

Aus der Arbeitsgruppe Zelluläre Neurowissenschaften
Max-Delbrück Zentrum für Molekulare Medizin, Berlin

DISSERTATION

iPSC Differenzierte Mikroglia: Charakterisierung und
Veränderungen nach Co-Kultivierung mit Gliomzellen

iPSC-Derived Microglia: Characterization and Changes Upon
Co-Cultivation with Glioma Cells

zur Erlangung des akademischen Grades
Doctor medicinae (Dr. med.)

vorgelegt der Medizinischen Fakultät
Charité – Universitätsmedizin Berlin

von

Marina Sophia Schnauß

aus Berlin

Datum der Promotion: 23.03.2024

Contents

Contents	2
Figures	10
Tables	14
Abbreviations	15
German Abstract	19
English Abstract	20
1. Introduction	21
1.1 <i>Microglia</i>	21
1.1.1 The Discovery of Microglia.....	21
1.1.2 The Role of Microglia	21
1.1.3 Microglial Ontogeny.....	21
1.2 <i>Glioma</i>	22
1.2.1 Glioma in Clinical Medicine	22
1.2.2 The Role of Microglia in Glioma.....	22
1.2.3 Transcriptional Changes in Glioma-Associated Microglia.....	23
1.2.4 Peripheral Monocytes in Glioma	23
1.3 <i>Microglia in Glioma Models</i>	24
1.3.1 Differences Between Human and Murine Microglia	24
1.3.2 Previous Experimental Setups Utilizing Human Microglia	24
1.4 <i>iPSC</i>	25
1.4.1 Pluripotency	25
1.4.2 Discovery of iPSC.....	25

1.4.3	iPSC Applications	25
1.5	<i>iPSC-Derived Microglia</i>	26
1.5.1	Applications of iPSC-Derived Microglia in Research	26
1.5.2	Differentiation Protocols for iMGL	26
1.5.2.1	Muffat et al.	26
1.5.2.2	Pandya et al.	27
1.5.2.3	Douvaras et al.	27
1.5.2.4	Haenseler et al.	27
1.5.2.5	Takata et al.	27
1.5.2.6	McQuade et al., Abud et al.	27
1.5.3	The “three flavors” of iMGL	28
1.5.3.1	iMGL in Brain Organoids	28
1.5.3.2	Xenotransplantation of iMGL	28
1.6	<i>Research Question</i>	30
2.	Methods	31
2.1	<i>Methods: Cell Culture</i>	31
2.1.1	Glioma Cell Culture	31
2.1.1.1	Cultivation of Glioma Cells.....	31
2.1.1.2	Passaging of Glioma Cells.....	31
2.1.2	THP-1 Cell Culture	31
2.1.2.1	THP-1 Cultivation.....	31
2.1.2.2	Passaging of THP-1 Cells.....	32
2.1.2.3	Differentiation of THP-1 Cells	32

2.2	<i>Methods: Stem Cell Culture</i>	32
2.2.1	iPSC Origin.....	32
2.2.1.1	Origin of BJFF.6 iPSC.....	32
2.2.1.2	Origin of XMOO1 iPSC.....	32
2.2.1.3	Thawing of iPSC.....	33
2.2.1.4	iPSC culture.....	33
2.2.1.5	Passaging of iPSC.....	33
2.2.1.6	Freezing of iPSC.....	34
2.3	<i>Stem Cell Differentiation</i>	34
2.3.1	Overview.....	34
2.3.2	Hematopoietic Differentiation.....	35
2.3.2.1	Clustersplit on Day -1.....	35
2.3.2.2	Well Selection and Start of Hematopoietic Differentiation on Day 0.....	36
2.3.2.3	Further Hematopoietic Differentiation.....	36
2.3.2.4	HPC Harvest and Reseeding.....	36
2.3.3	Differentiation Towards a Microglial Phenotype.....	37
2.3.3.1	Microglial Differentiation Medium.....	37
2.3.3.2	Day 0 of Microglial Differentiation.....	38
2.3.3.3	Days 2, 4, 6, 8, 10, 14, 16, 18, 20, 22 and 24 of Microglial Differentiation.....	38
2.3.3.4	Day 12 of Microglial Differentiation.....	38
2.3.3.5	Day 25 of Microglial Differentiation.....	38
2.3.3.6	Day 27 of Microglial Differentiation.....	38

2.3.3.7	IMGL Harvest	38
2.4	<i>Basic Characterization of iMGL Derived from XMOO1 iPSC Cell Line</i>	39
2.4.1	Upregulation of Microglia-Characteristic Gene Markers in Comparison to HPCs, THP-1 and U87 Cells Measured with Quantitative Polymerase Chain Reaction (qPCR)	39
2.4.1.1	IMGL Seeding	39
2.4.1.2	Cell Harvest and RNA Isolation	39
2.4.1.3	Reverse Transcription	39
2.4.1.4	QPCR	39
2.4.1.5	Statistical Analysis	40
2.4.2	Immunohistochemical Staining for Iba1, SLC2A5, TMEM119 and P2RY12	40
2.4.2.1	Immunohistochemical Staining	40
2.4.2.2	Confocal Microscopy	41
2.4.2.3	Quantification	41
2.4.3	Proinflammatory Response to LPS Stimulations	41
2.4.3.1	IMLG Stimulation with LPS	41
2.4.3.2	Cell Harvest, RNA Isolation and qPCR	41
2.4.3.3	Statistical Analysis	42
2.5	<i>Migration Assay</i>	42
2.5.1	Migration of XMOO1 iPSC-Derived iMGL	42
2.5.1.1	Cell Seeding	42
2.5.1.2	Scratching and Scanning	42

2.5.1.3	Analysis	42
2.6	<i>Phagocytosis Assay</i>	44
2.6.1	Phagocytosis of Carboxylate Beads by iMGL	44
2.6.1.1	Cell Seeding	44
2.6.1.2	Incubation with Carboxylate Microspheres	44
2.6.1.3	Cell Staining	44
2.6.1.4	Flow Cytometry	44
2.6.1.5	Analysis	45
2.6.1.6	Statistical Analysis	45
2.7	<i>Co-Cultivation Experiments</i>	45
2.7.1	Co-Cultivation of iMGL with glioma Cells	45
2.7.1.1	Day -1	45
2.7.1.2	Day 0	45
2.7.1.3	Days 1, 3 and 5	45
2.7.2	Gene Expression Analysis for GAM-Characteristic Genes.....	46
2.7.2.1	Cell Harvest, RNA Isolation, Reverse Transcription, qPCR.....	46
2.7.2.2	Statistical Analysis	47
2.7.3	Morphologic Analysis of iMGL Co-Cultivated with Glioma Cells.....	47
2.7.3.1	Cell Seeding and Co-Cultivation.....	47
2.7.3.2	Immunohistochemical Staining.....	47
2.7.3.3	Confocal Microscopy.....	48
2.7.3.4	Quantification of Morphology	48

2.7.3.5	Statistical Analysis	48
2.8	<i>Direct Co-Cultivation Experiments</i>	49
2.8.1	Direct Co-Cultivation of BJFF.6 iMGL and U87 mCherry	49
2.8.1.1	Cell Seeding and Co-Cultivation.....	49
2.8.1.2	Immunohistochemical Staining.....	49
2.8.1.3	Confocal Microscopy.....	49
2.8.1.4	Quantification of GPNMB and SPP1 Intensity and Statistical Analysis	50
2.8.1.5	Quantification of Morphology.....	50
2.8.1.6	Statistical Analysis	50
2.9	<i>Proinflammatory Stimulation of iPSC-Derived Microglia</i>	51
2.9.1	TLR2 Stimulation of iPSC-Derived Microglia.....	51
2.9.1.1	Cell Seeding	51
2.9.1.2	Cell Stimulation with Pam2CSK4	51
2.9.1.3	Cell Harvest, RNA Isolation, Reverse Transcription and QPCR	51
2.9.1.4	Statistical Analysis	52
2.10	<i>Statistical Analysis</i>	52
3.	Results	54
3.1	<i>Basic Characterization of iMGL Derived from XMOO1 iPSC Cell Line</i>	54
3.1.1	XMOO1-Derived iMGL Upregulate Microglia-Characteristic Genes P2RY12, SLC2A5 and TMEM119 Compared to HPCs, THP-1	54
3.1.2	XMOO1-Derived iMGL Do Not Upregulate Monocyte- Characteristic Genes Compared to HPCs, THP-1 and U87	55

3.1.3	Immunohistochemical Staining of iMGL Derived from XMOO1 iPSC Cell Line for Iba1, SLC2A5, TMEM119 and P2RY12.....	56
3.1.4	XMOO1 iMGL Upregulate Proinflammatory Genes Upon LPS Stimulation	58
3.1.5	Migration	59
3.1.6	FACS-Based Phagocytosis Assay – Proof of Concept with Cell Sorter and Phase Contrast Microscopy	61
3.1.7	FACS-Based Phagocytosis Assay – Analysis with LSRFortessa™ Analyzer and Quantification	63
3.2	<i>Expression of Genes Characteristic for GAM</i>	65
3.3	<i>Morphology of iMGL Co-Cultivated with Glioma Cells</i>	71
3.3.1	Representative Images and Description.....	71
3.3.2	Quantification of Morphology	77
3.4	<i>Direct Co-Cultivation with U87 mCherry</i>	80
3.4.1	Changes in SPP1 Upon Direct Co-Cultivation with U87 mCherry.....	80
3.4.2	Changes in GPNMB Upon Direct Co-Cultivation with U87 mCherry.....	83
3.4.3	Changes in Morphology Upon Direct Co-Cultivation.....	85
3.5	<i>TLR2 Stimulation</i>	86
3.5.1	TLR2 Stimulation Upregulates Proinflammatory Genes in BJFF.6-derived iMGL	86
3.5.2	TLR2 Stimulation Does Not Significantly Change GAM-Characteristic Gene Expression.....	87
3.5.3	TLR2 Stimulation Does Not Significantly Upregulate MMP9 and MMP14 Expression in BJFF.6-derived iMGL	88
4.	Discussion	89
4.1	<i>XMOO1-derived iMGL Exhibit Fundamental Microglia-Specific Properties</i> .89	
4.2	<i>iMGL Co-Cultivated with Human Glioma Cell Lines in a Transwell Setup Do Not Consistently Upregulate GAM-Characteristic Genes</i>	92

4.3	<i>iMGL Co-Cultivated with Human Glioma Cells in a Transwell Setup</i>	
	<i>Exhibit a Morphology Not Typic for GAM</i>	94
4.4	<i>iMGL Upregulate GPNMB in Co-Culture with Direct Intercellular Contact</i> ...	94
4.5	<i>TLR2 Stimulation Upregulates Pro-Inflammatory but Not</i>	
	<i>GAM-Characteristic Genes in iMGL</i>	95
5.	Outlook and Conclusion	98
6.	References	101
7.	Statutory Declaration	111
8.	German Curriculum Vitae	113
9.	Publication List	114
10.	Statistical Certification	115
11.	Aknowlegements	116

Figures

Nr.	Summary	page
1	Summary of differentiation of iPSC towards a microglial phenotype.	35
2	Workflow of the scratch wound assay done for this project.	43
3	Schematic description of co-cultivation protocol.	46
4	Gene expression of microglial signature genes P2RY12, TMEM119 and SLC2A5 in U87, THP-1, XMOO1 HPC and XMOO1 iMGL cells.	54
5	Gene expression of monocytic signature genes GDA, EMILIN2, HP and SELL in U87, THP-1, HPC and XMOO1 iMGL cells.	55
6	Staining of XMOO1-derived iMGL for canonical microglial markers Iba1, SLC2A5, TMEM119 and P2RY12.	56
7	Staining of XMOO1 iMGL for Iba1, P2RY12, TMEM119 and SLC2A5.	57
8	Genes upregulated by XMOO1 iMGL upon stimulation with LPS for 6 hours.	58
9	Scratch wound over a time range of 48 hours	59
10	Wound confluency of XMOO1 iMGL in a Woundmaker™-based scratch assay as calculated by IncuCyte Zoom® software (Sartorius, Göttingen, GER) for a total time of 48 hours.	60

11	Gating of XMOO1-derived iMGL by Aria II cell sorter for proof of concept.	61
12	Cell sorting results of XMOO1-derived iMGL that had been left to phagocytose fluorescently marked carboxylate microspheres.	62
13	Gating of XMOO1-derived iPSC by LSRFortessa™ (BD, Franklin Lakes, NJ, USA).	63
14	Quantification of phagocytosis.	64
15	Changes of expression of GAM-characteristic genes SPP1 and TGM2 after 72 and 144 hours of co-cultivation with U87, U251MG and LN229 glioma cells.	65
16	Fold-change relative to control of expression of GAM-characteristic genes GPNMB and IL6 after 72 and 144 hours of co-cultivation with U87, U251MG and LN229 glioma cells.	68
17	Co-cultivation of BJFF.6-derived iMGL with U87 glioma cells for 72 hours.	74
18	Co-cultivation of BJFF.6-derived iMGL with U87 glioma cells for 144 hours.	74
19	Co-cultivation of BJFF.6-derived iMGL with U251MG glioma cells for 72 hours.	75
20	Co-cultivation of BJFF.6-derived iMGL with U251MG glioma cells for 144 hours.	76

21	Co-cultivation of BJFF.6-derived iMGL with LN229 glioma cells for 72 hours.	76
22	Co-cultivation of BJFF.6-derived iMGL with LN229 glioma cells for 144 hours.	77
23	Volumes in μm^3 of iMGL co-cultivated with U87 glioma cells in a transwell setup and respective controls for 72 hours and 144 hours.	77
24	Sphericity as defined by Wadell was computed for iMGL co-cultivated with U87 glioma cells in a transwell setup versus monocultivated controls for 72 hours and 144 hours.	78
25	Nucleus to cytoplasm volume ratio of iMGL co-cultivated with U87 glioma cells in a transwell setup and respective controls for 72 hours and 144 hours.	79
26	Staining of XMOO1-derived iPSC directly co-cultivated with mCherry U87 glioma cells.	80
27	Staining of XMOO1-derived iPSC seeded on coverslips without mCherry U87 glioma cells as a control.	81
28	Staining of mCherry U87 glioma cells as a control.	81
29	BJFF.6-derived iMGL were stained for SPP1 with a secondary AF488-conjugated antibody.	82
30	Staining of XMOO1-derived iPSC directly co-cultivated with mCherry U87 glioma cells.	83

31	Staining of XMOO1-derived iPSC seeded on coverslips without mCherry U87 glioma cells as a control.	83
32	Staining of mCherry U87 glioma cells as a control.	84
33	Mean intensity per μm^3 of BJFF.6-derived iMGL stained with AF488-conjugated secondary antibody bound to primary anti-GPNMB antibody.	84
34	Volumes in μm^3 and sphericities of iMGL co-cultivated with U87 under direct cell-cell contact and respective controls.	85
35	Upregulation of proinflammatory markers in BJFF.6 -derived iMGL upon TLR2 stimulation.	86
36	Foldchanges of GAM-characteristic genes of BJFF.6-derived iMGL upon TLR2 stimulation with Pam2CSK4.	87
37	Foldchanges in MMP9 and MMP14 expression of XMOO1- and BJFF.6 derived iMGL upon TLR2 stimulation with Pam2CSK4.	88

Tables

Nr.	Summary	page
1	Ingredients of iMGL basal medium as published by McQuade et al. (McQuade, 2018).	37
2	Annotation of significance levels as used in this thesis.	53
3	Mean Fold-Changes, p-value, t-value and significance of changes in SPP1 gene expression for co-cultivation for 72 and 144 hours with U87, U251MG and LN229 for BJFF.6- and XMOO1-derived iMGL.	66
4	Mean Fold-Changes, p-value, t-value and significance of changes in TGM2 gene expression for co-cultivation for 72 and 144 hours with U87, U251MG and LN229 for BJFF.6- and XMOO1-derived iMGL.	67
5	Mean Fold-Changes, p-value, t-value and significance of changes in GPNMB gene expression for co-cultivation for 72 and 144 hours with U87, U251MG and LN229 for BJFF.6- and XMOO1-derived iMGL.	69
6	Mean Fold-Changes, p-value, t-value and significance of changes in IL-6 gene expression for co-cultivation for 72 and 144 hours with U87, U251MG and LN229 for BJFF.6- and XMOO1-derived iMGL.	70
7	Approximate cell sizes of iMGL on representative images for each glioma cell line used for co-cultivation, duration of co-cultivation and condition (see Figure 17, Figure 18, Figure 19, Figure 20, Figure 21, Figure 22).	73

Abbreviations

bFGF	Basic Fibroblast Growth Factor
BMP4	Bone Morphogenic Protein 4
BORG	Brain ORGanoids (iPSC-derived brain-like structures)
CD200	Cluster of Differentiation 200
CD68	Cluster of Differentiation 68
cDNA	Complementary Deoxyribonucleic Acid
CNS	Central Nervous System
CX3CL1	Chemokine C-X3-C motif ligand 1 / Fractalkine
DAPI	4',6-Diamidin-2-phenylidol
DMEM	Dulbecco's Modified Eagle's Medium
ELISA	Enzyme-Linked Immunosorbent Assay
EMP	Erythromyeloid Precursor
FACS	Fluorescence-Activated Cell Sorting
FCS	Fetal Calve Serum
FLT3	Fms related receptor tyrosine kinase 3
GAM	Glioma-Associated Microglia

GER	Germany
GPNMB	Glycoprotein Non-metastatic Melanoma Protein B
HLA	Human Leukocyte Antigen
HPC	Hematopoietic progenitor cells
IL-10	Interleukin 10
IL-1 β	Interleukin 1 beta
IL-34	Interleukin 34
IL-6	Interleukin 6
iMGL	iPSC-derived Microglia-Like cells
iNOS	Inducible Nitric Oxide Synthase
iPSC	Induced Pluripotent Stem Cells
Klf4	Kruppel-like factor 4
LPS	Lipopolysaccharide
M-CSF	Macrophage Colony-Stimulating Factor / Colony Stimulating Factor 1
MACS	Magnetic-Activated Cell Sorting
MMP14	Matrix Metalloproteinase 14
MMP9	Matrix Metalloproteinase 9
NO	Nitric Oxide

OBS	Organotypic Brain Slices (here: mouse brain slices kept in culture for up to several weeks)
OCT3/4	Octamer-Binding Transcription factors 3/4
oMG	Organoid Microglia
PBS	Phosphate Buffered Saline
PI	Propidium Iodide
qPCR	Quantitative Polymerase Chain Reaction
RNA	Ribonucleic Acid
SCF	Stem Cell Factor
Sox2	Sex determining region Y box 2
SPP1	Secreted Phosphoprotein 1, also known as Osteopontin
TBP	TATA-Binding Protein
TBS	Tris-Buffered Saline
TGF- β 1	Transforming Growth Factor Beta 1
TGM2	Transglutaminase 2
TLR2	Toll-like Receptor 2
TLR4	Toll-like Receptor 4
TNF α	Tumor Necrosis Factor Alpha
TPO	Thrombopoietin

UDP	Uridine Diphosphate
USA	United States of America
VEGF	Vascular Endothelial Growth Factor
VEGFA	Vascular Endothelial Growth Factor A
WHO	World Health Organization
xMG	Xenotransplanted Microglia

German Abstract

Glioblastome sind die häufigsten Hirntumore des Menschen und sind mit einer infausten Prognose verbunden (Schwartzbaum, 2006). Bis zu 30 % der Zellen eines Glioblastoms können Makrophagen oder Mikroglia, die gewebständigen Makrophagen des Gehirns, sein (Charles, 2011) (Badie, 2000). Der Anteil infiltrierender Mikroglia und Makrophagen innerhalb eines Glioblastoms korreliert mit einer schlechten Prognose (Engler, 2012) (Feng, 2015). Bis dato waren gesunde menschliche Mikroglia und Makrophagen für Forschungszwecke nur schwer erhältlich. Neue Erkenntnisse zur Ontologie der Mikroglia (Ginhoux, 2010) bildeten die Grundlage für mehrere Protokolle, die es ermöglichen, induzierte pluripotente Stammzellen (iPSC) zu iPSC-generierten mikroglia-ähnlichen Zellen (iMGL) zu differenzieren (Abud, 2017) (Gutmann, 2019) (Hasselman, 2020). Hier erforschen wir, ob iMGL, welche wie von McQuade et al. publiziert differenziert wurden (McQuade, 2018), ein geeignetes Modell sind, um über Mikroglia im Kontext von Gliomen zu forschen. Zuerst wurden iMGL, welche aus der iPSC Zelllinie XMOO1 generiert wurden, gründlich charakterisiert. Dann analysierten wir die Genexpression und Morphologie von iMGL, welche mithilfe von Transwell Inserts co-kultiviert wurden. Außerdem betrachten wir die Gliom-typischen Marker SPP1 und GPNMB (Szulzewsky, 2016) in einem direkten co-Kultur Modell, sowie Veränderungen der Genexpression infolge von TLR2 Stimulation.

English Abstract

Glioblastomas are the most common primary human brain tumor entities and have a very poor prognosis (Schwartzbaum, 2006). Up to 30 % of glioblastoma cells can be peripheral macrophages or microglia, the brain's resident macrophages (Charles, 2011) (Badie, 2000). Higher numbers of infiltrating microglia and peripheral macrophages have been correlated with a poor glioma prognosis (Engler, 2012) (Feng, 2015). To date, healthy human microglia and human glioma-associated microglia are scarcely available for research purposes. Novel findings on microglial ontology (Ginhoux, 2010) were the foundation of several protocols which differentiate induced pluripotent stem cells (iPSC) into iPSC-derived microglia-like (iMGL) cells (Abud, 2017) (Gutmann, 2019) (Hasselmann, 2020). Here, we investigate whether iMGL, differentiated as published by McQuade et al. (McQuade, 2018), are a suitable model to investigate microglia in the context of glioma. First, we characterize iMGL differentiated from the iPSC cell line XMOO1 thoroughly. Then, we analyze gene expression and morphology of iMGL co-cultivated with glioma cells in a transwell setting, microglial marker expression in a direct co-cultivation setting, and gene expression in response to TLR2 stimulation.

1. Introduction

1.1 Microglia

1.1.1 The Discovery of Microglia

Microglia are the resident immune cells of the brain. Historically, a glue-like mass called neuroglia was first described by Rudolph Virchow in 1856 (Virchow, 1862). Mihály von Lenhossek then postulated that glia consist of cells and used the term “astrocyte” for the first time (Lenhossek, 1895). In 1913, Santiago Ramon y Cajal published a staining protocol that allowed him to specifically stain astrocytes (y Cajal, 1913). Some cells remained unstained by this method, including microglia. In 1919, Pio del Rio-Hortega furthered these findings to describe microglia in four publications. The first publication describes two staining protocols for microglia and subsequent observations on microglial morphology, types (neuronal, vascular and astroglial satellites) and density in different brain regions (Rio-Hortega, 1919). The second publication is about the amoeboid transformation of microglia under pathologic conditions. It identifies microglia as the previously observed cells that are characteristic for certain brain pathologies, such as the “Stäbchenzellen” described by Alois Alzheimer (Rio-Hortega, 1919). The third publication argues that microglia most likely have a mesodermal origin (Rio-Hortega, 1919). Remarkably, this has recently been confirmed (Ginhoux, 2010). The fourth publication describes the migration and phagocytosis of microglia (Rio-Hortega, 1919).

1.1.2 The Role of Microglia

Based on these publications, it has been elucidated that microglia are relevant for the pathophysiology of a myriad of neurological diseases, including Alzheimer’s disease, psychiatric disorders such as autism spectrum disorder and schizophrenia, stroke, brain trauma, viral infections and glioma (Wolf, 2017). Microglia constantly screen the brain parenchyme for pathogens, are activated by a broad range of stimuli and secrete a broad variety of cytokines, growth factors, and chemokines. They also play a key role in brain development, as they conduct synaptic pruning (Paolicelli, 2011).

1.1.3 Microglial Ontogeny

Microglia have a distinct ontogeny from monocytes and most other macrophages. They originate from mesodermal, yolk-sac derived erythromyeloid precursors (EMPs) that

migrate to the neuroepithelium at embryonic Day 8 in mice (Ginhoux, 2010), and not from hematopoietic stem cells (Schulz, 2012). The c-kit⁺ EMPs develop into CD45⁺ c-kit^{lo} CX3CR1⁻ A1 cells, then into CD45⁺c-kit⁻CX3CR1⁺ A2 cells, which migrate into the early brain utilizing matrix metalloproteinases (Kierdorf, 2013).

1.2 Glioma

1.2.1 Glioma in Clinical Medicine

Glioma are the most common brain tumor entities in humans and constitute a devastating diagnosis (Schwartzbaum, 2006). In Germany, glioma comprise about 1.6 % of tumors in males and 1.4 % of tumors in females (Robert Koch Institut, 2017). Central nervous tumors are classified by the World Health Organization's (WHO) classification (Louis, 2016). The WHO classification considers tumor histology, as well as genetic deviations. Glioma are brain tumor entities comprising astrocytoma, glioblastoma, oligodendroglioma and ependymal tumors, amongst others. Furthermore, brain tumors are graded by WHO grading I-IV, based on histologic malignancy criteria. WHO grading is a base for prognostic assessment of patients affected by glioma. Glioblastoma, the most common primary brain tumor, shows a median survival of 14.5 months when treated with operative resection, radiotherapy and chemotherapy, chiefly since glioma exhibit a highly infiltrative growth (Stupp, 2009).

1.2.2 The Role of Microglia in Glioma

Glioma maintain a complex tumor ecosystem consisting not only of neoplastic cells, but also of non-neoplastic cells (Hambardzumyan, 2016) (Gutmann, 2019). Glioma contain more microglia and macrophages than healthy brain tissue (Engler, 2012). Up to 30 % of glioma mass can consist of microglia (Charles, 2011). Microglia do not only fail to effectively fight tumor cells, but on the contrary foster glioma growth (Feng, 2015) (Hu, 2014). The amount of tumor-infiltrating microglia and macrophages was shown to be linked with a worse prognosis in patients (Wang, 2016).

Glioma cells trigger microglial motion towards them and convert microglia into a protumorigenic phenotype, whose gene profile only partially overlaps with microglia stimulated with inflammatory mediators (Ellert-Miklaszewska, 2013). Microglia of the protumorigenic phenotype sustain tumor growth through a variety of mechanisms,

including upregulation of matrix metalloproteinase 14 (MMP14) mainly via toll-like receptor 2 (TLR2), which enhances glioma migration (Vinnakota, 2013) and invasion-promoting IL-6 via toll-like receptor 4 (TLR4) (a Dzaye, 2016). Also, microglia-derived TGF- β was shown to be relevant for glioma invasion (Wesolowska, 2008).

1.2.3 Transcriptional Changes in Glioma-Associated Microglia

It has been shown that glioma-associated microglia (GAM) express a number of characteristic genes. In two gene expression studies, one including murine data and one using data from human glioma samples, Szulzewski et al. showed that tumor-associated microglia and macrophages express higher levels of GPNMB and SPP1 (Szulzewski, 2015, Szulzewski F. S., 2017). SPP1 is mostly secreted by glioma-associated microglia and macrophages and SPP1 knock-down has led to enhanced tumor progression, decreased apoptosis in glioma cells, decreased tumor vascularization and increased microglial infiltration. GPNMB stands for glycoprotein non-metastatic melanoma protein B and is upregulated in various cancers. It is associated with a poor prognosis for glioma patients (Szulzewski, 2016). Previously, Kuan et al. produced some recombinant immunoproteins targeting GPNMB and tested its applications for malignant glioma and melanoma in athymic rats (Kuan, 2011). Also, a study by Walentynowicz et al. showed that TGM2 is upregulated in various glioma-associated microglia apart from GPNMB (Walentynowicz, 2018). TGM2 stands for transglutaminase 2, an acyltransferase situated on the plasma membrane that catalyzes Ca²⁺-dependent protein modifications, serves as G-protein and as part of certain integrins, making it relevant to membrane stabilization as well as phagocytosis (Szondy, 2017). Also, TGM2 has been linked to apoptotic signaling pathways as well as the TGF- β 1 pathway in microglia. It is furthermore known to be expressed as a vast majority of cells and cellular compartments and has been associated with a broad variety of diseases.

1.2.4 Peripheral Monocytes in Glioma

Next to microglia, brain tissue infiltration by peripheral monocytes from the bone marrow, especially the skull bone marrow, is also likely relevant for central nervous system (CNS) pathologies such as glioma (Herisson, 2018). This has been complicating research on microglia under pathologic conditions, as it has been difficult to distinguish tissue-resident microglia from invading monocytes. Recently, a study

with a metanalytic bioinformatic approach showed that in mice, P2RY12, SLC2A5, TMEM119 and FCRL5 are reliable markers for microglia in health and disease, whereas EMILIN2, GDA, HP and SELL are monocyte markers (Haage, 2019).

1.3 Microglia in Glioma Models

1.3.1 Differences Between Human and Murine Microglia

It has become increasingly clear that murine microglia possess a clearly distinct phenotype from their human counterparts (Smith, 2014). Furthermore, transcriptomic differences between human microglia isolated post mortem and murine microglia have been shown (Galatro, 2017) (Szulzewsky, 2016). Also, the lipopolysaccharide receptor TLR4, which is highly expressed in murine microglia and strongly activates them, seems to be less important in humans (Wolf et al.). Moreover, sialic acid binding immunoglobulin-like lectins (Siglecs), a molecule family involved in innate immune responses, were shown to be represented by almost twice as many genes in humans compared to mice. This might lead to a higher variation in Siglec proteins in humans, which might have an influence in Alzheimer's disease (Linnartz-Gerlach, 2019). Furthermore, it has been shown in murine models that TGF- β 1 down regulates expression of the antigen-presenting protein class human leukocyte antigen (HLA). This is not the case in human microglia (Smith, 2013). However, as in murine microglia, M-CSF could downregulate HLA expression, also TGF- β 1 reduced microglial cell numbers, suggesting that TGF- β 1 may act on human microglia through another pathway. Another difference between human and murine microglia lies in their production of nitric oxide (NO) through the inducible NO synthase (iNOS). Human microglia necessitate a stronger and different stimulation than rodent microglia to produce NO, also human microglia generally produce less NO (Smith, 2014) (Landry, 2012). Moreover, as opposed to rodent microglia, human microglia do not downregulate their NO production upon COX-2 inhibition (Janabi, 2002). As NO production often is used to measure microglia activation, this might lead to a bias when analyzing microglial activation in different species.

1.3.2 Previous Experimental Setups Utilizing Human Microglia

Several studies have used microglia isolated post mortem from human subjects, even though this poses a high logistic challenge. Other studies were done with human brain tissue samples from patients that underwent brain surgery due to conditions such as

epilepsy, glioma or trauma. These experimental setups have pitfalls. It is likely that microglia isolated post mortem or from brain surgery samples exhibit unphysiological activation or undetected pathologic changes. Moreover, it has been shown that a long-term cultivation of these acutely isolated microglia may lead to significant transcriptomic changes and a different enhancer landscape, both for human (Gosselin, 2017) and rodent microglia (Bohlen, 2017) (Butovsky, 2014). Also, in rodent microglia microglial signature genes were downregulated with a half-life of less than an hour under culture conditions (Bohlen, 2017).

1.4 iPSC

1.4.1 Pluripotency

Pluripotency is a cell's ability to differentiate into any cell of the three germ layers, namely mesoderm, ectoderm and endoderm. They can therefore become any cell of the human body. Pluripotent cells are unlike totipotent cells, which can give rise to a whole organism and multipotent cells, which can only develop into a fraction of an organism's cells. Pluripotent stem cells are cells that are not only pluripotent, but also have an unlimited ability for self renewal. Examples for pluripotent stem cells are embryonic carcinoma cells, embryonic stem cells and iPSC.

1.4.2 Discovery of iPSC

Murine embryonic stem cells were first established by Evans et al. in 1981 (Evans, 1981), human embryonic stem cells were first described by Thomson et al. in 1998 (Thomson, 1998).

In 2006, Takahashi et al. showed that murine adult fibroblasts and embryonic stem cells can be reprogrammed towards pluripotency by introducing the four transcription factors Oct3/4, Sox2, c-Myc and Klf4 (Takahashi, 2006). In 2007, the same authors reported the generation of human iPSC, alongside with Thomson et al. (Takahashi, 2007) (Yu, 2007). The Nobel Prize in Physiology or Medicine was awarded to Shinya Yamanaka and Sir John B. Gurdon in 2012 for the discovery of iPSC.

1.4.3 iPSC Applications

Since then, iPSC have been used for a broad variety of applications, including disease modeling and organoid cultivation for research, but also in clinical practice for

personalized medicine approaches (Scudellari, 2016). Furthermore, iPSC are thought to be a promising tool for regenerative therapies. However, few clinical trials including iPSC have been done up to date.

1.5 iPSC-Derived Microglia

1.5.1 Applications of iPSC-Derived Microglia in Research

In the past, research on microglia has been hampered by poor availability of human microglia in a physiologic state. Microglia extracted post-mortem or intraoperatively are generally affected by brain pathologies, acute brain trauma or stress (Wolf, 2017). In consequence, microglial research has chiefly been conducted on murine microglia.

Therefore, novel approaches seek to establish models where microglia are obtained by differentiation of human pluripotent stem cells to iPSC-derived microglia-like cells (iMGL). The obtained iMGL may become new tools for basic research, enabling discovery of new and specification of known pathways in order to find cues to innovative therapies. Furthermore, iMGL may also be an opportunity for genetics research, since new techniques such as CRISPR/Cas9 allow targeted insertion of mutations into these cells. However, developing protocols for iPSC differentiation into iMGL cells has been a challenge, since microglia undergo a complex embryologic development (Ginhoux, 2010). They originate in the yolk sac as EMPs, then become primitive macrophages, that seed in the neural tube. There, they develop a distinct microglial phenotype due to environmental cues, including IL-34 and TGF β -1.

1.5.2 Differentiation Protocols for iMGL

Several protocols to differentiate iPSC to iMGL have been published in recent years.

1.5.2.1 Muffat et al.

In 2016, Muffat et al. published a protocol for iMGL derivation from iPSC relying on embryoid body formation (Muffat, 2018). Eventually, embryoid bodies evolve to yolk sac embryoid bodies, which release immature iMGL approximately 30 days later. Maturation of iMGL takes another 30 days. A serum-free neuroglial differentiation medium supplemented with M-CSF and IL-34 is used for this protocol.

1.5.2.2 Pandya et al.

Pandya et al. published a protocol that differentiates iPSC to hematopoietic progenitor cells (HPCs), then HPCs to iMGL using a co-culture with astrocytes and supplementation with GM-CSF, M-CSF and IL3 (Pandya, 2017).

1.5.2.3 Douvaras et al.

Douvaras et al. developed a differentiation protocol where microglial progenitor cells can be isolated from culture supernatant by fluorescence-activated cell sorting (FACS) or magnetic-activated cell sorting (MACS) several times over 15 days (Douvaras, 2017). Microglial progenitors were previously obtained by adding BMP4, bFGF, SCF, VEGFA, IL3, TPO, M-CSF, FLT3 and GM-SCF to culture medium in different combinations for 25 days. After isolating microglial progenitor cells, cells are left to mature for 20 days in presence of IL-34 or GM-CSF.

1.5.2.4 Haenseler et al.

Haenseler et al.'s differentiation protocol relies on co-cultivation with iPSC-derived neurons (iNeurons) (Haenseler, 2017). In a first step, embryoid bodies are produced by cultivation with BMP4, VEGF and SCF. Then, supplementation with IL3 and M-CSF induces myeloid differentiation. After three to four weeks, macrophage precursor cells can be harvested from supernatant. Co-cultivation with iNeurons in medium containing IL-34 then led to the induction of a microglia-like phenotype in macrophage precursor cells.

1.5.2.5 Takata et al.

Takata et al. published an article that describes two ways to differentiate murine and human iPSC into microglia-like cells (Takata, 2017). First, iPSC are differentiated into primitive macrophages, which are then co-cultivated with iPSC-derived neurons or transferred into developing mouse brains. This also led to the development of a microglia-like phenotype.

1.5.2.6 McQuade et al., Abud et al.

In 2018, McQuade et al. published a protocol for iPSC differentiation to iMGL that abstains from embryoid body formation, co-culture and cell sorting, therefore significantly simplifying the process (McQuade, 2018). It is based on the differentiation

of iPSC into hematogenic progenitor cells (HPCs), which are then further differentiated to iMGL by exposing them to cytokines that are key for their *in vivo* development, namely M-CSF, IL-34, TGF- β 1, CX3CL1 and CD200.

The same group then further investigated iMGL cells obtained by their new protocol (Abud, 2017). For that, they conducted developmental and transcriptomic analyses. Also, they analyzed proinflammatory cytokine secretion of iMGL, migration, calcium transients and phagocytosis. Moreover, they performed differential gene expression analysis of iMGL co-cultured with rat hippocampal neurons and separated by FACS. Finally, they implanted iMGL into transgenic mice and human brain organoids and characterized microglial integration.

1.5.3 The “three flavors” of iMGL

In a recently published review, Hasselmann et al. refer to different models involving iMGL as the “three flavors” of iMGL, namely iPSC-derived microglia (iMGL), organoid microglia (oMG) and xenotransplanted microglia (xMG) (Hasselmann, 2020). iMG are the base for various in-vitro models, which are especially suited to study monogenetic diseases.

1.5.3.1 iMGL in Brain Organoids

A protocol to derive brain organoids (BORG) from iPSC was first published by Lancaster et al. in 2013 (Lancaster, 2013). In 2017, Abud et al. co-cultivated iMGL differentiated *in vitro* with BORG and were able to show a microglia-typical morphology and injury response (Abud, 2017). Furthermore, in 2018 Ormel et al. could induce the intrinsic development of microglia-like cells within BORG by slightly modifying the protocol by Lancaster et al. (Ormel, 2018). These microglia-like cells were PU.1, CD68 and Iba1 positive; they also expressed P2RY12 and TMEM119, albeit in lesser amounts than human ex vivo microglia. Furthermore, the microglia-like cells could phagocytose and also seemed to conduct synaptic pruning.

1.5.3.2 Xenotransplantation of iMGL

In 2017, Abud et al. transplanted human iMGL into immunodeficient MITRG mice with a quadruple knock-in for human M-CSF, GM-CSF, IL3 and thrombopoietin (Abud, 2017). The xenotransplanted microglia expressed microglia characteristic markers Iba1, TMEM119 and P2RY12; furthermore, they exhibited a microglia-typic ramified

morphology. Two years later, Hasselmann et al. published their experiments involving xenotransplantation of HPCs, the progenitors of iMGL in their differentiation protocol (Hasselmann, 2019). They used MITRG mice which had a knock-in for human M-CSF only. The HPC differentiated into mature-microglia like cells, which showed a typical morphology, expressed microglia-characteristic markers and had a transcriptomic signature similar to human *in vivo* microglia. Also, numerous microglial subpopulations with niche-characteristic morphologies and phenotypes emerged, such as parenchymal, perivascular and meningeal microglia. XMG surveyed their environment and responded to laser ablation, trauma and intraperitoneal lipopolysaccharide (LPS). Also, xMG showed disease-characteristic changes in response to A β plaques and had Alzheimer's disease-specific transcriptomic alterations that are unique to human microglia. Svoboda et al. transplanted microglial precursors into neonatal mouse brains and showed that iMGL integrated in the brains and produced a microglia-characteristic gene signature as well as morphology (Svoboda, 2019). The resulting microglia-like cells also responded to stimulation with LPS and transcriptionally resembled *in vivo* human microglia in the context of disease.

1.6 Research Question

To date, research on microglia has chiefly utilized murine models. Nevertheless, it has been shown that human microglia differ from murine microglia in terms of transcriptome (Galatro, 2017) (Szulzewsky, 2016) and function (Wolf, 2017) (Smith, 2014) (Landry, 2012). Over the last decade, a whole string of scientific discoveries has strongly improved our knowledge of microglial embryology (Ginhoux, 2010) (Schulz, 2012) (Kierdorf, 2013). This was the groundwork for the development of several protocols aiming to differentiate iMGL towards a microglial phenotype (Muffat, 2018) (Haenseler, 2017) (Abud, 2017) (McQuade, 2018). Nevertheless, to date (March 2020), there are no publications on glioma where iMGL were utilized. Therefore, we would like to investigate whether iMGL are a suitable model for studying GAM and whether a co-culture setting can steer microglia towards a GAM-like phenotype. The basis for this will be the differentiation of XMOO1 and BJFF.6 iPSC towards a microglial phenotype using the differentiation protocol from McQuade et al. (McQuade, 2018). The resulting iMGL will be assessed for their expression of microglia marker genes (Haage, 2019) and known microglia-characteristic properties. These include migration, phagocytosis and response to LPS stimulation. Then, we would like to investigate how a co-culture setting can steer microglia towards a GAM-like phenotype. A transwell setup will be used to investigate microglial changes in gene expression and morphology. Protein expression of GAM-markers SPP1 and GPNMB (Szulzewsky, 2016) will be investigated by immunohistochemistry in a direct co-culture setup. TLR2 stimulation has been shown to be crucial for MMP14 expression in GAMs and glioma expansion (Vinnakota, 2013). Hence, we will investigate whether TLR2 stimulation upregulates GAM-characteristic genes in iMGL.

2. Methods

2.1 Methods: Cell Culture

2.1.1 Glioma Cell Culture

2.1.1.1 Cultivation of Glioma Cells

Human glioma cell lines U87 (ECACC, Porton Down, UK, 89081402), U251MG (ECACC, Porton Down, UK, 89181403) and LN229 (ATCC, Manassas, VA, USA, CRL-2611) were used. They were cultivated in Dulbecco's Modified Eagle's Medium (DMEM) (Life Technologies, Carlsbad, USA, 41965062), supplemented with 10 % Pierce™ Bovine Serum (Life Technologies, Carlsbad, USA, 23209) and 1 % Penicillin-Streptomycin-Glutamine (Life Technologies, Carlsbad, USA, 10378016). Cells were grown in vented cell culture flasks with 25 cm² surface (Sarstedt, Nümbrecht, GER, 83.3910.002).

2.1.1.2 Passaging of Glioma Cells

For passaging, cells were washed with phosphate buffered saline (PBS) (Life Technologies, Carlsbad, USA, 14190-169) once, then released from flasks using approximately 2 ml Trypsin/EDTA (VWR, Radnor, PA, USA, L2163). Flasks were kept at room temperature or if necessary at 37°C, until cells were visibly released. Then, the enzyme activity of Trypsin/EDTA was stopped with 10 ml DMEM, 10 % fetal bovine serum (FBS), 1 % Penicillin-Streptomycin-Glutamine (PSG) by washing cells off the flask bottom and resuspending them in the medium multiple times. Cells were centrifuged for five minutes at 800 rpm. Then, supernatant was discarded and the remaining cell pellet was resuspended in DMEM, 10 % FBS, 1 % PSG. Cells were counted with Neubauer chamber (Roth, Karlsruhe, GER, T729.1) and cell counter (Roth, Karlsruhe, GER, EE53.1). Then, cells were reseeded into new cell culture flasks at desired density and incubated at 37°C normoxia.

2.1.2 THP-1 Cell Culture

2.1.2.1 THP-1 Cultivation

THP-1 cells were cultivated in glutamate-free RPMI 1640 (Life Technologies, Carlsbad, USA, 31870025) supplemented with 1 % PSG (Life Technologies, Carlsbad, USA, 10378016), 10 % Pierce™ Bovine Serum (Life Technologies, Carlsbad, USA, 23209) and 0,35 % 2-mecaptoethanol (Sigmaaldrich, St Louis, MO, USA, M3148). Cells were

grown in suspension at a density between 200'000 / ml and 1'000'000 / ml with medium change every other day.

2.1.2.2 Passaging of THP-1 Cells

Cells were split at 800'000 / ml. Cells were grown in flasks with 25 cm² surface (Sarstedt, Nümbrecht, GER, 83.3910.002). For splitting, they were moved into a 15 ml Falcon® (Corning, Corning, NY, USA, 352096), then counted with Trypan Blue (Sigmaaldrich, St Louis, MO, USA, T8154) and centrifuged for five minutes at 800 rpm. Then, their old medium was suctioned off and replaced with an appropriate amount of new medium.

2.1.2.3 Differentiation of THP-1 Cells

For differentiation, cells were plated in a 12-well plate (Sarstedt, Nümbrecht, GER, 83.3921) at 150'000 cells per well. They were then supplemented with 100 ng/ml phorbol 12-myristate 12-acetate for 48 hours. Then, the medium was changed back to regular THP-1 medium and cells were incubated for another 24 to 48 hours.

2.2 Methods: Stem Cell Culture

2.2.1 iPSC Origin

2.2.1.1 Origin of BJFF.6 iPSC

Stem cell line BJFF.6 was provided by Prof Gutmann's laboratory at Washington University in St Louis. BJFF.6 cells were derived from P6 foreskin fibroblasts from a healthy male at Washington University, the cell line been used in a publication by Chen et al., amongst others (Chen, 2018).

2.2.1.2 Origin of XMOO1 iPSC

XMOO1 cells (hPSCreg name: HMGUi001-A, BioSamples name: SAMEA5727779, Cellosaurus name: CVCL_WJ49, BIH name: BIHi043-A) were provided by the MDC Stem Cell Core Facility. They were initially produced by Institute of Diabetes and Regeneration Research (IDR) at Helmholtz Zentrum München. They were derived from a healthy Caucasian female's upper arm fibroblasts. The detailed generation and differentiation into pancreatic progenitor cells of this cell line have been described (Wang, 2018).

2.2.1.3 Thawing of iPSC

Flasks with stem cells frozen in Bambanker serum-free cell freezing medium (NIPPON Genetics Europe GmbH, Dueren, Germany, BB01) were gently swirled in a 37°C waterbath to thaw. Then, cells were added to 10 ml StemMACS iPS-Brew XF medium (Miltenyi, Bergisch Gladbach, Germany, 130-104-368), supplemented with 0,5 mM Thiazovivin (Stemcell Technologies, Vancouver, BC, Canada, 72254) at a ratio of 1:1000. Cells were centrifuged at 300 g for five minutes, then supernatant was removed and cells were resuspended in 2 ml StemMACS also supplemented with Thiazovivin. Then, the suspension was added to a 6-well plate coated with Geltrex (life technologies, Carlsbad, CA, USA, A14133-02) in a dropwise manner and incubated at 37°C and hypoxia.

2.2.1.4 iPSC culture

BJFF.6 stem cells were cultivated in 2 ml StemMACS iPS-Brew XF (Miltenyi, Bergisch Gladbach, Germany, 130-104-368). XMOO1 cells were cultivated in E8 medium, which is self-made by MDC stem cell core facility. E8 home supplements contain PBS (LifeTechnologies, Carlsbad, CA, USA, REF14190-144), sterile water (LifeTechnologies, Carlsbad, CA, USA, REF10977-035), L-ascorbic acid 2-phosphate (Sigmaaldrich, St Louis, MO, USA, A8960), Insulin, human Transferrin (Sigmaaldrich, St Louis, MO, USA, T375), sodium selenite (Sigmaaldrich, St Louis, MO, USA, S5261), FGF2 (Peprotech, Rocky Hill, NJ, USA, AF-100-18B) and TGFβ1 (Peprotech, Rocky Hill, NJ, USA, AF-100-21C). PH was adjusted with HCl (Roth, Karlsruhe, GER, 4625.1) and NaOH (Roth, Karlsruhe, GER, 8655.1). Stem cell media were renewed every other day. Stem cells were thawed and kept in culture for approximately three weeks and used for a number of differentiations.

2.2.1.5 Passaging of iPSC

Single cell passaging was performed when cells reached 60-70 % confluency. This usually was the case after two to seven days. Usually, a split ratio between 1:3 and 1:20 was chosen. In preparation of the split, wells were coated with Geltrex (life technologies, Carlsbad, CA, USA, A14133-02) diluted 1:100 in ice-cold DMEM-F12 (life technologies, Carlsbad, CA, USA, 41965062) and incubated at 37°C for at least 30 minutes. Cells were released from 6-well plates using 1 ml Accutase (Life technologies, Carlsbad, CA, USA, A11105-01) per well. After three minutes of

incubation at 37°C, their detachment was assessed under the microscope. If necessary, incubation time was prolonged, however, a maximal incubation time of nine minutes was not exceeded.

Once the cells were sufficiently detached, enzymatic activity of Accutase was stopped with 2 ml StemMACS iPS-Brew XF supplemented with Thiazovivin. Cells were resuspended with a serological pipette such as to reach a single cell suspension, then centrifuged at 300 g for five minutes. After centrifugation, medium supernatant was aspirated, cells were flipped and resuspended in 3 ml StemMACS supplemented with Thiazovivin using a 1000 µl pipette. Then, a fraction of the cell suspension according to selected split ratio was added to a Geltrex-coated well prefilled with 2 ml prewarmed StemMACS medium. Finally, cells were evenly distributed in the well by rocking the cell culture plate in a North-South and East-West motion and incubated at 37°C hypoxia.

2.2.1.6 Freezing of iPSC

Cells were frozen in Bambanker serum-free cell freezing medium (NIPPON Genetics Europe GmbH, Dueren, Germany, BB01) using Mr. Frosty™ Freezing Container (Thermo Fisher Sc., Waltham, MA, USA, 5100-0001) according to the manufacturer's instructions. Briefly, cells were released with 1 ml Accutase (life technologies, Carlsbad, CA, USA, A11105-01) per well of a 6-well plate and centrifuged at 300 g for five minutes, similar as to when they were passaged. Supernatant was removed, cells were flipped and slowly resuspended thrice in 1 ml Bambanker serum-free cell freezing medium with a 1000 µl pipette. Then, cells were counted in a 96-well plate with Trypan blue and Bambanker volume was adjusted in order to reach approximately one million cells in 1 ml per cryovial. Then, the Bambanker and cell solution was aliquoted into cryogenic vials (Corning, Corning, NY, USA, 430488) containing 1 ml each and the vials were stored at -80°C in Mr. Frosty™ Freezing Container overnight, then put in liquid nitrogen tanks for long-term storage.

2.3 Stem Cell Differentiation

2.3.1 Overview

Stem cells were differentiated to a microglial phenotype according to a protocol published by McQuade et al. (McQuade, 2018). Stem cell differentiation includes a first

step that consists of differentiation towards a CD34-positive hematopoietic progenitor cell (HPC) using Stemdiff Hematopoietic Kit (Stemcell Technologies, Vancouver, BC, Canada, 5310). Then, HPCs are directed towards a microglial phenotype in a specially composed maturation medium supplemented with the cytokines TGF- β 1, M-CSF and IL-34. For the last three days of differentiation, the cytokines CX3CL1 and CD200 are also added. Figure 1 summarizes the steps of iPSC differentiation. Stem cell differentiation was performed in Falcon® 6-well cell culture plates (Corning, Corning, NY, USA, 353046).

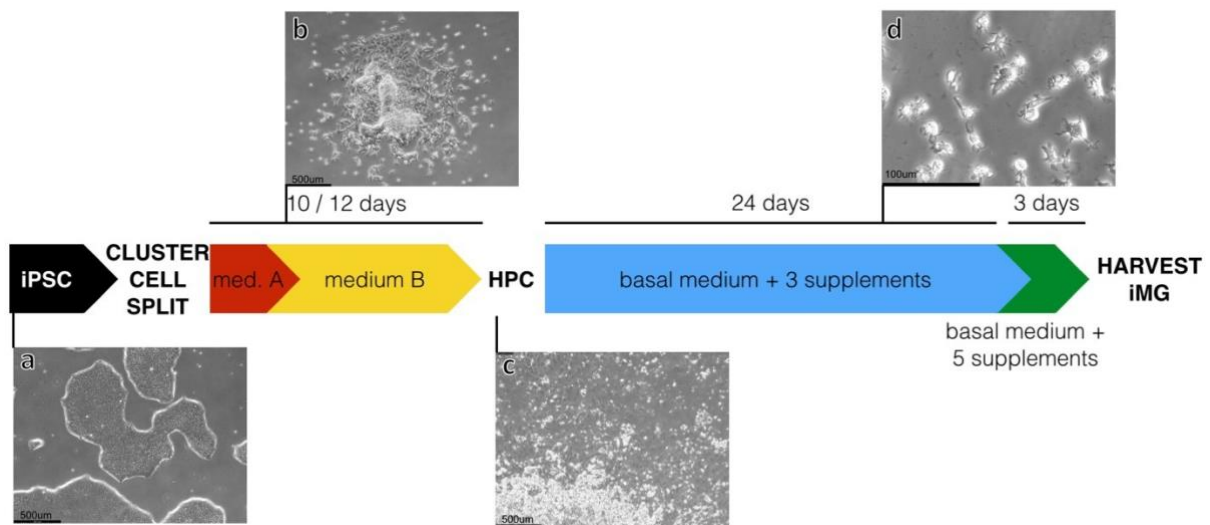


Figure 1 Summary of differentiation of iPSC towards a microglial phenotype. a: XMOO1 iPSC, the stem cell colonies are clearly demarcated, b: day 3 of HPC differentiation, the cell colonies popped and are no longer clearly demarcated, c: day 10 of HPC differentiation, HPCs are now visible as small, round and very light cells, d: day 10 of differentiation towards a microglial phenotype (day 20 or 22 overall), the cells are now larger, generally not clustered and show a delicate ramification.

2.3.2 Hematopoietic Differentiation

2.3.2.1 Clustersplit on Day -1

One day before the beginning of hematopoietic differentiation, a clustersplit was performed. Its aim was to obtain aggregates comprising about 100 iPSC with a diameter of 100-200 μ m, which were then seeded. For that, cell medium was removed and cells were exposed to a thin film of ReLeSR (Stem Cell Technologies, Vancouver, BC, Canada, 05872), then incubated at room temperature for a maximum of ten minutes. After onset of microscopically visible cell detachment, 1 ml of StemMACS iPS-Brew XF per well was added in order to stop the reaction. Cells were further detached mechanically by tapping the plate border for 30-60 seconds. Then, detached cell aggregates were resuspended with a 1000 μ l pipette till an aggregate size of

100-200 μm was reached. Aggregate counts were performed, cluster size and homogeneity were assessed. If necessary, resuspension was repeated. Otherwise, cell aggregates were plated at three to six different densities (e.g. 40, 60, 80 and 100 aggregates per well) into wells precoated with Geltrex and filled with 2 ml StemMACS iPS-Brew XF. Then, cells were further incubated at 37°C hypoxia.

2.3.2.2 Well Selection and Start of Hematopoietic Differentiation on Day 0

Thereafter, the well with optimal colony size and density was selected. A colony size between 150 and 250 μm was considered optimal, along with a density of 50-65 colonies per well, including at least 20 well-sized colonies. Also, differentiation was discontinued if the clusters were suspected to show differentiation, where one cluster was disproportionately large or the well contained plenty of small clusters. Disproportionally large or numerous undersized clusters may suppress growth of the other normal-sized clusters in a well. Medium in selected well was replaced by 2 ml medium A from Stemdiff Hematopoietic Kit (Stemcell Technologies, Vancouver, BC, Canada, 5310) and cells were incubated at 37°C normoxia from there on in.

2.3.2.3 Further Hematopoietic Differentiation

On Day 2 of hematopoietic differentiation (hence after 48 hours), 1 ml of medium A was replaced with fresh medium A. On Day 3, all of medium A was aspirated and replaced by 2 ml of medium B, also from Stemdiff Hematopoietic Kit (Stemcell Technologies, Vancouver, BC, Canada, 5310). On Days 5, 7 and 9, further 1 ml of medium B was added to each well.

2.3.2.4 HPC Harvest and Reseeding

On Days 10 and 12, the HPCs resulting from this step were collected. For that, supernatant was removed carefully without touching the well ground and resuspended thrice in a falcon. HPCs were counted with Trypan blue, centrifuged at 300 g for five minutes and 130'000 cells were replated into each Geltrex-precoated wells in a final volume of 2ml microglial differentiation medium (see below). At Day 10, supernatant resulting from centrifugation was added back to the well. Days 10 and 12 provide a first opportunity to assess differentiation quality and to estimate the number of cells that will be yielded from that particular differentiation.

2.3.3 Differentiation Towards a Microglial Phenotype

2.3.3.1 Microglial Differentiation Medium

Microglial differentiation medium was produced weekly by combining the following ingredients for 50 ml: 45,75 ml DMEM/F12 (Thermo Fisher Sc., Waltham, MA, USA, 11039-021), 1 ml Insulin-Transferrin-Selenium (ITS -G) (Thermo Fisher Sc., Waltham, MA, USA, 41400045), 2 ml serum free B27 (Thermo Fisher Sc., Waltham, MA, USA, 17504-044), 250 µl N2 supplement (Thermo Fisher Sc., Waltham, MA, USA, 17502048), 500 µl Glutamax (Thermo Fisher Sc., Waltham, MA, USA, 35050061), 1,731 µl Monothioglycerol (Sigmaaldrich, St Louis, MO, USA, MKCG1462), 25 µl Insulin (PromoCell, Heidelberg, Germany, C-52310) and 500 µl Non-essential amino acids (NEAA) (Thermo Fisher Sc., Waltham, MA, USA, 11140-035), see Table 1.

Table 1 Ingredients of iMGL basal medium as published by McQuade et al. (McQuade, 2018).

Ingredient	Amount in 50ml
DMEM-F12	45,75 ml
B27	2 ml
Non-Essential Amino Acids	0,5 ml
N2	0,25 ml
Insulin-Transferrin Selenite	1 ml
Glutamax	0,5 ml
Insulin	25 µl
Monothioglycerol	1,731 µl

2.3.3.2 Day 0 of Microglial Differentiation

Differentiation of HPCs towards a microglial phenotype predominantly occurs in a floating state. On day 0, 130'000 HPCs were plated in Falcon® 6-well cell culture plates (Corning, Corning, NY, USA, 353046) in 2 ml microglial differentiation medium.

2.3.3.3 Days 2, 4, 6, 8, 10, 14, 16, 18, 20, 22 and 24 of Microglial Differentiation

Immediately before each supplementation with fresh medium, microglial differentiation medium was supplemented with 100 ng/ml IL-34 (Peprotech, Rocky Hill, NJ, USA, 200-34-500), 50 ng/ml TGFβ1 (Peprotech, Rocky Hill, NJ, USA, 100-21C-250) and 25 ng/ml M-CSF (Peprotech, Rocky Hill, NJ, USA, 300-25-250) taken from single use aliquots. On days 2, 4, 6, 8, 10, 14, 16, 18, 20, 22 and 24 another ml of freshly supplemented differentiation medium was added to the wells.

2.3.3.4 Day 12 of Microglial Differentiation

On Day 12, 6 ml of differentiation medium were removed from the wells, leaving 1 ml behind. Then, the removed medium was centrifuged at 300 g for five minutes, supernatant was removed and the cells were resuspended in 1 ml of fresh differentiation medium and added back to the well.

2.3.3.5 Day 25 of Microglial Differentiation

On Day 25, all medium but 2 ml was collected and centrifuged at 300 g for five minutes. Supernatant was removed and cells were resuspended in 1 ml maturation medium, which contains 100 ng/ml CD200 (Novoprotein, Summit, NJ, USA, C311) and 100 ng/ml CXCL1 (Peprotech, Rocky Hill, NJ, USA, 300-31-250) in addition to the supplements of differentiation medium.

2.3.3.6 Day 27 of Microglial Differentiation

Finally, at Day 27 another 1 ml of maturation medium containing five supplements was added to the wells.

2.3.3.7 IMGL Harvest

Starting at Day 28, cells could be collected for functional assays or cultivated in maturation medium for one to two more weeks. At this point, the differentiation could be assessed a second time in terms of cell yield.

2.4 Basic Characterization of iMGL Derived from XMOO1 iPSC Cell Line

2.4.1 Upregulation of Microglia-Characteristic Gene Markers in Comparison to HPCs, THP-1 and U87 Cells Measured with Quantitative Polymerase Chain Reaction (qPCR)

2.4.1.1 iMGL Seeding

600'000 iMGL derived from three independent differentiations of XMOO1 iPSC were seeded in a 24-well plate overnight, in order to be harvested the next day.

2.4.1.2 Cell Harvest and RNA Isolation

The next day, supernatant was carefully removed and centrifuged for five minutes at 300 g. Meanwhile, 100 µl LBA-TG buffer from ReliaPrep™ ribonucleic acid (RNA) Cell Miniprep System (Promega, Fitchburg, USA) was added to the wells and cells were collected from the wellground with a cell scraper (Sarstedt, Nümbrecht, GER, 83.1832). Consecutively, supernatant from centrifuged eppitubes was carefully discarded and the remaining cell pellet was pooled with the cells from the wellground. THP-1 and U87 cells were harvested the same way. HPCs were harvested on Day 10 or 12 as indicated by our iPSC differentiation protocol, then centrifuged at 300 g for five minutes. Supernatant was discarded and cells were resuspended in LBA-TG. Afterwards, RNA was extracted using ReliaPrep™ RNA Cell Miniprep System and stored at -80°C.

2.4.1.3 Reverse Transcription

RNA purity and concentration were measured using NanoDrop 8000 spectrometer (Thermo Fisher Scientific, Schwerte, Germany). In the next step, RNA was converted to complementary DNA (cDNA) using PrimeScript RT Reagent Kit (Takara Bio Inc., Mountain View, California) following manufacturer's instructions. Briefly, RNA dilution with constant RNA concentrations were prepared, then mixed with Takara master mix containing oligo dT primers as well as random hexamers, a buffer and an enzyme mix.

2.4.1.4 QPCR

QPCR was performed with 7500 Fast Real-Time thermocycler (Applied Biosystems, Carlsbad, USA) using the SYBR Select Master Mix (Applied Biosystems, Carlsbad, USA). TATA-binding protein (TBP) was used as housekeeping gene. Used primers were:

- human P2RY12 forward	5'-CACTGCTCTACACTGTCCTGT-3',
- human P2RY12 reverse	5'-AGTGGTCCTGTTCCCAGTTTG-3',
- human SLC2A5 forward	5'-GAGGCTGACGCTTGTGCTT-3',
- human SLC2A5 reverse	5'-CCACGTTGTACCCATACTGGA-3',
- human TMEM119 forward	5'-GAGGAGGGACGGGAGGAG-3',
- human TMEM119 reverse	5'-CAGAAGGATGAGGAGGCTGG-3',
- human EMILIN2 forward	5'-GTGCGCCTACATCGTGAACA-3',
- human EMILIN2 reverse	5'-AGCACCTCCATTCCAAGTGTG-3',
- human HP forward	5'-CAGCACAGTCCCCGAAAAGAA-3',
- human HP reverse	5'-CAGTCGCATACCAGGTGTCC-3',
- human GDA forward	5'-GCTGGAAGTAGCATAGACCTGC-3',
- human GDA reverse	5'-TCTTCTGCAAAGTCGATGTTCTG-3',
- human SELL forward	5'-ACCCAGAGGGACTTATGGAAC-3'
- human SELL reverse	5'-GCAGAATCTTCTAGCCCTTTGC-3'

2.4.1.5 Statistical Analysis

Statistical analysis was done in GraphPad Prism (version 8.4.0 for MacOS, GraphPad Software, La Jolla California USA, www.graphpad.com). One-way ANOVA was done, along with Dunnett's multiple comparisons test.

2.4.2 Immunohistochemical Staining for Iba1, SLC2A5, TMEM119 and P2RY12

2.4.2.1 Immunohistochemical Staining

After regular iMGL harvest, cells were seeded on glass coverslips overnight, then stained. Three PBS washing steps, each of five minutes duration on a shaker were performed, then cells were fixed for 20 minutes in 4 % PFA and washed in PBS again. After permeabilization in tris-buffered saline (TBS) with 5 % donkey serum (DKS) and 0,1 % Triton, cells were incubated with primary antibodies on a shaker at 4°C overnight. Then, cells were washed thrice in TBS and incubated with a secondary antibody in TBS for two hours, as well as 4',6-diamidino-2-phenylindole (DAPI) 1:200 for nuclear staining. Coverslips were mounted on slides using Aqua Poly/Mount (Polysciences Inc., Warrington, USA) and placed at room temperature overnight protected from light, then stored at 4°C. Used Primary antibodies were goat anti-Iba1 (Abcam, Cambridge, UK, product code: ab5076) 1:600, rabbit anti-P2RY12 (Genetex, Irvine, CA, product code: GTX54796) 1:250, rabbit anti-TMEM119 (Abcam,

Cambridge, UK, product code: ab185333) 1:100 as well as mouse anti-SLC2A5 (Genetex, Irvine, CA, product code: ABIN1498473) 1:100. Secondary Alexa Fluor 647-conjugated antibodies were from either affine to goat (Dianova GmbH, Hamburg, Germany, product code: 705-605-147) 1:200, mouse (Dianova GmbH, Hamburg, Germany, product code: 715-605-151) 1:125 or rabbit (Dianova GmbH, Hamburg, Germany, product code: 711-605-152) 1:200, depending on primary antibody origin.

2.4.2.2 Confocal Microscopy

Microscopy was done using Carl Zeiss 710 Microscope (Carl Zeiss AG, Oberkochen, Germany) with 20X objective for counting of positively stained cells and 40X oil immersion objective for representative images.

2.4.2.3 Quantification

For quantification of cells that stained positive, nuclei and positively stained cells were counted independently by hand on at least five images with 20X magnification.

2.4.3 Proinflammatory Response to LPS Stimulations

2.4.3.1 IMLG Stimulation with LPS

For stimulation with LPS, 600'000 cells were seeded in a 24-well plate (Sarstedt, Nümbrecht, GER, 83.3922.500) in 50 % conditioned medium the cells had been differentiated in and 50 % fresh maturation medium with five supplements. The cells were incubated at normoxia overnight; on the following day the medium amount was adjusted and 1 µg/ml LPS (Enzo Life Sciences, ALX-581-007-L002) diluted in LAL water (InvivoGen, San Diego, CA, USA, h2olal-25) was added. Cells were then incubated at normoxia for six hours.

2.4.3.2 Cell Harvest, RNA Isolation and qPCR

Cells were harvested, RNA was isolated, rtPCR and qPCR were performed as described above. Primers used were:

- human TBP forward 5'-AGCGCAAGGGTTTCTGGTTT-3',
- human TBP reverse 5'-CTGAATAGGCTGTGGGGTCA-3',
- human IL-6 forward 5'-AACCTGAACCTTCCAAAGATGG-3',
- human IL-6 reverse 5'-TCTGGCTTGTTCCCTCACTACT-3',
- human TNF forward 5'-ATGAGCACTGAAAGCATGATCC-3',

- human TNF reverse 5'-GAGGGCTGATTAGAGAGAGGTC-3',
- human IL-10 forward 5'-TCAAGGCGCATGTGAACTCC-3',
- human IL-10 reverse 5'-GATGTCAAACCTCACTCATGGCT-3',
- human IL-1 forward 5'-CAGCTACGAATCTCCGACCAC-3',
- human IL-1 reverse 5'-GGCAGGGAACCAGCATCTTC-3',
- human TGF-1 forward 5'-CAATTCCTGGCGATACCTCAG-3',
- human TGF-1 reverse 5'-GCACAACTCCGGTGACATCAA-3'

2.4.3.3 Statistical Analysis

Statistical analysis was done in GraphPad Prism (version 8.4.0 for MacOS, GraphPad Software, La Jolla California USA, www.graphpad.com), using a two-tailed ratio paired t-test.

2.5 Migration Assay

2.5.1 Migration of XMOO1 iPSC-Derived iMGL

Cell migration was assessed using IncuCyte® Cell Migration kit (Sartorius, Göttingen, GER).

2.5.1.1 Cell Seeding

100'000 iMGL were seeded in a 96-well ImageLock™ plate (Sartorius, Göttingen, GER, ref. nr. 4806) in the 50 % conditioned medium the iMGL had previously been differentiated in and 50 % fresh medium with five supplements (M-CSF, TGF-β1, IL-34, CX3CL1, CD200) and left to adhere for four hours. Conditions were performed at least in duplicates.

2.5.1.2 Scratching and Scanning

Next, scratches were made in all wells simultaneously with WoundMaker™ (Sartorius, Göttingen, GER). The plates were then placed into IncuCyte Zoom® device (Sartorius, Göttingen, GER) where an image was taken every hour over a total of 48 hours at a 4X magnification. Selected scan type was “scratch wound”.

2.5.1.3 Analysis

For analysis, scratch wound analysis tool from IncuCyte Zoom® software was used. It computes a cell mask based on contrasts. To set optimal analysis parameters, for each

experiment image collections of three to five representative images of wells from $t = 0$ and $t = 24$ hours were created. Then, a new processing definition was set by adjusting the segmentation bias between 1,7 and 1,9 and setting a minimal object area of $500 \mu\text{m}^2$. Scratch wound mask was computed by determining the cell-free area at $t = 0$. Then, the proportion of scratch wound surface covered by migrating cells was determined for each timepoint. This metric in % is called “confluency”. For analysis, the confluency values were normalized to 0 % confluency at $t = 0$.

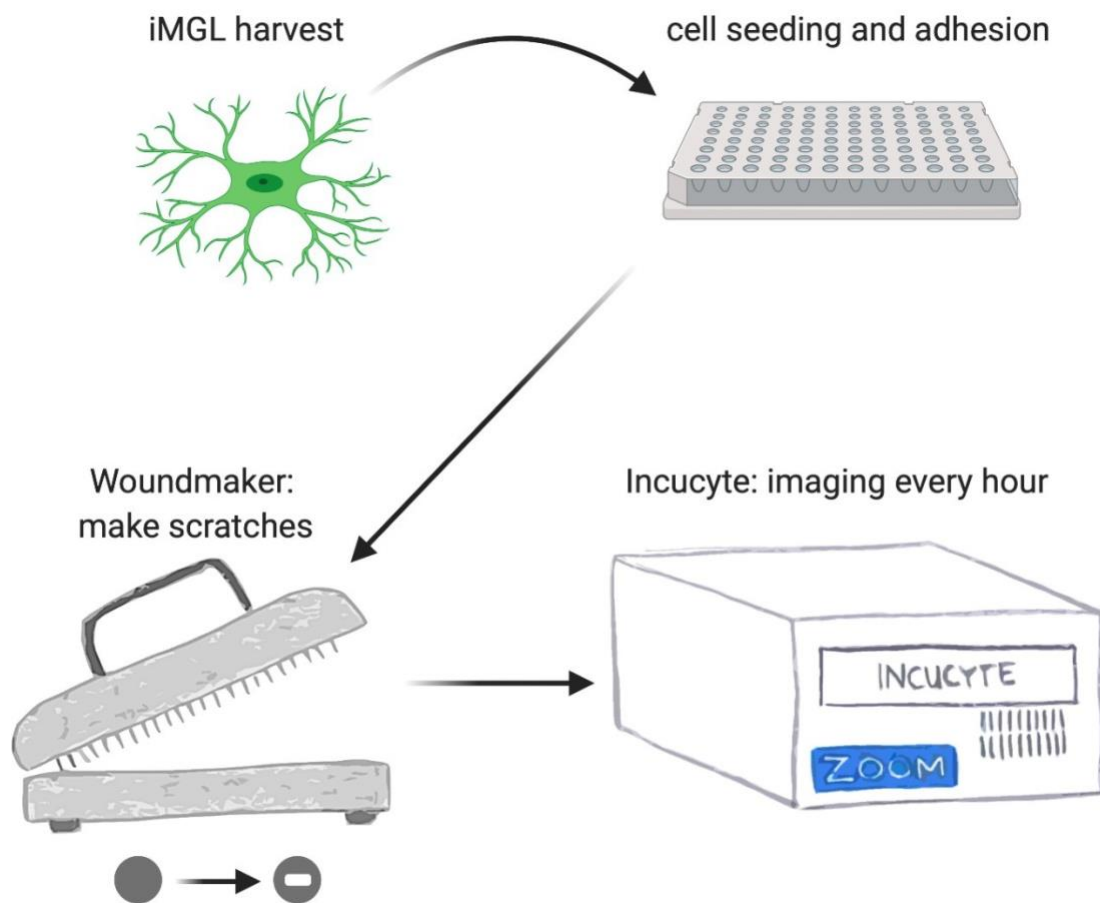


Figure 2 Workflow of the scratch wound assay done for this project. Briefly, iMGL were harvested onto a 96-well ImageLock™ plate (Sartorius, Göttingen, GER, ref. nr. 4806) and left to adhere for 4 hours. Then, identical scratches were made in all wells using WoundMaker™ (Sartorius, Göttingen, GER) and plates were set in the incucyte, where images were made every hour for 48 hours. Created with BioRender.com.

2.6 Phagocytosis Assay

2.6.1 Phagocytosis of Carboxylate Beads by iMGL

2.6.1.1 Cell Seeding

iMGL were seeded in a 24-well plate (Sarstedt, Nümbrecht, GER, 83.3922.500) and incubated overnight at 37°C normoxia.

2.6.1.2 Incubation with Carboxylate Microspheres

3.0 nm Fluoresbrite® carboxylate microspheres (Polysciences Inc., Warrington, USA) with a yellow-green emission maximum at 486 nm and an excitation maximum of 441 nm were resuspended in FBS, shaken, centrifuged and resuspended in 10 µl PBS and added directly to medium of iMGL. If necessary, stimulants were added along with the beads, namely 5 µg/ml cytochalasin D (Sigmaaldrich, St Louis, MO, USA, C2618) or 100 µmol/l uridine diphosphate (UDP) (Abcam, Cambridge, UK, product code: ab120383). Thereafter, microglia and beads were incubated for 45 minutes at 37°C normoxia.

2.6.1.3 Cell Staining

Cells were then washed off the well bottom and centrifuged at 300 g for five minutes. Meanwhile, anti-CD11b PE-Cy7 conjugated monoclonal antibody (Invitrogen, Carlsbad, CA, USA, ref. nr. 25-0112.82) was added to flow medium consisting of PBS and 2 % FBS at a 1:50 concentration. After centrifugation, cell supernatant was discarded and replaced with 50 µl flow medium with antibody. Cells were dissolved by resuspension, then incubated with anti-CD11b antibody in flow medium for ten minutes at 4°C. Then, 400 µl of flow medium was added to the suspension and another centrifugation at 300 g for five minutes was carried out. Supernatant was again discarded and replaced with 300 µl flow medium. Then, cells and medium were filtered into a FACS tube (Corning, Corning, NY, USA, 352235).

2.6.1.4 Flow Cytometry

Cell sorting was done using FACSAria™ II (BD, Franklin Lakes, NJ, USA), flow cytometry with LSRFortessa™ (BD, Franklin Lakes, NJ, USA). Unstained cells only, stained cells only, and also beads only were used as negative controls. Propidium iodide (PI) (Sigmaaldrich, St Louis, MO, USA, P4170) was used as a viability marker.

2.6.1.5 Analysis

Analysis was done using FlowJo™ (version 10.6.1, Becton Dickinson, Ashland, OR). To estimate the number of beads phagocytosed per cell, mean intensity in the B-530_30-A channel of PI negative and PE-Cy7 positive cells and of PI negative, PE-Cy7 positive and B-530_30-A positive cells (i.e. of cells, that had phagocytosed) was computed and exported from FlowJo™. Then, to obtain an estimate of phagocytosed beads per cell, the mean intensity per cell was divided by the approximate intensity of one bead.

2.6.1.6 Statistical Analysis

Statistics were done in GraphPad Prism (version 8.4.0 for MacOS, GraphPad Software, La Jolla California USA, www.graphpad.com) with two-tailed ratio paired t-test.

2.7 Co-Cultivation Experiments

2.7.1 Co-Cultivation of iMGL with glioma Cells

Following their harvest, iMGL were co-cultivated with glioma cell lines U87, U251MG and LN229 for 72 and 144 hours.

2.7.1.1 Day -1

On Day 1, 250'000 iMGL were seeded in a 24-well plate in 500 µl medium, consisting of 50 % iMGL maturation medium with five supplements and 50 % iMGL conditioned medium the cells had previously been cultivated in. On the same day, 50'000 glioma cells were seeded in a 24-well transwell insert (Sarstedt, Nümbrecht, GER, 83.3932.041).

2.7.1.2 Day 0

On Day 0, the transwell inserts were set into the wells containing iMGL. 100 µl unconditioned DMEM complete was added into the control transwell inserts that did not contain glioma cells.

2.7.1.3 Days 1, 3 and 5

Then, on Days 1, 3 and 5 150 µl differentiation medium containing three supplements was added to the iMGL. Co-cultures were kept at normoxia.

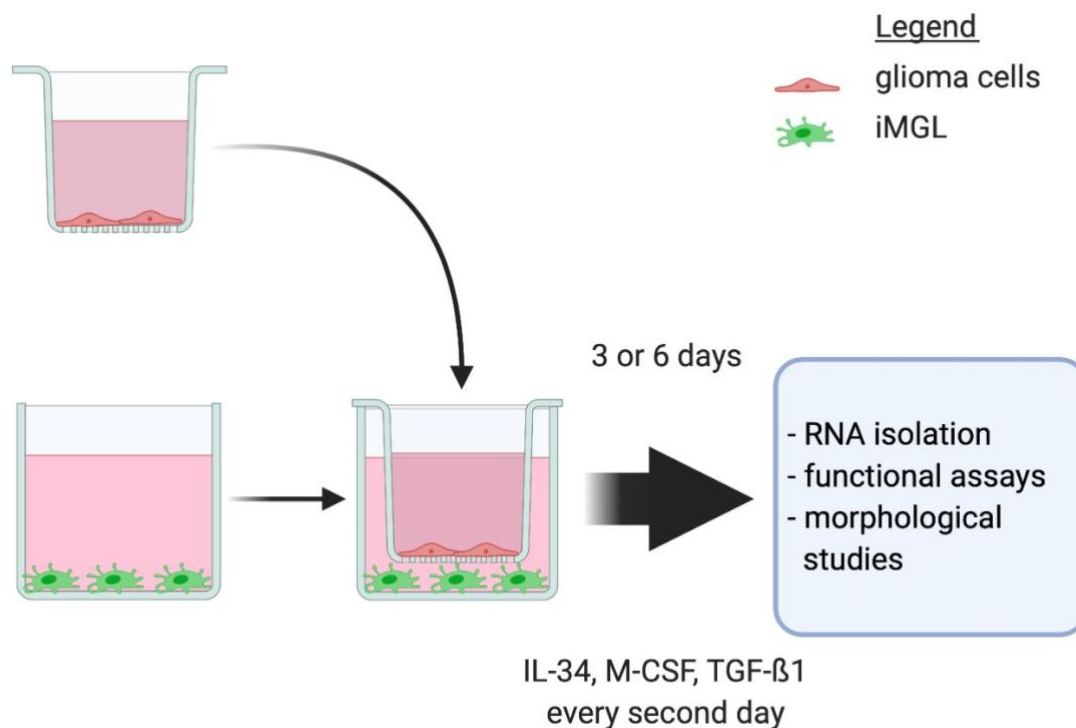


Figure 3 Schematic description of co-cultivation protocol. On Day 1, iMGL were seeded on the ground of 24-well plates, glioma cells were seeded into transwell inserts (Sarstedt, Nümbrecht, GER, 83.3932.041). On Day 0, transwell inserts were hung into the wells and iMGL were hence co-cultivated with glioma cells for three or six days, adding the three protein supplements M-CSF, IL-34 and TGF-β1 every other day. After co-cultivation, iMGL were harvested and used for RNA isolation, functional assays or morphological studies. Created with BioRender.com.

2.7.2 Gene Expression Analysis for GAM-Characteristic Genes

2.7.2.1 Cell Harvest, RNA Isolation, Reverse Transcription, qPCR

After 72 or 144 hours of co-culture, transwell inserts containing glioma cells were removed and iMGL RNA was harvested as described above. After that, RNA purity was measured and RNA was converted to cDNA as described above. QPCR was again performed with 7500 Fast Real-Time thermocycler (Applied Biosystems, Carlsbad, USA) utilizing SYBR Select Master Mix (Applied Biosystems, Carlsbad, USA). TBP was selected as a housekeeping gene. Sequences of used primers applied were:

- human forward TBP 5'-AGCGCAAGGGTTTCTGGTTT-3',
- human reverse TBP 5'-CTGAATAGGCTGTGGGGTCA-3',

- human IL-6 forward 5'-AACCTGAACCTTCCAAAGATGG-3',
- human IL-6 reverse 5'-TCTGGCTTGTTCCCTCACTACT-3',
- human GPNMB forward 5'- TGCGGTGAACCTGATATTCCC -3',
- human GPNMB reverse 5'- GTCCTCTGACCATGCTGTCC -3',
- human forward SPP1 5'-CTCCATTGACTCGAACGACTC-3',
- human reverse SPP1 5'-CAGGTCTGCGAACTTCTTAGAT-3',
- human forward TGM2 5'-CGTGACCAACTACAACCTCGG-3',
- human reverse TGM2 5'-CATCCACGACTCCACCCAG-3'

2.7.2.2 Statistical Analysis

Statistical analysis was carried out in GraphPad Prism (version 8.4.0 for MacOS, GraphPad Software, La Jolla California USA, www.graphpad.com) with two-tailed ratio paired t-test.

2.7.3 Morphologic Analysis of iMGL Co-Cultivated with Glioma Cells

2.7.3.1 Cell Seeding and Co-Cultivation

For morphological measurements, 50'000 iMGL were seeded on glass coverslips on Day 1 of co-cultivation. After leaving them to adhere for 15 minutes, co-cultivation was performed as described above.

2.7.3.2 Immunohistochemical Staining

After 72 and 144 hours, transwell inserts were removed and cells were stained. For this, cells were washed thrice on a shaker for five minutes in PBS with pH 7,4, fixed with 4 % PFA for 20 minutes, then washed with PBS three times again. Thereafter, cells were permeabilized in TBS, with 5 % donkey serum (DKS) and 0,1 % Triton and incubated with goat anti-Iba1 (Abcam, Cambridge, UK, product code: ab5076) 1:600 in TBS and 5 % DKS on a shaker at 4°C overnight. The next day, cells were washed thrice for five minutes on a shaker with TBS and incubated with secondary antibodies donkey anti-goat Alexa Fluor 647 (Dianova GmbH, Hamburg, Germany, product code: 711-545-152) 1:200 in TBS for two hours, as well as DAPI 1:200 for nuclear staining. Coverslips were mounted on slides using Aqua Poly/Mount (Polysciences Inc., Warrington, USA) and stored overnight protected from light at 4°C.

2.7.3.3 Confocal Microscopy

Microscopy was performed using Zeiss 710 confocal microscope with a 63X oil immersion objective using Zen 2.1 software (Carl Zeiss AG, Oberkochen, Germany). For quantitative analysis, TCS SPE microscope from Leica was used (Leica Microsystems GmbH, Wetzlar, GER). 20X objective was used along with z-stacks (step size 1 μm , 30 steps) as well as 405 and 635 nm lasers.

2.7.3.4 Quantification of Morphology

Cell morphology was analyzed using Imaris 9.2 software (Bitplane, Zurich, Switzerland). FindCells function based on cell nuclei and Iba1 staining was used to identify cells. All images were analyzed using batch function, in order to ensure a consistent analysis. Then, for each cell respective volume, nucleus to cytoplasm volume ratio and sphericity ψ as defined by Wadell in 1935 was issued. Sphericity is the ratio of the surface area of a sphere with the examined object's volume divided by the examined object's actual surface area.

$$\psi = \frac{\pi^{\frac{1}{3}} (6V)^{\frac{2}{3}}}{A}$$

ψ : Sphericity

V: Particle volume

A: Particle area

2.7.3.5 Statistical Analysis

The obtained values of morphology were analyzed in GraphPad Prism (version 8.4.0 for MacOS, GraphPad Software, La Jolla California USA, www.graphpad.com) using a two-tailed unpaired t-test. For each distinct iPSC differentiation and co-cultivation, the average morphological parameters were computed and considered as one sample in statistical analysis. However, for clearer and more intuitive data representation, a representative subset of morphological data from single cells was plotted in Figure 23, Figure 24 and Figure 25.

2.8 Direct Co-Cultivation Experiments

2.8.1 Direct Co-Cultivation of BJFF.6 iMGL and U87 mCherry

2.8.1.1 Cell Seeding and Co-Cultivation

For direct co-cultivation, 50'000 U87 (ECACC, Porton Down, UK, 89081402) were seeded on glass coverslips placed in 24-well plates (Sarstedt, Nümbrecht, GER, 83.3922.500) in DMEM complete containing DMEM (Life Technologies, Carlsbad, USA, 41965062), 10 % Pierce™ Bovine Serum (Life Technologies, Carlsbad, USA, 23209) and 1 % Penicillin-Streptomycin-Glutamine (Life Technologies, Carlsbad, USA, 10378016). Next, 20'000 iMGL were seeded on top of glioma cells and directly on coverslips for control in 50 % conditioned medium the cells had been differentiated in, and 50 % maturation medium containing M-CSF, IL-34, TGF-β1, CX3CR1 and CD200 in the concentrations noted above, supplemented with 10 % Pierce™ Bovine Serum (Life Technologies, Carlsbad, USA, 23209) and 1 % Penicillin-Streptomycin-Glutamine (Life Technologies, Carlsbad, USA, 10378016). Cells were co-cultivated for 48 hours at 37°C normoxia.

2.8.1.2 Immunohistochemical Staining

Cells were stained as described using two antibody combinations. On the one hand, goat anti-human GPNMB (R&D Systems, Minneapolis, MN, USA, product code: AF2550) 1:100 and rabbit anti-human Iba1 (Abcam, Cambridge, UK, product code: ab178847) 1:600 were used as primary antibodies and donkey anti-goat Alexa Fluor 488 (Dianova GmbH, Hamburg, Germany, product code: 705-545-147) 1:200 in addition to donkey anti-goat Alexa Fluor 647 (Dianova GmbH, Hamburg, Germany, product code: 711-605-152) 1:200 were used as secondary antibodies. On the other hand, anti-human SPP1 (Abcam, Cambridge, UK, product code: ab195541) 1:50 and anti-human Iba1 (Abcam, Cambridge, UK, product code: ab5076) 1:600 were used as primary antibodies; secondary antibodies were donkey anti-rabbit Alexa Fluor 488 (Dianova GmbH, Hamburg, Germany, product code: 711-605-152) 1:200 and donkey anti-goat Alexa Fluor 647 (Dianova GmbH, Hamburg, Germany, product code: 711-605-152) 1:200. In both cases, DAPI 1:600 was used as nuclear staining.

2.8.1.3 Confocal Microscopy

Microscopy was carried out using Zeiss 710 confocal microscope with 20X objective (Carl Zeiss AG, Oberkochen, Germany) and z-stack acquisition (step size 1µm, 30

steps). 405, 488, 561 and 633 nm lasers were used. At least three images per coverslip were taken.

2.8.1.4 Quantification of GPNMB and SPP1 Intensity and Statistical Analysis

Analysis was conducted using Imaris 9.2 software (Bitplane, Zurich, Switzerland). Batch analysis was done to ensure that all images were analyzed the same. Strongly Iba1-positive sections, which likely correspond to microglia, were rendered as surfaces. Cells with high mCherry expression, which more likely correspond to glioma cells, were excluded. Then, the sum of intensity on channel 4 (corresponding to AF488, labelling anti-GPNMB or anti-SPP1) inside the surfaces and the volume of surfaces was extracted from the statistics on computed surfaces. For each experiment, mean surface intensity per μm^3 was computed using R (Version 1.1.447 for MacOS, RStudio Team, Boston, MA, USA, <http://www.rstudio.com/>). Finally, a two-tailed ratio paired t-test was performed in GraphPad Prism (version 8.4.0 for MacOS, GraphPad Software, La Jolla California USA, www.graphpad.com).

2.8.1.5 Quantification of Morphology

Morphological analysis of cell volume and sphericity was based on Iba1-positive surfaces determined as described above (see 2.8.1.4). CSV files issued by Imaris 9.2 software (Bitplane, Zurich, Switzerland) were opened in Microsoft Excel Version 16.37 (Microsoft Corporation, Redmond, WA, USA). Surfaces with an XY distance to image border less than $2\ \mu\text{m}$ were excluded from analysis, as well as surfaces with a volume smaller than $100\ \mu\text{m}^3$, since these were likely debris. For each experiment, mean cell volume and sphericity was computed. Sphericity as defined by Wadell was used. For a detailed definition of this, please refer to section 2.7.3.4. A large value for sphericity indicates that the examined object is nearly spherical.

2.8.1.6 Statistical Analysis

Obtained values were analyzed in GraphPad Prism (version 8.4.0 for MacOS, GraphPad Software, La Jolla California USA, www.graphpad.com) using a two-tailed ratio paired t-test. Average morphological parameters computed for each distinct co-cultivation were considered as one sample in statistical analysis. Nevertheless, data points plotted in Figure 34 correspond to morphological data of a subset of representative cells.

- human reverse MMP14 5'-GATGGCCGCTGAGAGTGAC-3'

For primers of TBP, IL6, IL-1 β , IL10, TNFa, SPP1, GPNMB and TGM2 see above.

2.9.1.4 Statistical Analysis

For statistical analysis, GraphPad Prism (version 8.4.0 for MacOS, GraphPad Software, La Jolla California USA, www.graphpad.com) was selected. A two-tailed ratio paired t-test was used.

2.10 Statistical Analysis

In this thesis, the following statistical tests were applied: a one-way ANOVA followed by Dunnett's multiple comparisons test, a two-tailed ratio paired t-test and two-tailed unpaired t-test. The significance level or alpha was set two-sided at 0.05. Due to the explorative character of this work, no p-value adaptation was done for Dunnett's multiple comparisons test, which followed ANOVA or for t-tests. As already mentioned, GraphPad Prism (version 8.4.0 for MacOS, GraphPad Software, La Jolla California USA, www.graphpad.com) was used for statistical analysis in this thesis.

In this thesis, significance levels were used as is common in this field and as issued by GraphPad Prism (version 8.4.0 for MacOS, GraphPad Software, La Jolla California USA, www.graphpad.com):

Table 2 Annotation of significance levels as used in this thesis.

Symbol	Meaning
ns	$P > 0.05$
*	$P \leq 0.05$
**	$P \leq 0.01$
***	$P \leq 0.001$
****	$P \leq 0.0001$

3. Results

3.1 Basic Characterization of iMGL Derived from XMOO1 iPSC Cell Line

3.1.1 XMOO1-Derived iMGL Upregulate Microglia-Characteristic Genes P2RY12, SLC2A5 and TMEM119 Compared to HPCs, THP-1 and U87

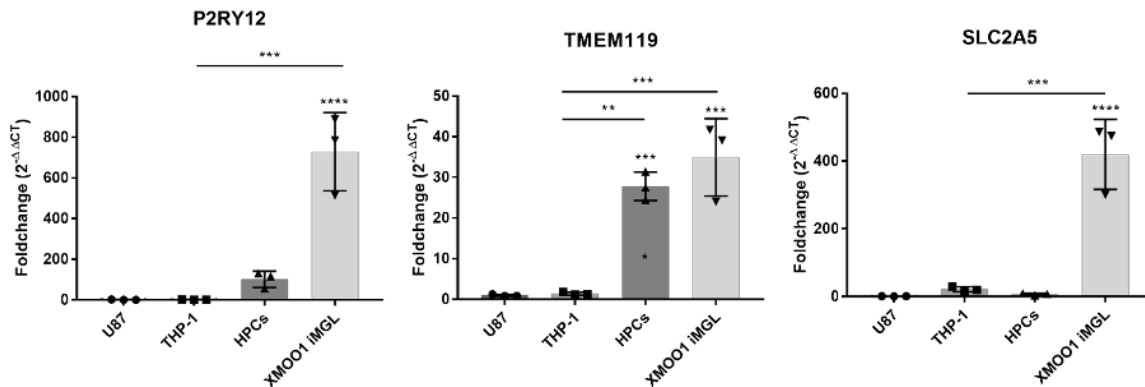


Figure 4 Gene expression of microglial signature genes P2RY12, TMEM119 and SLC2A5 in U87, THP-1, XMOO1 HPC and XMOO1 iMGL cells. Genes expression was quantified as fold-change compared to miscellaneous U87 glioma cells. P2RY12, TMEM119 and SLC2A5 are significantly upregulated in XMOO1 iMGL compared to U87 and THP-1. Furthermore, TMEM119 is also significantly upregulated in HPCs compared to U87 and THP-1 cells. For statistical analysis, one-way ANOVA followed by Dunnett's multiple comparisons test was used.

All of the three investigated microglia-characteristic genes were significantly upregulated in iMGL in comparison to U87 (P2RY12: $p < 0.0001$, TMEM119: $p = 0.0001$, SLC2A5: $p < 0.0001$). Also, they were upregulated in iMGL in comparison to THP-1 (P2RY12: $p = 0.0004$, TMEM119: $p = 0.0008$, SLC2A5: $p = 0.0004$). TMEM119 was upregulated in HPCs compared to U87 ($p = 0.0005$) and to THP-1 ($p = 0.0027$).

In comparison to U87, iMGL displayed a 729-fold expression of P2RY12, a 419.96-fold expression of SLC2A5 and a 34.94-fold expression of TMEM119. HPCs, the progenitors of iMGL in our differentiation protocol, displayed a 101.76-fold expression of P2RY12, a 7.3-fold expression of SLC2A5 and a 32.27-fold expression of TMEM119. THP-1 had a 0.99-fold expression of P2RY12, a 21.74-fold expression of SLC2A5 and a 1.4-fold expression of TMEM119.

3.1.2 XMOO1-Derived iMGL Do Not Upregulate Monocyte-Characteristic Genes Compared to HPCs, THP-1 and U87

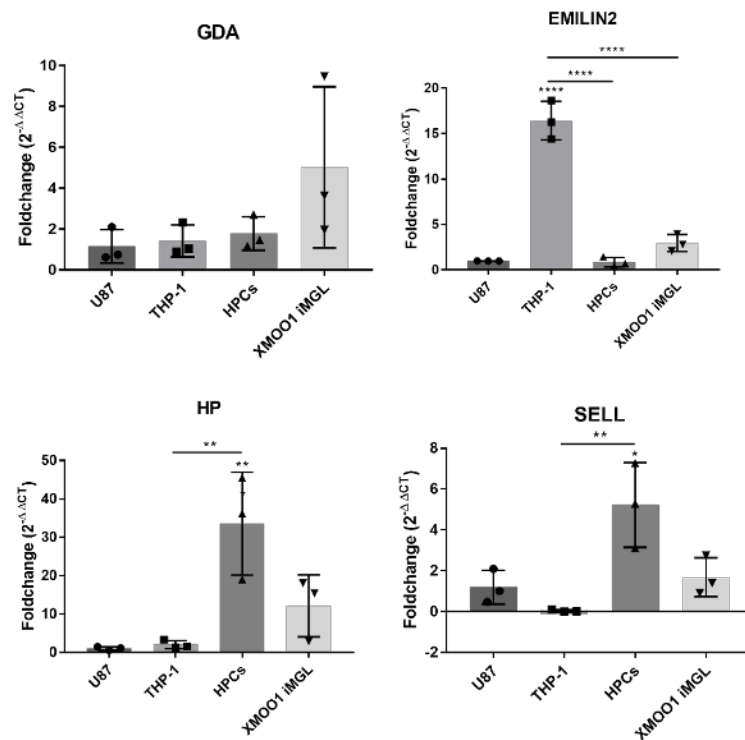


Figure 5 Gene expression of monocytic signature genes GDA, EMILIN2, HP and SELL in U87, THP-1, HPC and XMOO1 iMGL cells. iMGL do not show an upregulation of any of these genes compared to the other cell types. EMILIN2 is strongly upregulated in THP-1, HPCs strongly express HP and SELL compared to the other cell types. For statistical analysis, one-way ANOVA followed by Dunnett's multiple comparisons test was used.

EMILIN2 was upregulated in THP-1 significantly compared to iMGL ($p < 0.0001$), U87 ($p < 0.0001$) and HPCs ($p < 0.0001$). THP-1 displayed a 16.45-fold expression to U87, whereas iMGL displayed a 2.97-fold higher expression compared to U87. For GDA, there were no significant differences in gene expression between U87, THP-1, HPCs and iMGL.

HP was significantly upregulated in HPCs compared to U87 ($p = 0.0025$) and THP-1 ($p = 0.0095$), but not in iMGL. iMGL had a 12.14-fold higher HP expression than U87.

SELL was also significantly upregulated in HPCs compared to U87 ($p = 0.0093$) and THP-1 ($p = 0.0053$), but not in iMGL. iMGL had a 1.68-fold higher HP expression than U87. iMGL had a 1.68-fold expression of SELL compared to U87.

3.1.3 Immunohistochemical Staining of iMGL Derived from XMOO1 iPSC Cell Line for Iba1, SLC2A5, TMEM119 and P2RY12

XMOO1-derived iMGL exhibit a microglia-characteristic morphology, including a clear, oftentimes bipolar ramification, mostly central nuclei and little cell clustering.

99 % of depicted XMOO1 iMGL stained positive for Iba1, 97 % for SLC2A5, 99.2 % for TMEM119 and 87 % for P2RY12 (Figure 6).

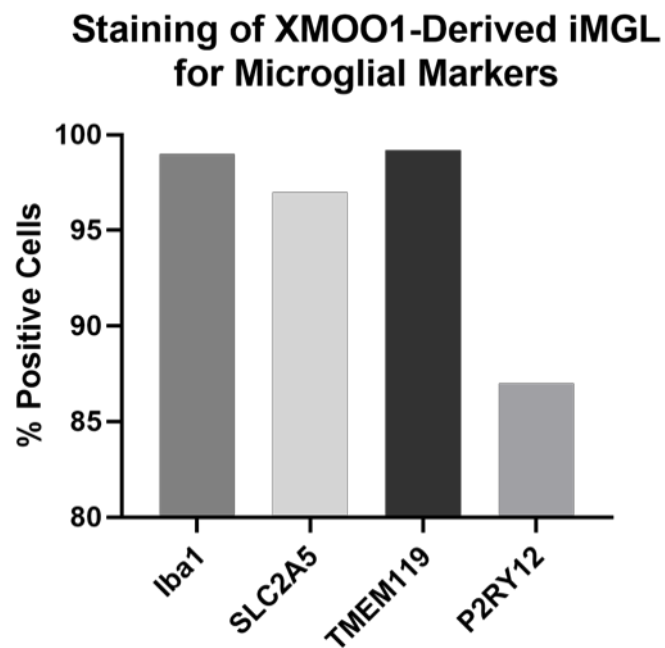


Figure 6 Staining of XMOO1-derived iMGL for canonical microglial markers Iba1, SLC2A5, TMEM119 and P2RY12. 99 % of cells were positive for Iba1, 97 % for SLC2A5, 99.2 % for TMEM119 and 87 % for P2RY12. Cells were counted by hand.

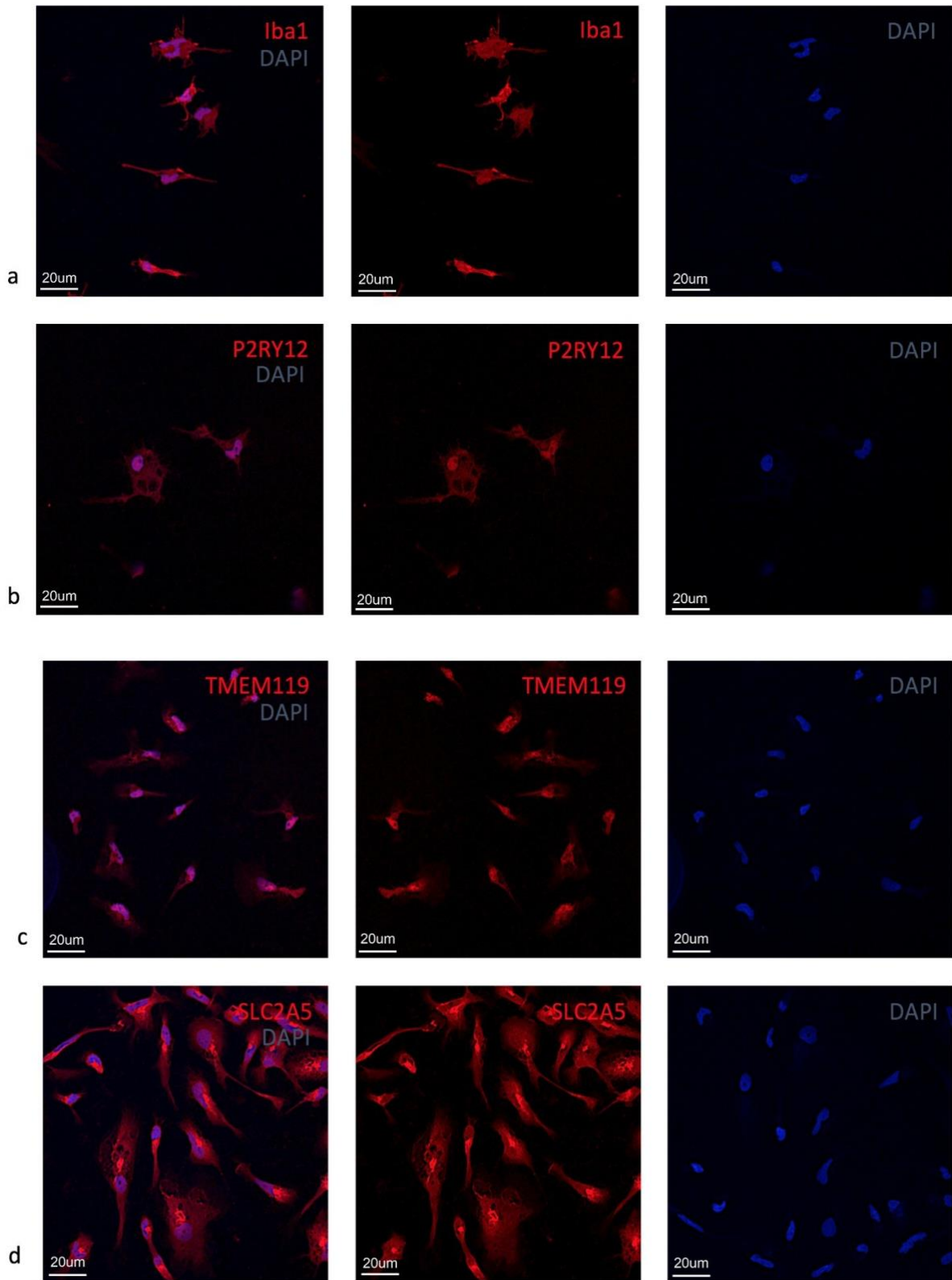


Figure 7 Staining of XMOO1 iMGL for (a) Iba1, (b) P2RY12, (c) TMEM119 and (d) SLC2A5. Staining was done in triplicates at least. Cells that stained positive were quantified by independently counting stained nuclei and cells on at least 5 images with 20X magnification. 99 % of iMGL stained positive for Iba1, 97 % stained positive for SLC2A5, 99.2 % for TMEM119 and 87 % for P2RY12.

3.1.4 XMOO1 iMGL Upregulate Proinflammatory Genes Upon LPS Stimulation

Proinflammatory Gene Expression after 6h LPS Stimulation

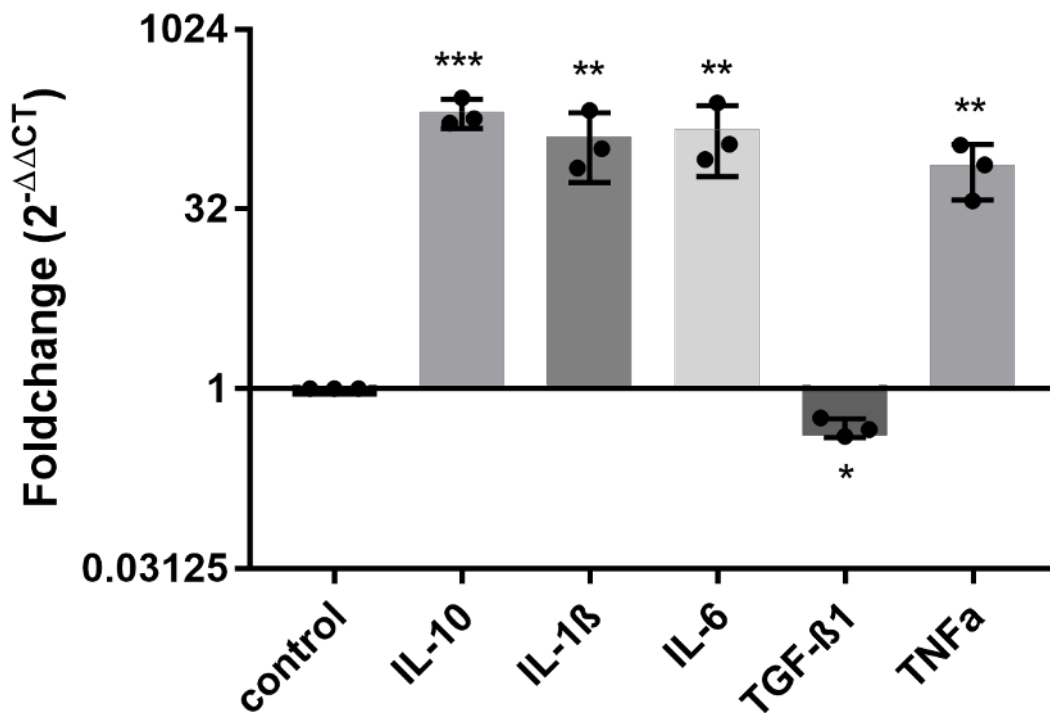


Figure 8 Genes upregulated by XMOO1 iMGL upon stimulation with LPS for six hours. The typically upregulated genes are expressed at a significantly higher level, whereas TGF-β1, which is normally downregulated by inflammation, is significantly less-expressed upon LPS stimulation. For statistical analysis, a two-tailed ratio paired t-test was performed.

Upon stimulation with LPS, XMOO1 iMGL showed significant upregulation of IL-10 ($p = 0.0008$, $t = 35.18$), IL-1β ($p = 0.0047$, $t = 14.57$), IL-6 ($p = 0.0044$, $t = 15.06$) and TNFα ($p = 0.0055$, $t = 13.42$), whereas TGF-β1 was significantly downregulated ($p = 0.0184$, $t = 7.265$). On average, there was a 208.47-fold change of IL-10, 129.31-fold change of IL-1β, 147.93-fold change of IL-6, 0.48-fold change of TGF-β1 and a 74.36-fold change of TNFα.

3.1.5 Migration

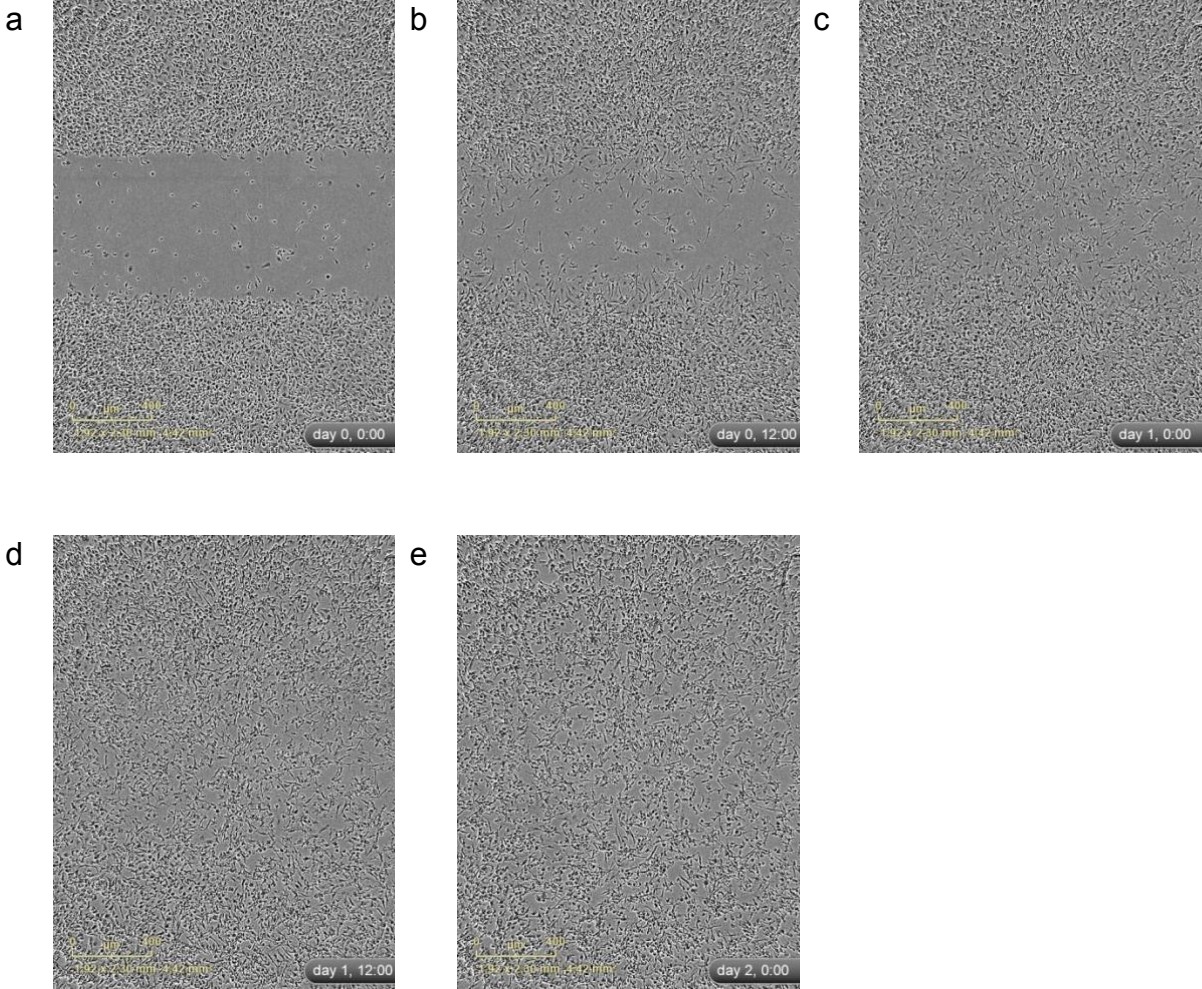


Figure 9 Scratch wound over a time range of 48 hours, images were taken every 12 hours. At $t = 0$, a clearly demarcated scratch wound is still visible (a). Then, cells migrate into the scratch (b, c, d), resulting in a nearly homogenous cell distribution after 48 hours (e).

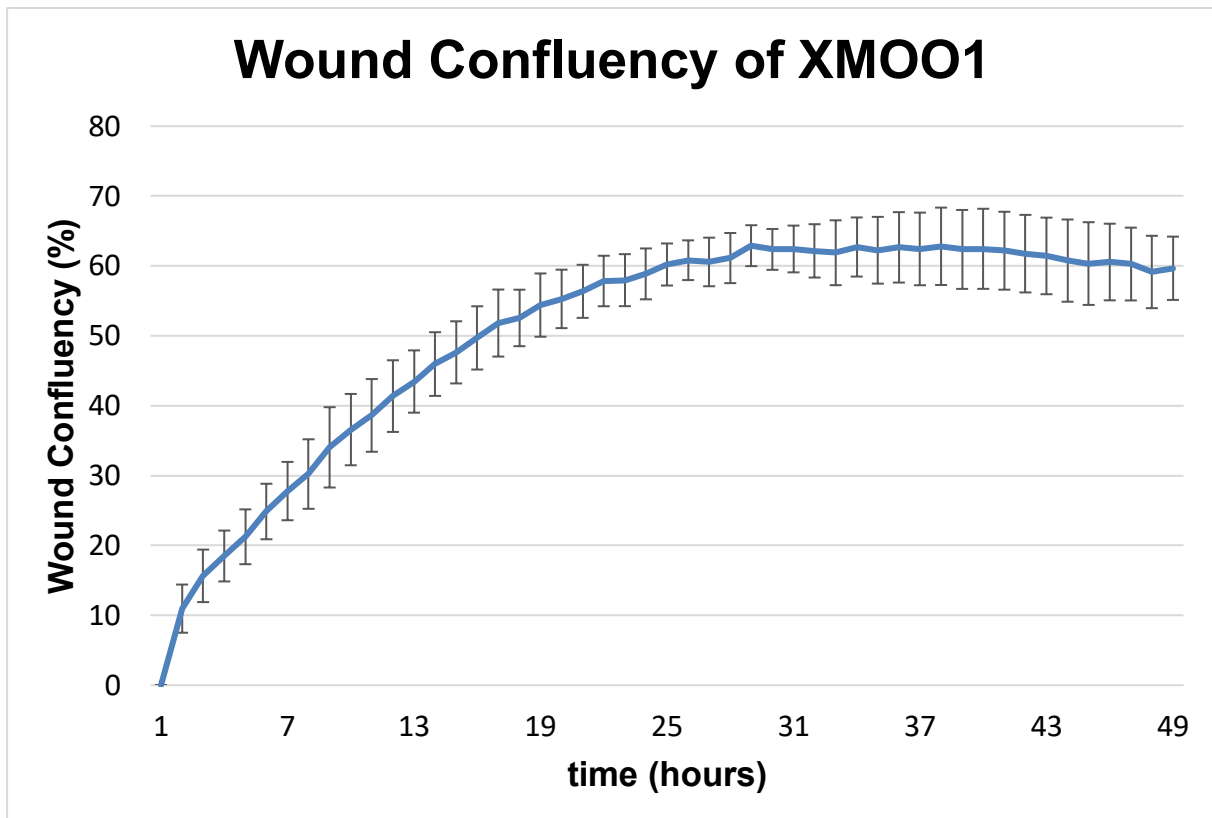


Figure 10 Wound confluency of XMOO1 iMGL in a Woundmaker™-based scratch assay as calculated by IncuCyte Zoom® software (Sartorius, Göttingen, GER) for a total time of 48 hours. Images were taken on an hourly basis. For analysis, a contrast-based cell mask was computed and the scratch wound mask was defined as cell-free area at $t = 0$. Confluency, the percentage of scratch wound mask area covered by cells, was then computed for each timepoint. The resulting growth curve is logarithmic and reaches its maximum after about 28 hours at approximately 62 % confluency.

Over the course of 48 hours, XMOO1 iMGL migrate into a standardized scratch wound produced by Woundmaker™ (Sartorius, Göttingen, GER), until the cells are nearly homogeneously distributed (Figure 9). Here, we used the metric confluency to quantify the migration of cells into the scratch wound. Confluency is defined as the percentage of area covered by cells within a scratch wound area. Scratch wound area is defined as cell-free area at $t = 0$. The average confluency for our scratch assay experiments using XMOO1 iMGL is graphed in Figure 10. Evidently, cell migration into scratch wound follows the pattern of logarithmic growth. After about 28 hours, the maximal confluency is reached with 60 % of scratch wound being covered by migrated cells.

3.1.6 FACS-Based Phagocytosis Assay – Proof of Concept with Cell Sorter and Phase Contrast Microscopy

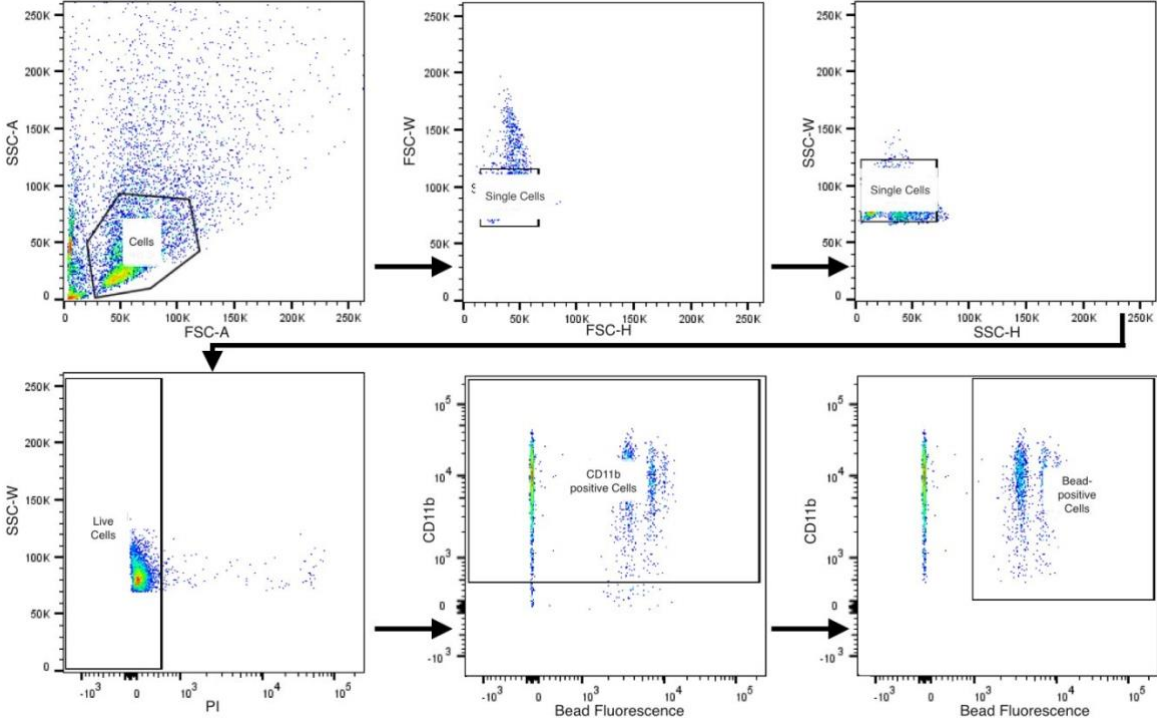


Figure 11 Gating of XMOO1-derived iMGL by Aria II cell sorter for proof of concept. First, the population consisting of cells was selected using forward scatter area and sideward scatter area. Then, doublet cells were excluded using forward scatter width and height, as well as sideward scatter width and height. In the next step, PI positive cell were excluded. CD11b positive cells were selected and finally, cells positive for fluorescent signal of the carboxylate microspheres were sorted into a 96-well plate for imaging under a phase-contrast microscope (see Figure 12).

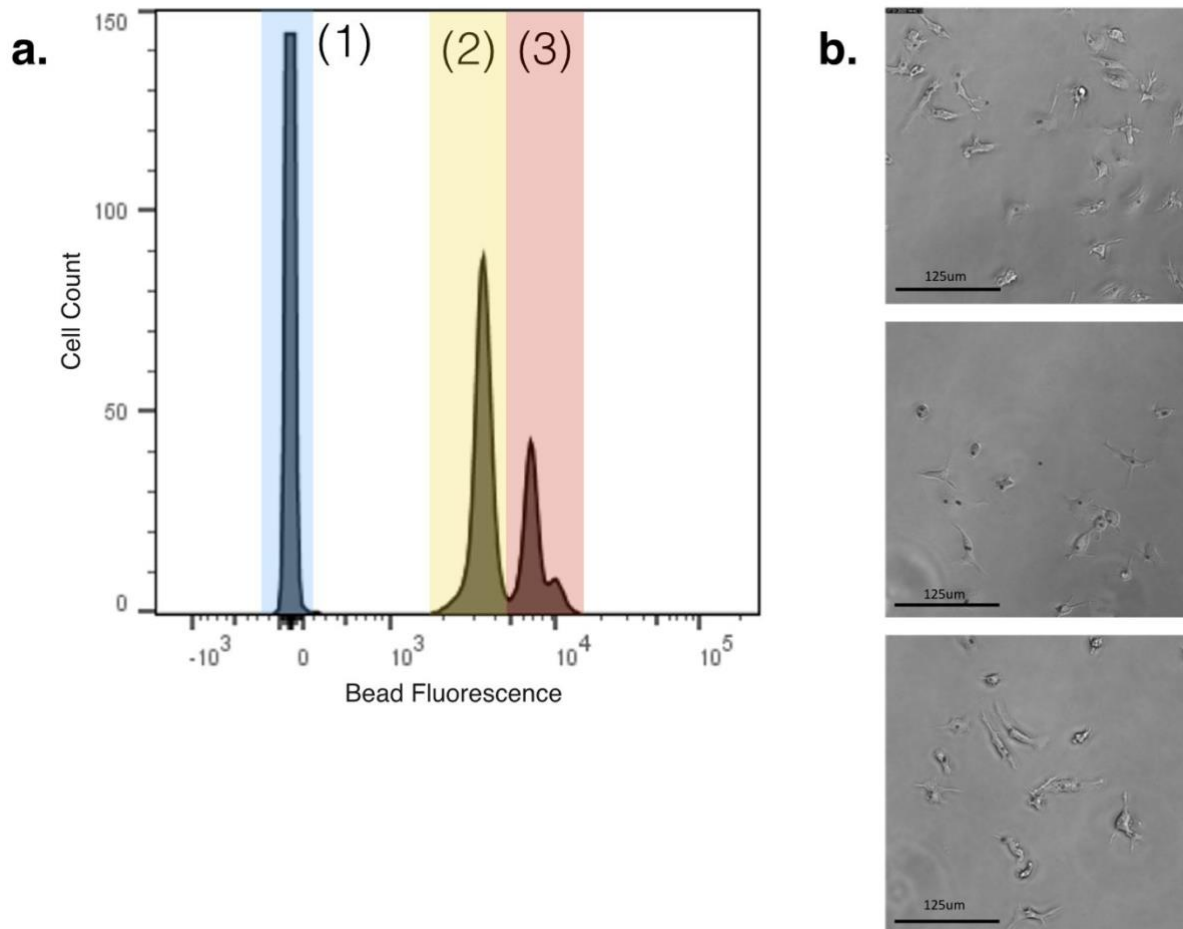


Figure 12 Cell sorting results of XMOO1-derived iMGL that had been left to phagocytose fluorescently marked carboxylate microspheres. Cells were sorted as described in Figure 11. This experiment was conducted as a proof of principle for FACS-based phagocytosis assay. (a) Histogram of PI negative, CD11b positive single cell's fluorescence in B-530_30-A channel measuring bead fluorescence. Three main populations are recognizable: cells that did not phagocytose a bead (1), cells that phagocytosed one bead (2) and cells that phagocytosed two beads or more (3). (b) After cell sorting, cells that had phagocytosed a bead were sorted into a 96-well plate and phase contrast microscopy was performed. Note that the vast majority of depicted cells phagocytosed one or two beads. This goes in line with the nearly dicrotic population of B-530_30-A positive cells (see Figure 11).

For proof of concept, XMOO1-derived iMGL were sorted into a 96-well plate with FACSARIA™ II (BD, Franklin Lakes, NJ, USA), then imaged via phase contrast microscopy. Gating is depicted in Figure 11. Cells were selected based on their forward scatter and sideward scatter area. After that, doublet cells were identified by their tell-tale relationship between area and height in side and forward scatter and gaited out from downstream analysis. Then, dead PI positive cells were excluded and CD11b negative cells were discarded. Finally, cells positive for B-530_30-A, corresponding to fluorescence of carboxylate beads, were sorted into a 96-well plate. Cell count as a function of intensity for B-530_30-A channel is shown in Figure 12. Note that

fluorescence distribution of B-530_30-A positive cells is nearly dicrotic. Thereafter, phase-contrast microscopy was performed (Figure 12). The vast majority of cells phagocytosed one bead or two beads, which fits dicrotic distribution of B-530_30-A positive cells.

3.1.7 FACS-Based Phagocytosis Assay – Analysis with LSRFortessa™ Analyzer and Quantification

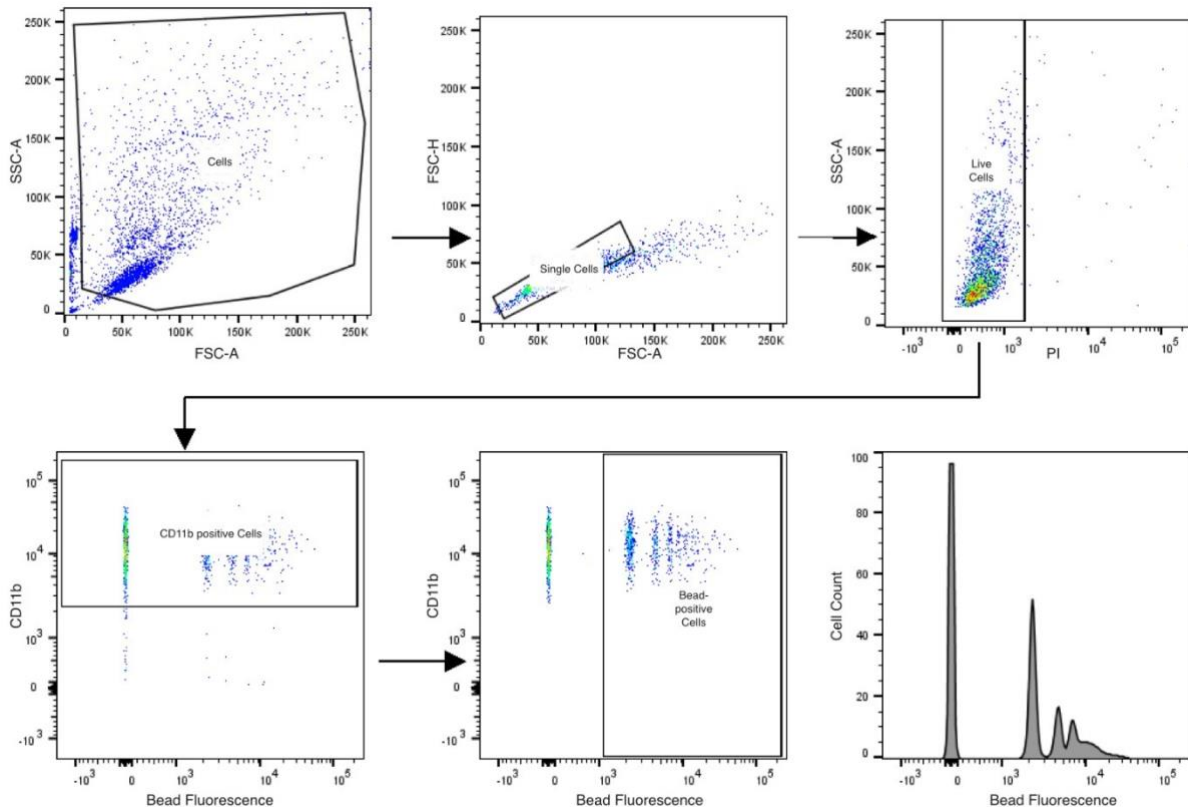


Figure 13 Gating of XMOO1-derived iPSC by LSRFortessa™ (BD, Franklin Lakes, NJ, USA). Analysis was done in FlowJo™ (version 10.6.1, Becton Dickinson, Ashland, OR). First, cells were sorted using sideward scatter area and forward scatter area. Then, doublet cells were excluded, taking forward scatter height and area into account. Thereafter, live cells, hence PI negative cells, were selected. Next, CD11b negative cells were excluded so that all cells positive for fluorescent bead signal could be examined and quantified.

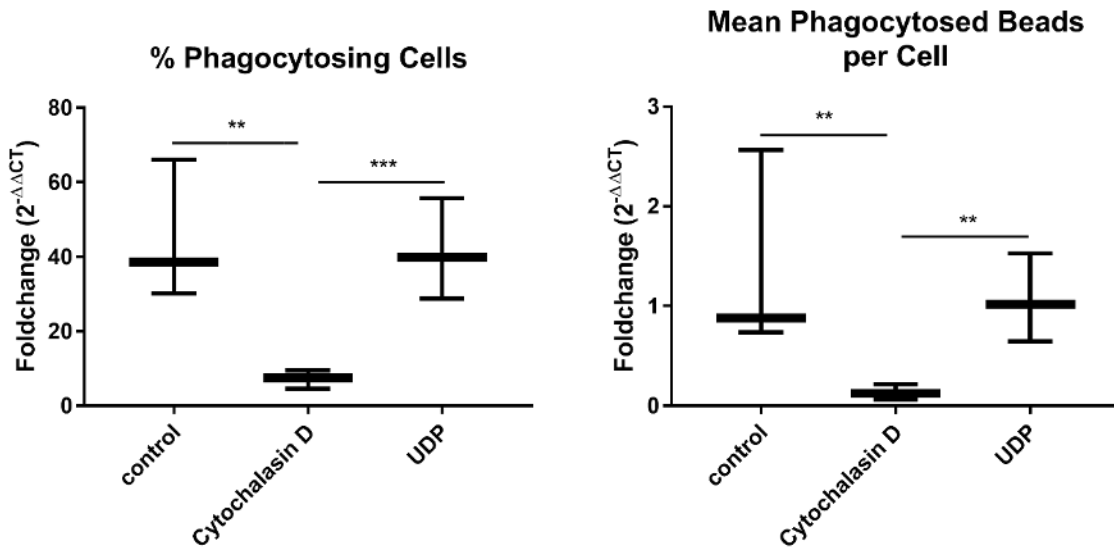


Figure 14 Quantification of phagocytosis. Cytochalasin D significantly downregulated both the fraction of phagocytosing cells ($p = 0.0026$) and the mean number of phagocytosed beads per cell ($p = 0.0054$). UDP did not significantly affect phagocytosis. However, compared to cells treated with Cytochalasin D, significantly more cells stimulated with UDP phagocytosed ($p = 0.0008$) and more beads per cell were phagocytosed ($p = 0.0025$). For statistical analysis, two-tailed ratio paired t-test was performed.

Cell sorting for FACS analysis was done using LSRFortessa™ (BD, Franklin Lakes, NJ, USA). Gating is described in Figure 13. As in the section above (chapter 3.1.6), a population of CD11b positive live single cells is positive for B-530_30-A. Evidently, these cells had most likely phagocytosed the Fluoresbrite® carboxylate microspheres. Quantification of the percentage of phagocytosing cells and the mean number of phagocytosed beads per cell (Figure 14) reveals that mycotoxin cytochalasin D, an inhibitor of actin polymerization, significantly downregulated both the percentage of phagocytosing cells and the number of phagocytosed beads per cell. While under control conditions an average of 44,93 % of cells had been phagocytically active, a treatment with cytochalasin D significantly reduced the fraction of phagocytosing cells to 7,17 % on average ($p = 0,0026$, $t = 19,7$). Also, the mean number of phagocytosed beads per cell was reduced. While under control conditions, a cell phagocytosed 1,39 beads on average, cells treated with cytochalasin D phagocytosed 0,13 beads per cell, hence significantly less ($p = 0,0054$, $t = 13.61$). Treatment with UDP did not significantly change phagocytosis, 41,47 % of cells phagocytosed on average (comparison to control: $p = 0,4151$, $t = 1,02$) and an average of 1,06 beads per cell was phagocytosed (comparison to control: $p = 0,4784$, $t = 0,8645$).

3.2 Expression of Genes Characteristic for GAM

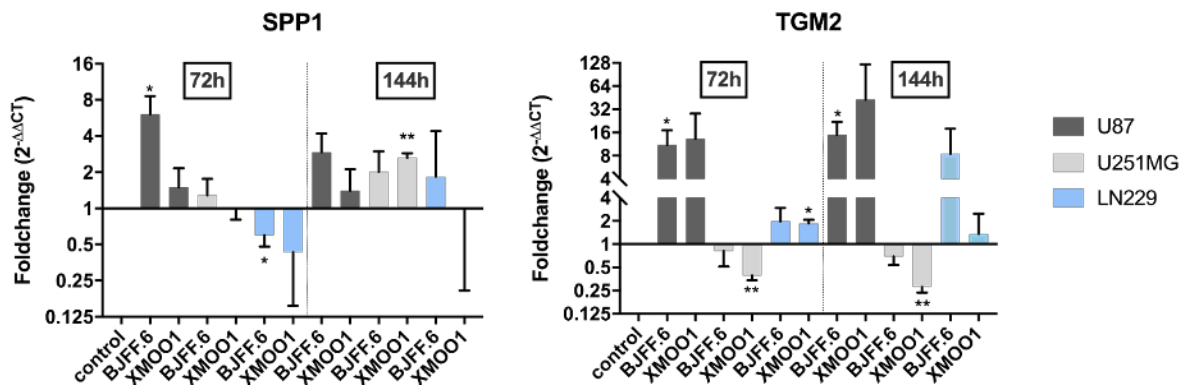


Figure 15 Changes of expression of GAM-characteristic genes SPP1 and TGM2 after 72 and 144 hours of co-cultivation with U87, U251MG and LN229 glioma cells. Experiments were performed for BJFF.6 and XMOO1 iMGL. For statistical analysis, a two-tailed ratio paired t-test was performed.

After 72 hours of co-cultivation with U87, BJFF.6-derived iMGL significantly upregulated SPP1 ($p = 0.0205$, $t = 6.887$). SPP1 was also upregulated in XMOO1-derived iMGL after 144 hours of co-cultivation with U251MG ($p = 0.0028$, $t = 18.89$). SPP1 was downregulated in BJFF.6-derived iMGL after 72 hours of co-cultivation with LN229 ($p = 0.0478$, $t = 4.409$).

After 72 hours of co-cultivation, TGM2 was significantly upregulated in BJFF.6-derived iMGL co-cultivated with U87 ($p = 0.0186$, $t = 7.232$) and in XMOO1-derived iMGL co-cultivated with LN229 ($p = 0.0118$, $t = 9.136$). After 72 hours, TGM2 was downregulated in XMOO1-derived iMGL co-cultivated with U251MG ($p = 0.0078$, $t = 11.29$). After 144 hours of co-culture, TGM2 was significantly upregulated in BJFF.6-derived iMGL co-cultivated with U87 ($p = 0.0112$, $t = 9.368$) and downregulated in XMOO1-derived iMGL co-cultivated with U251MG ($p = 0.0046$, $t = 14.71$).

Table 3 Mean Fold-Changes, p-value, t-value and significance of changes in SPP1 gene expression for co-cultivation for 72 and 144 hours with U87, U251MG and LN229 for BJFF.6- and XMOO1-derived iMGL.

<u>SPP1</u>						
Time	Glioma Cell Line	iPSC Cell Line	Mean Fold-Change	p-value	t-value	Significance
72 hours	U87	BJFF.6	6.077329	0.0205	6.877	*
		XMOO1	1.50223067	0.3871	1.097	NA
	U251MG	BJFF.6	1.28634367	0.4928	0.8322	NA
		XMOO1	0.99585933	0.8953	0.1489	NA
	LN229	BJFF.6	0.59622233	0.0478	4.409	*
		XMOO1	0.42982833	0.1078	2.794	NA
144 hours	U87	BJFF.6	2.93694767	0.0797	3.327	NA
		XMOO1	1.4012785	0.3479	1.216	NA
	U251MG	BJFF.6	2.01351333	0.1344	2.445	NA
		XMOO1	2.64058433	0.0028	18.89	**
	LN229	BJFF.6	1.832845	0.8515	0.2124	NA
		XMOO1	0.99654167	0.6888	0.4631	NA

Table 4 Mean Fold-Changes, p-value, t-value and significance of changes in TGM2 gene expression for co-cultivation for 72 and 144 hours with U87, U251MG and LN229 for BJFF.6- and XMOO1-derived iMGL.

<u>TGM2</u>						
Time	Glioma Cell Line	iPSC Cell Line	Mean Fold-Change	p-value	t-value	Significance
72 hours	U87	BJFF.6	11.067759	0.0186	7.232	*
		XMOO1	13.3056333	0.0916	3.073	NA
	U251MG	BJFF.6	0.81438433	0.4070	1.041	NA
		XMOO1	0.393848	0.0078	11.29	**
	LN229	BJFF.6	1.978672	0.1730	2.080	NA
		XMOO1	1.86145333	0.0118	9.136	*
144 hours	U87	BJFF.6	14.963782	0.0112	9.368	*
		XMOO1	42.7402905	0.2130	1.804	NA
	U251MG	BJFF.6	0.69466067	0.1147	2.693	NA
		XMOO1	0.278747	0.0046	14.71	**
	LN229	BJFF.6	8.48926167	0.1659	2.138	NA
		XMOO1	1.36011267	0.9334	0.0944	NA

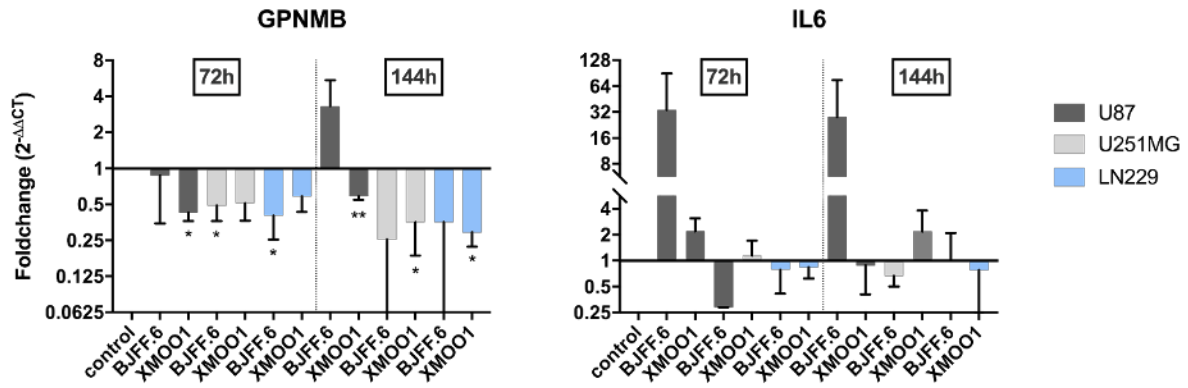


Figure 16 Fold-change relative to control of expression of GAM-characteristic genes GPNMB and IL6 after 72 and 144 hours of co-cultivation with U87, U251MG and LN229 glioma cells. Experiments were performed for BJFF.6 and XMOO1 iMGL. For statistical analysis a two-tailed ratio paired t-test was done.

After 72 hours, GPNMB was significantly downregulated in BJFF.6-derived iMGL co-cultivated with U251MG ($p = 0.0351$, $t = 5.196$) and LN229 ($p = 0.0416$, $t = 4.748$) and in XMOO1-derived iMGL co-cultivated with U87 ($p = 0.0100$, $t = 9.908$). After 144 hours, GPNMB was significantly downregulated in XMOO1-derived iMGL co-cultivated with U87 ($p = 0.0079$, $t = 11.20$), U251MG ($p = 0.0483$, $t = 4.383$) and LN229 ($p = 0.0112$, $t = 9.364$). There were no significant changes in IL-6 expression.

Table 5 Mean Fold-Changes, p-value, t-value and significance of changes in GPNMB gene expression for co-cultivation for 72 and 144 hours with U87, U251MG and LN229 for BJFF.6- and XMOO1-derived iMGL.

<u>GPNMB</u>						
Time	Glioma Cell Line	iPSC Cell Line	Mean Fold-Change	p-value	t-value	Significance
72 hours	U87	BJFF.6	0.871337	0.5240	0.7655	NA
		XMOO1	0.42636133	0.0100	9.908	*
	U251MG	BJFF.6	0.48899833	0.0351	5.196	*
		XMOO1	0.50996067	0.0512	4.246	NA
	LN229	BJFF.6	0.40298565	0.0416	4.748	*
		XMOO1	0.580373	0.0602	3.891	NA
144 hours	U87	BJFF.6	3.303927	0.2023	1.871	NA
		XMOO1	0.58385725	0.0079	11.20	**
	U251MG	BJFF.6	0.25376467	0.0970	2.972	NA
		XMOO1	0.35431767	0.0483	4.383	*
	LN229	BJFF.6	0.35503527	0.1112	2.743	NA
		XMOO1	0.29123667	0.0112	9.364	*

Table 6 Mean Fold-Changes, p-value, t-value and significance of changes in IL-6 gene expression for co-cultivation for 72 and 144 hours with U87, U251MG and LN229 for BJFF.6- and XMOO1-derived iMGL.

<u>IL-6</u>						
Time	Glioma Cell Line	iPSC Cell Line	Mean Fold-Change	p-value	t-value	Significance
72 hours	U87	BJFF.6	33.9222277	0.3024	1.377	NA
		XMOO1	2.190529	0.1313	2.481	NA
	U251MG	BJFF.6	0.286611	0.1178	2.650	NA
		XMOO1	1.14273233	0.9081	0.1306	NA
	LN229	BJFF.6	0.78290551	0.3871	1.097	NA
		XMOO1	0.83380833	0.2966	1.400	NA
144 hours	U87	BJFF.6	28.1513897	0.8738	0.1799	NA
		XMOO1	0.87917475	0.5138	0.7869	NA
	U251MG	BJFF.6	0.66152933	0.0902	3.099	NA
		XMOO1	2.17685967	0.2904	1.424	NA
	LN229	BJFF.6	1.01200421	0.5858	0.6436	NA
		XMOO1	0.7765395	0.6139	0.6937	NA

3.3 Morphology of iMGL Co-Cultivated with Glioma Cells

3.3.1 Representative Images and Description

The co-cultivation of iMGL with glioma cells induces a less spheroid and more ramified iMGL phenotype. iMGL were especially more ramified when co-cultivated with U251MG and LN229 glioma cells (see Figure 19, Figure 20, Figure 21, Figure 22). In general, cell ramification was rather scarce with few and thick short rami. iMGL were often polarized in a bipolar manner. There was no visible change in nucleus morphology.

Moreover, co-cultivation led to increased iMGL volume. On representative images, iMGL co-cultivated with U87 glioma cells for 72 hours had a diameter of approximately 20 μm , respective controls had a diameter of about 27 μm (see Figure 17). After 144 hours of co-cultivation with the same glioma cells, iMGL were approximately 13 μm large and controls had a diameter of about 19 μm (see Figure 18). Hence, after 72 hours of co-cultivation with U87 glioma cells, co-cultivated iMGL were approximately 7 μm larger than respective controls on the images below. After 144 hours, co-cultivated iMGL had a diameter approximately 6 μm larger than respective controls.

After 72 hours of co-cultivation with U251MG glioma cells, iMGL had a diameter of about 18 μm , whereas respective controls measured about 25 μm on representative images (see Figure 19). After 144 hours of co-cultivation with U251MG, iMGL measured about 15 μm and controls about 26 μm (see Figure 20). Therefore, after 72 hours iMGL co-cultivated with U251MG were approximately 7 μm larger than controls, after 144 hours co-cultivated and control iMGLs differed by about 11 μm on representative images.

On representative images, when co-cultivated with LN229 glioma cells for 72 hours, iMGL possessed a diameter of about 24 μm , respective controls were about 28 μm large (see Figure 21). After 144 hours, co-cultivated iMGL were about 13 μm large, while control iMGL were about 32 μm large (see Figure 22). Hence, after 72 hours iMGL co-cultivated with U251MG glioma cells were approximately 4 μm larger than respective controls on representative images and after 144 hours co-cultivated iMGL were approximately 19 μm larger.

For a summary of the numbers mentioned above, see Table 7. For a more systematic quantification of iMGL volume upon co-cultivation with U87 glioma cells, see 3.3.2.

On the representative images below, more co-cultivated iMGL than respective controls were depicted. Sixteen iMGL were depicted in total under co-cultivation while 14 iMGL were visible for respective controls.

For a quantification of morphology of iMGL co-cultivated with U87 glioma cells and respective controls, please consult 3.3.2.

Table 7 Approximate cell sizes of iMGL on representative images for each glioma cell line used for co-cultivation, duration of co-cultivation and condition (see Figure 17, Figure 18, Figure 19, Figure 20, Figure 21, Figure 22).

Glioma Cell Line	Co-Cultivation Duration	Condition	Approx. Cell Size
U87	72 h	control	20 μm
		co-culture	27 μm
	144 h	control	13 μm
		co-culture	19 μm
U251MG	72 h	control	18 μm
		co-culture	25 μm
	144 h	control	15 μm
		co-culture	26 μm
LN229	72 h	control	24 μm
		co-culture	28 μm
	144 h	control	13 μm
		co-culture	32 μm

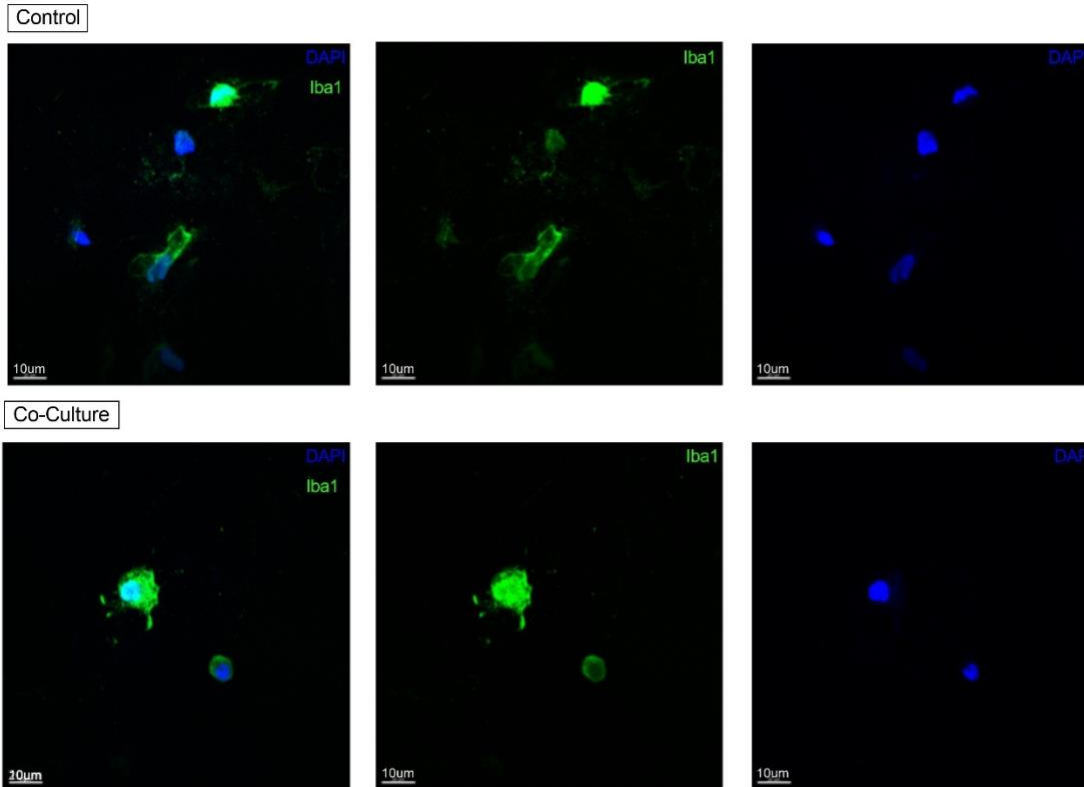


Figure 17 Co-cultivation of BJFF.6-derived iMGL with U87 glioma cells for 72 hours. Co-cultivated cells are larger and more ramified.

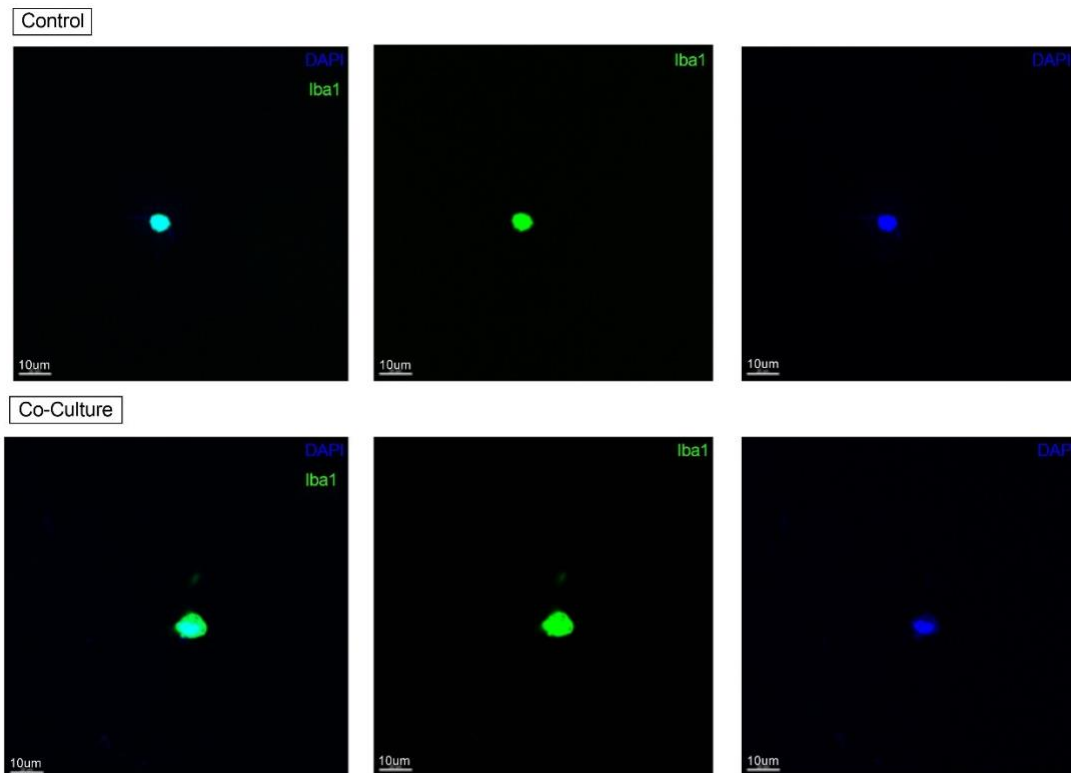


Figure 18 Co-cultivation of BJFF.6-derived iMGL with U87 glioma cells for 144 hours. Co-cultivated cells are slightly larger.

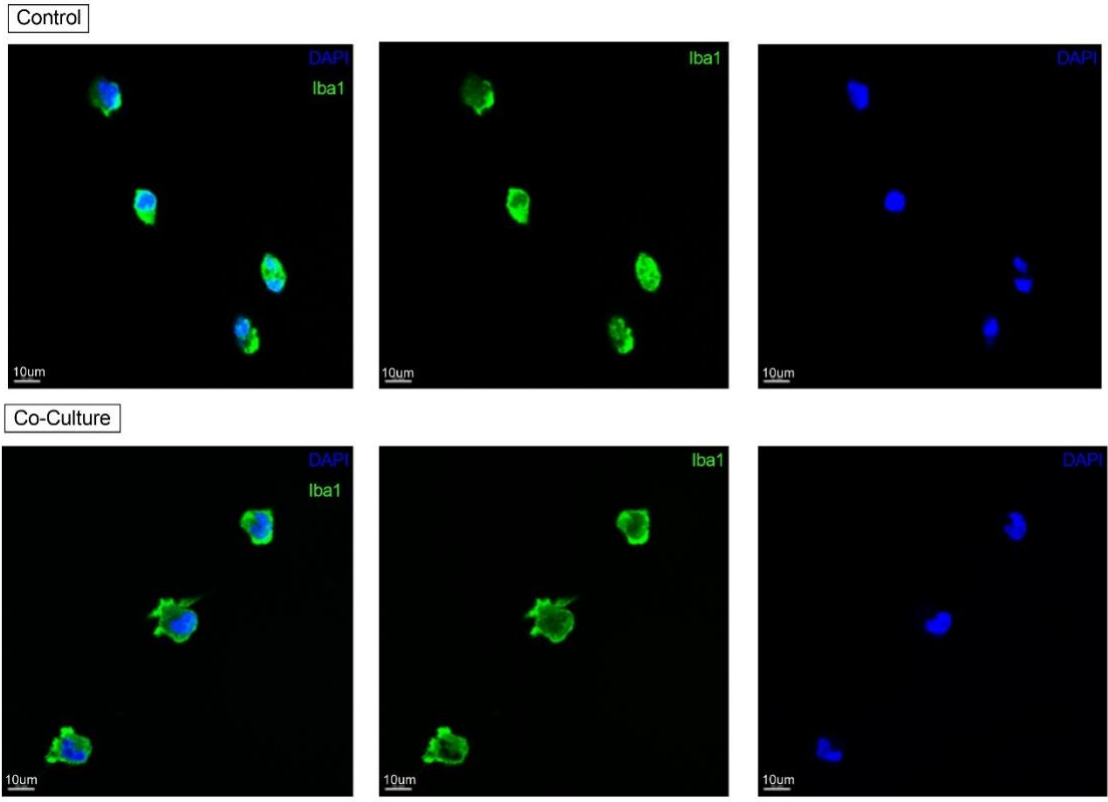


Figure 19 Co-cultivation of BJFF.6-derived iMGL with U251MG glioma cells for 72 hours. Co-cultivated cells are larger and have more ramifications.

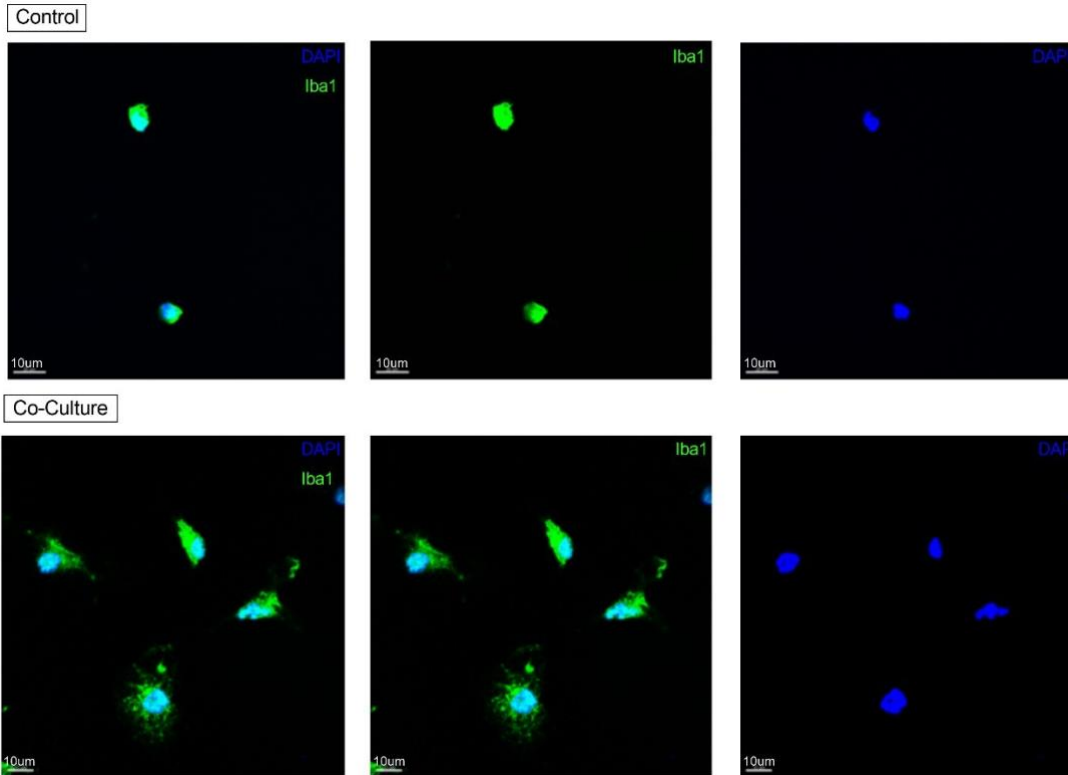


Figure 20 Co-cultivation of BJFF.6-derived iMGL with U251MG glioma cells for 144 hours. Co-cultivated cells exhibit a larger and more ramified phenotype.

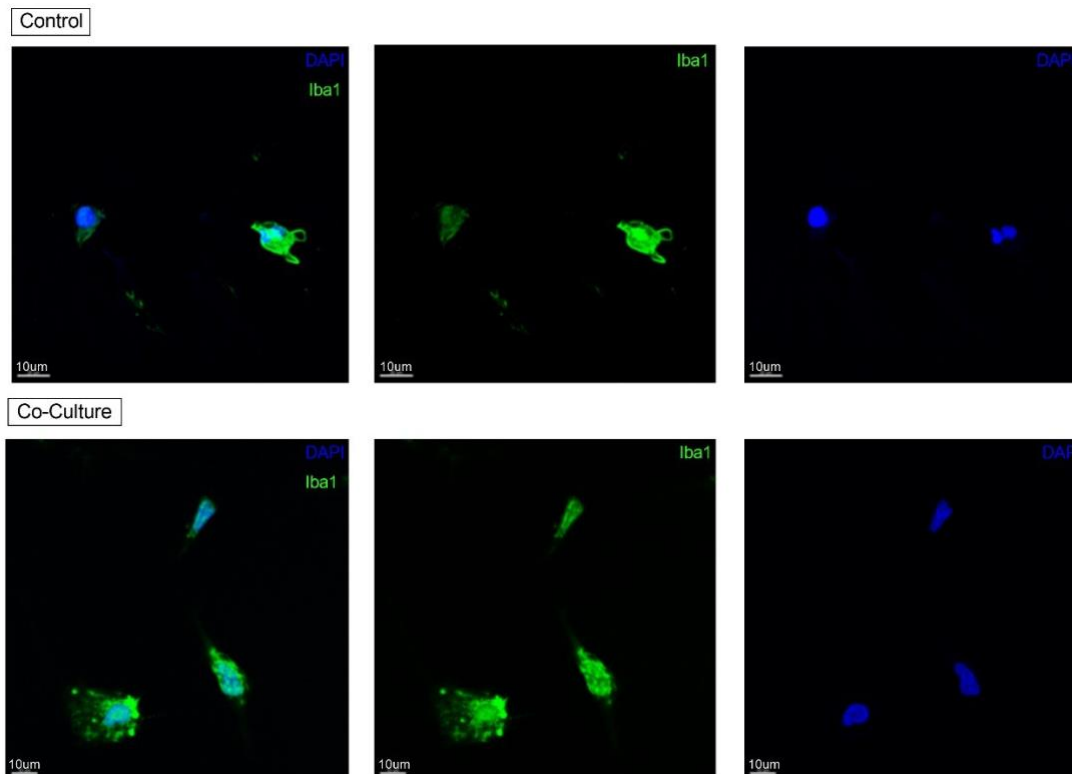


Figure 21 Co-cultivation of BJFF.6-derived iMGL with LN229 glioma cells for 72 hours. Co-cultivated cells are larger and possess more ramifications.

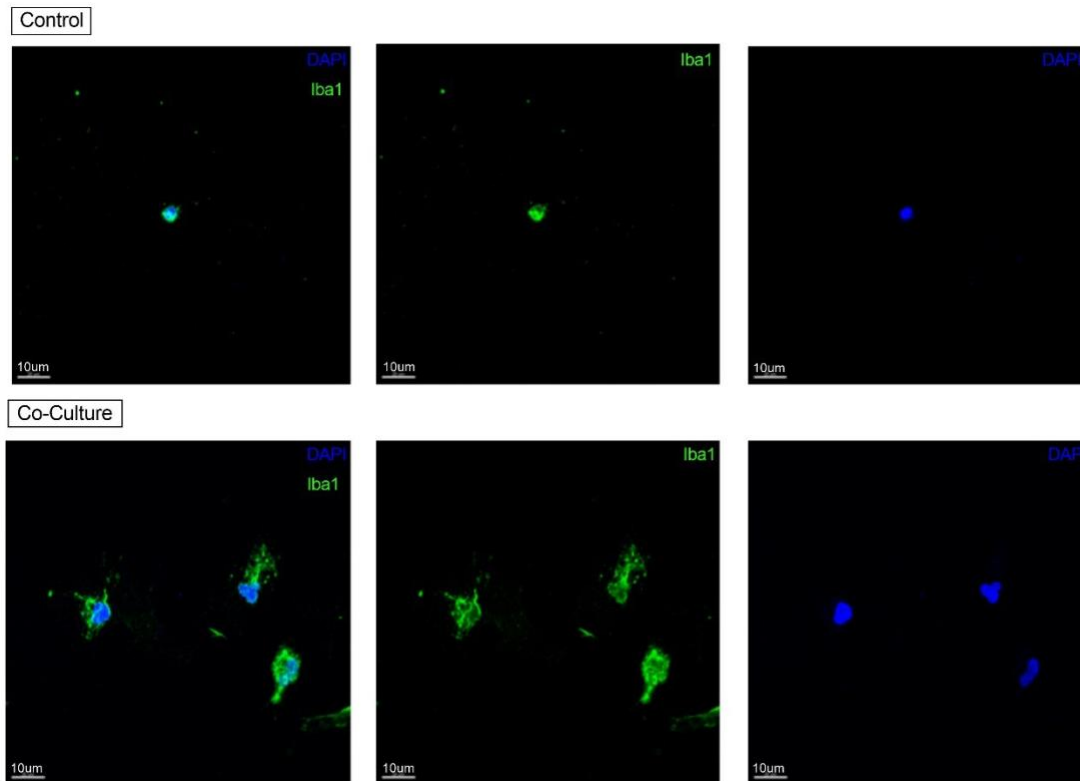


Figure 22 Co-cultivation of BJFF.6-derived iMGL with LN229 glioma cells for 144 hours. Co-cultivated cells are of a larger cell size and more ramified.

3.3.2 Quantification of Morphology

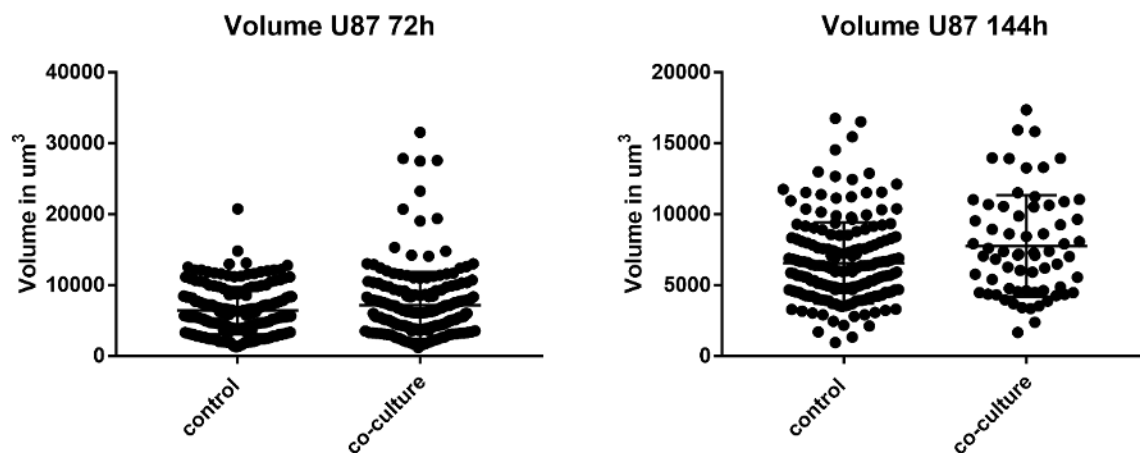


Figure 23 Volumes in μm^3 of iMGL co-cultivated with U87 glioma cells in a transwell setup and respective controls for 72 hours and 144 hours. Each dot represents an analyzed cell. There was no significant difference in volume between co-cultivated iMGL and controls. Disproportionally large statistical outliers most likely correspond to cells that were very proximal and hence challenging to distinguish for Imaris 9.2 software. For statistical analysis a two-tailed ratio paired t-test was performed. In

order to enable a clearer data visualization, only a representative set of datapoints was depicted in the graph above. Nevertheless, all collected data was included in statistical analysis.

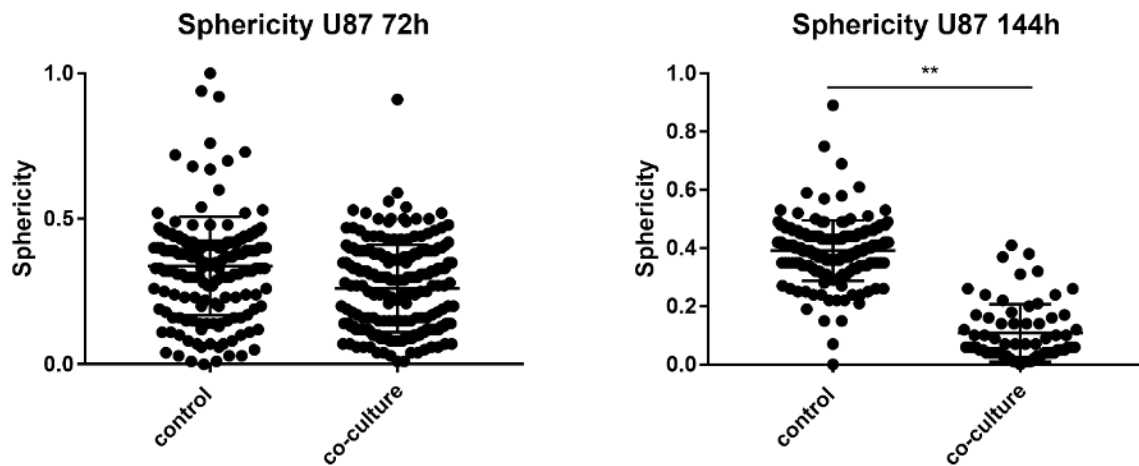


Figure 24 Sphericity as defined by Wadell was computed for iMGL co-cultivated with U87 glioma cells in a transwell setup versus monocultivated controls for 72 hours and 144 hours. Each dot represents an analyzed cell. Note that by Wadell, a perfectly spherical object is assigned a sphericity of 1. For more details on this metric please consult 2.7.3.4. After 144 hours of co-cultivation, iMGL co-cultivated with U87 cells were significantly less spherical, hence more ramified than monocultivated controls ($p=0,0014$). There was no significant difference in sphericity between co-cultivated iMGL and control cells after 72 hours of co-cultivation. For statistical analysis, a two-tailed ratio paired t-test was performed. For clearer data visualization, only a representative subset of datapoints was plotted above.

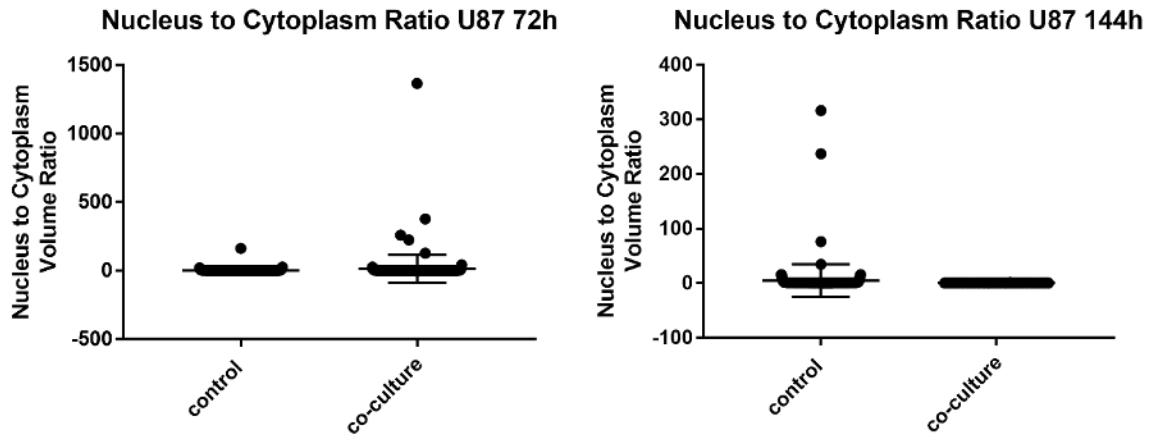


Figure 25 Nucleus to cytoplasm volume ratio of iMGL co-cultivated with U87 glioma cells in a transwell setup and respective controls for 72 hours and 144 hours. Each dot represents an analyzed cell. A significant difference in nucleus to cytoplasm volume ratio between co-cultivated iMGL and controls could not be found. Statistical outliers with a very large nucleus to cytoplasm ratio could be explained with exceptionally poor quality Iba1 cell staining. For statistical analysis, a two-tailed ratio paired student's t-test was performed. For the purpose of clearer data visualization, only a representative subset of datapoints is plotted above.

iMGL volume neither changed significantly after 72 hours of co-cultivation with U87 glioma cells ($p = 0,515$) nor after 144 hours of co-cultivation ($p = 0,5005$) compared to control.

Also, iMGL sphericity was not influenced by 72 hours of co-cultivation with U87 glioma cells ($p = 0,3441$). However, iMGL sphericity was significantly increased after 144 hours of co-cultivation with U87 glioma cells ($p = 0,0014$). Note that for sphericity a metric defined by Wadell was used. For details on this, please consult 2.7.3.4. Briefly, sphericity is the surface area of a perfect sphere of volume respective to the analyzed particle divided by the particle's real surface area. Hence, sphericity of a perfect sphere would be equal to one.

Moreover, the nucleus to cytoplasm volume ratio did not significantly change after 72 hours ($p = 0,4372$) or 144 hours ($p = 0,1$) of co-cultivation.

3.4 Direct Co-Cultivation with U87 mCherry

3.4.1 Changes in SPP1 Upon Direct Co-Cultivation with U87 mCherry

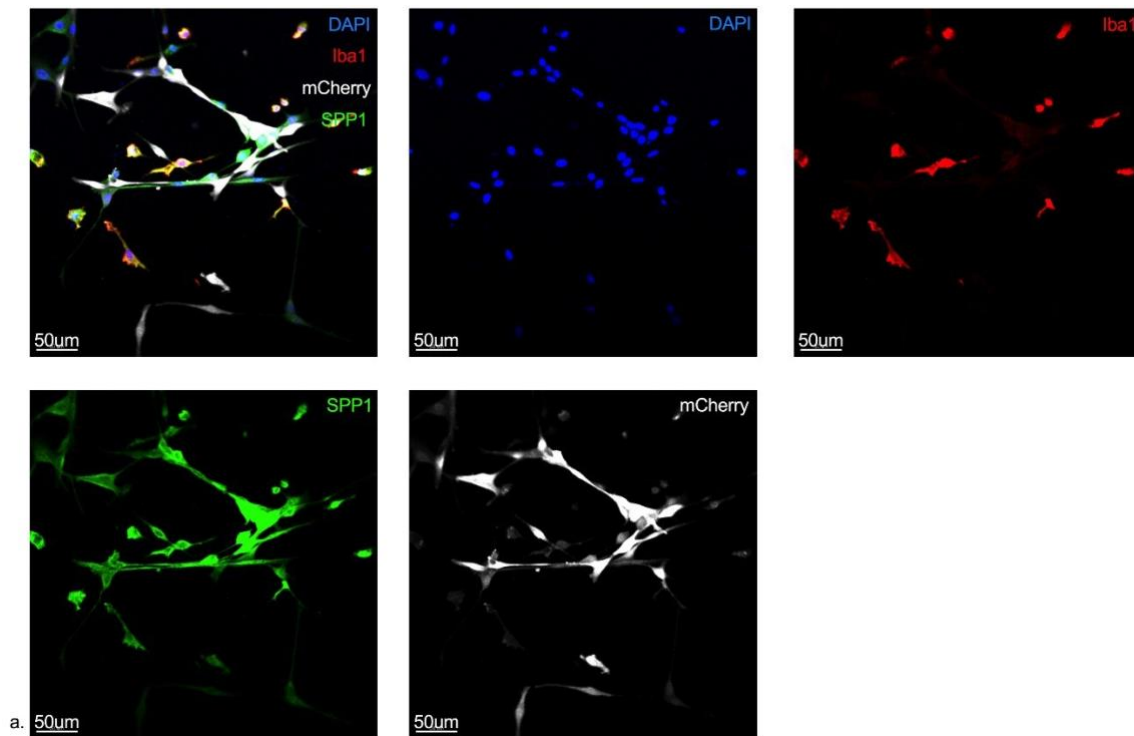


Figure 26 Staining of XMOO1-derived iPSC directly co-cultivated with mCherry U87 glioma cells. Cells were stained for Iba1 and SPP1, amongst other things. For quantitative analysis, Iba1 was used to distinguish microglia from glioma cells, SPP1 intensity within Iba1-positive microglia was then quantified. U87 glioma cells were tagged with mCherry. In quantitative analysis, Iba1-positive cells with a very high intensity of mCherry were excluded, as they were more likely to be glioma cells.

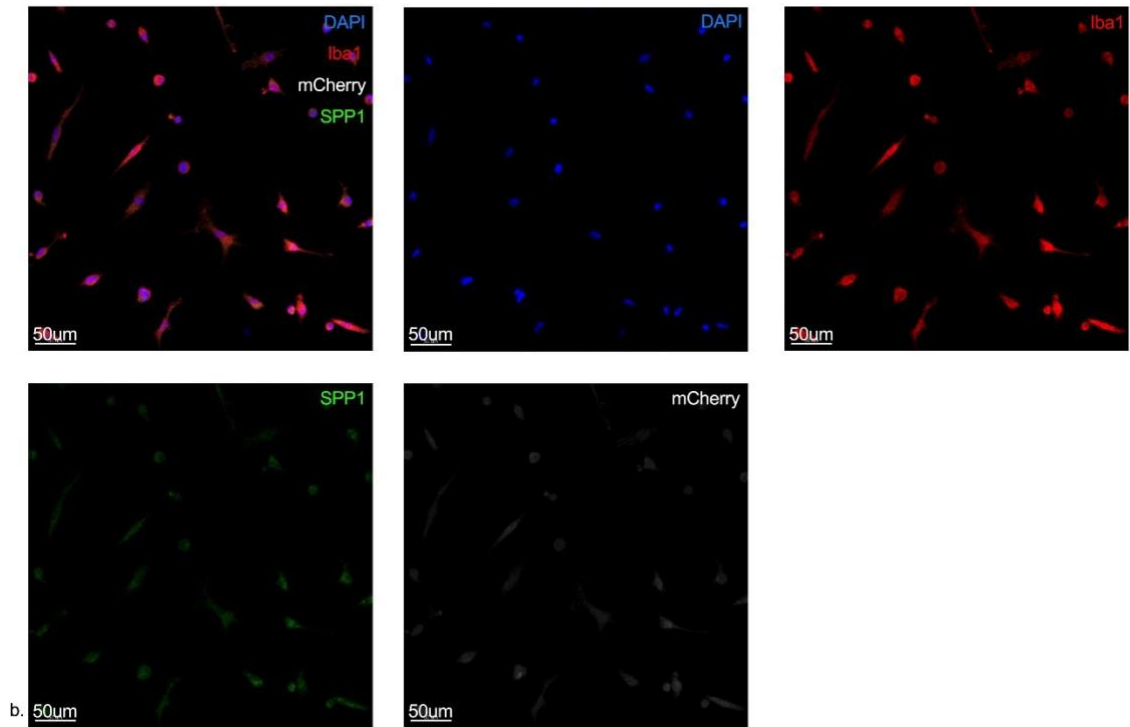


Figure 27 Staining of XMOO1-derived iPSC seeded on coverslips without mCherry U87 glioma cells as a control.

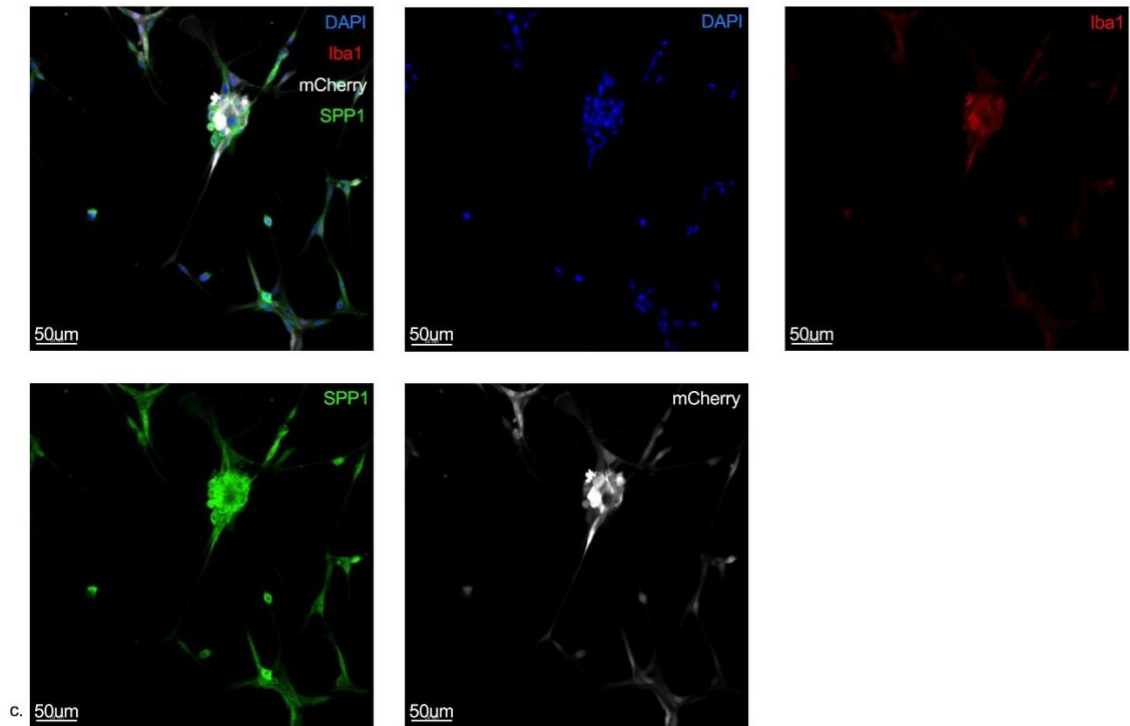


Figure 28 Staining of mCherry U87 glioma cells as a control. Evidently, glioma cells were positive for SPP1, in addition to iMGL. In quantitative analysis, this issue was solved by only quantifying SPP1 intensity inside of strongly Iba1-positive and mCherry negative surfaces. Glioma cells were highly positive for mCherry and only weakly positive for Iba1.

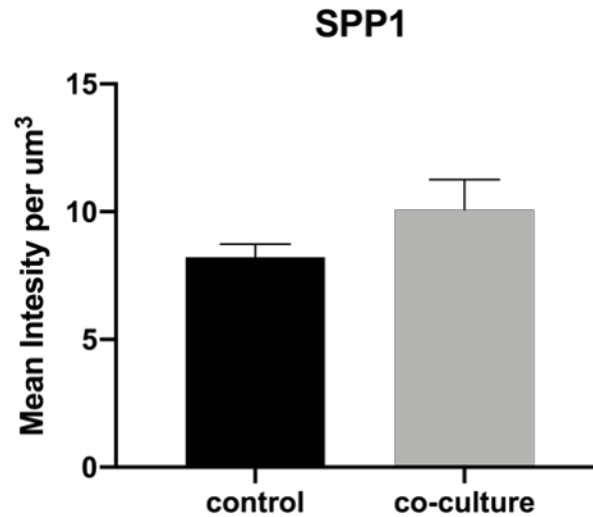


Figure 29 BJFF.6-derived iMGL were stained for SPP1 with a secondary AF488-conjugated antibody. Mean fluorescence intensity per μm^3 was computed for each experiment. Here, iMGL co-cultivated with U87 mCherry with direct cell-cell contact are compared with iMGL in monoculture. Co-cultivation with glioma cells did not significantly upregulate the fluorescence intensity of iMGL. For statistical analysis, a student's two-tailed ratio paired t-test was performed.

Here, BJFF.6-derived iMGL were either co-cultivated on coverslips with U87 mCherry glioma cells with direct cell-cell contact, or they were kept in monoculture. Then, cells were stained with microglia specific anti-Iba1 and anti-SPP1, in order to quantify intensity of secondary antibody bound to SPP1. After direct co-cultivation with U87 mCherry, BJFF.6-derived iMGL did not stain significantly more positive for SPP1 ($p = 0.1469$, $t = 2.313$).

3.4.2 Changes in GPNMB Upon Direct Co-Cultivation with U87 mCherry

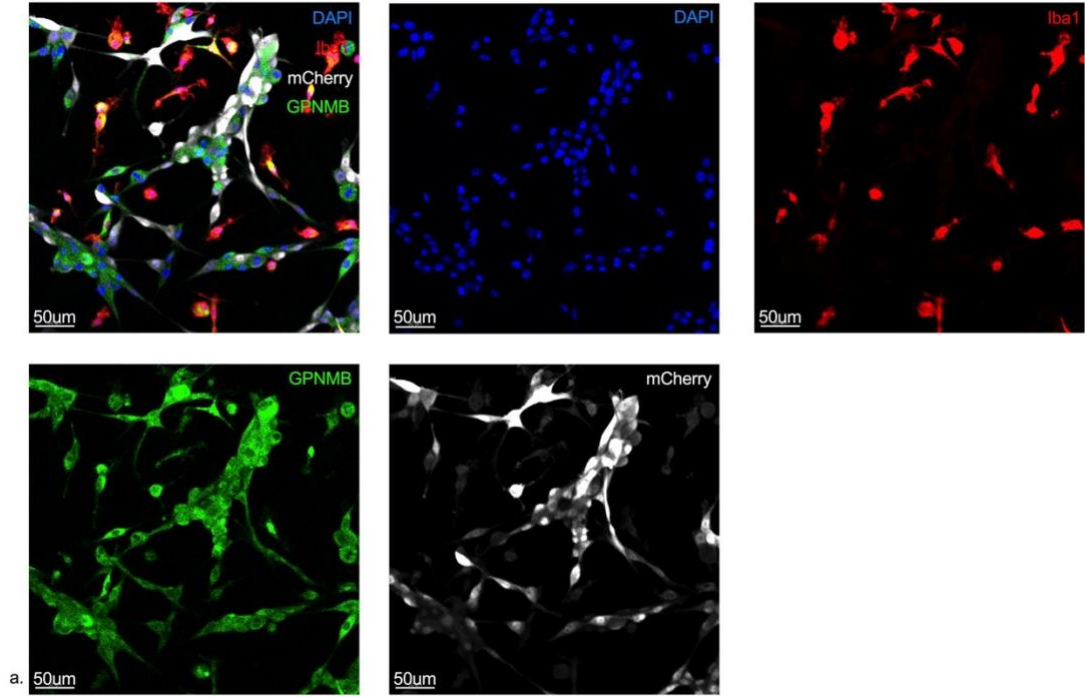


Figure 30 Staining of XMOO1-derived iPSC directly co-cultivated with mCherry U87 glioma cells. Cells were stained for Iba1 and GPNMB, amongst other things. Quantitative analysis was based on these stainings, for details consult the annotation of Figure 26.

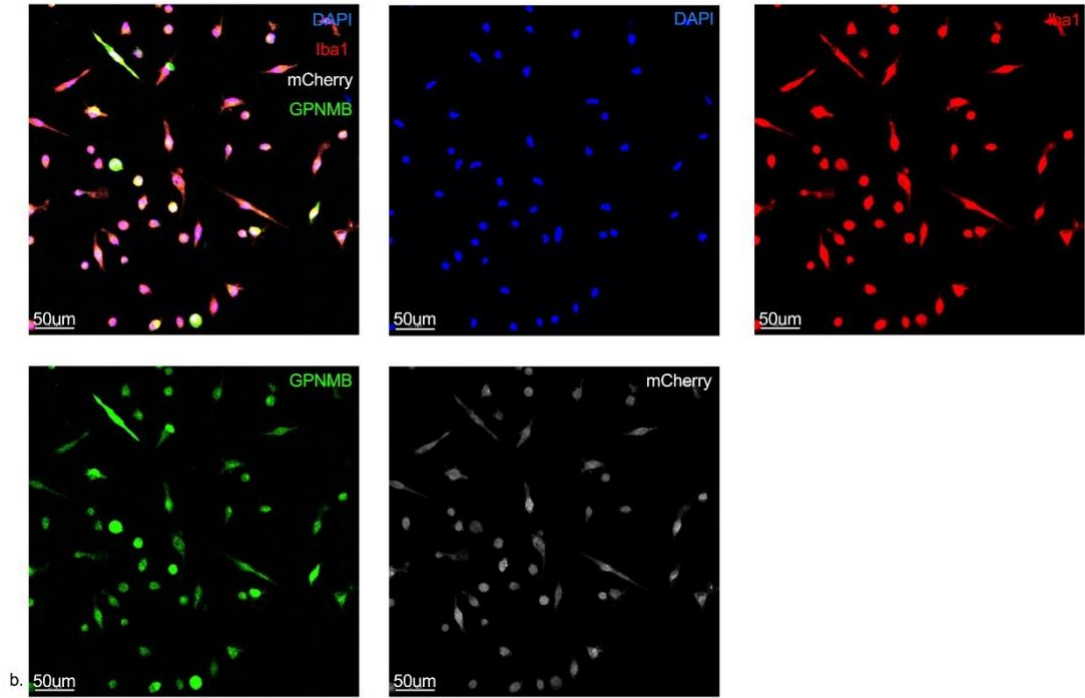


Figure 31 Staining of XMOO1-derived iPSC seeded on coverslips without mCherry U87 glioma cells as a control.

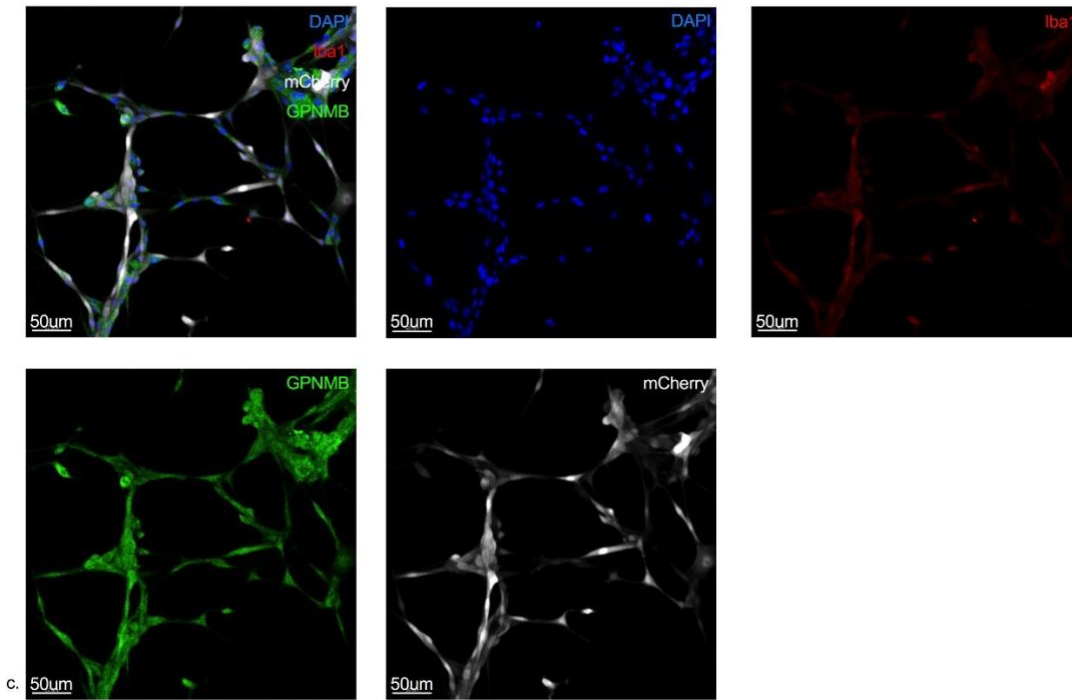


Figure 32 Staining of mCherry U87 glioma cells as a control. Visibly, iMGL and glioma cells were positive for GPNMB. However, iMGL could be recognized because they are strongly positive for Iba1 and negative for negative. Therefore, GPNMB intensity inside iMGL was quantified by measuring GPNMB intensity inside of strongly Iba1 positive and mCherry-negative surfaces only.

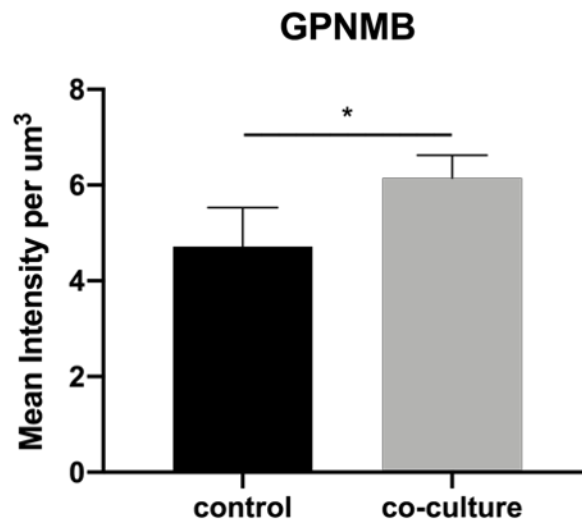


Figure 33 Mean intensity per μm^3 of BJFF.6-derived iMGL stained with AF488-conjugated secondary antibody bound to primary anti-GPNMB antibody. BJFF.6-derived iMGL co-cultivated under direct cell-cell contact with U87 mCherry and BJFF.6-derived iMGL in monoculture are compared. Under co-cultivation, fluorescence intensity of iMGL stained for GPNMB was significantly higher ($p = 0,0374$, $t = 5,027$), indicating an upregulation of GPNMB. For statistical analysis, a student's two-tailed ratio paired t -test was performed.

In this experiment, BJFF.6-derived iMGL co-cultivated under direct cell-cell contact with U87 mCherry glioma cells were compared to iMGL in monoculture. The fluorescence intensity of the secondary antibody bound to a primary anti-GPNMB antibody was quantified inside of Iba1-labelled microglia cells. Co-cultivation significantly increased staining intensity of iMGL ($p = 0.0374$, $t = 5.027$).

3.4.3 Changes in Morphology Upon Direct Co-Cultivation

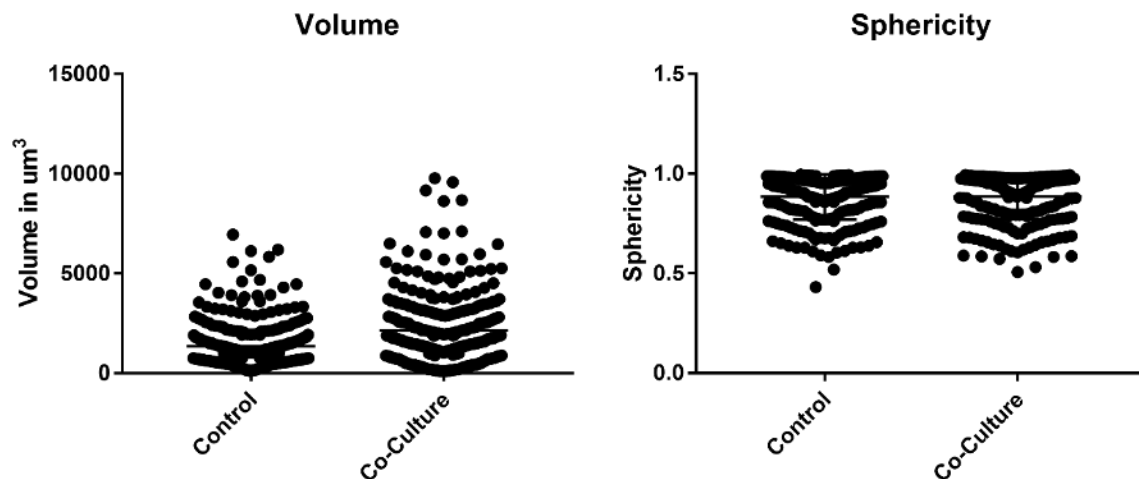


Figure 34 Volumes in μm^3 and sphericities of iMGL co-cultivated with U87 under direct cell-cell contact and respective controls. Each dot represents an analyzed cell. Sphericity was calculated as defined by Wadell. Thus, a perfectly spherical object would have been assigned a sphericity of one. For more details on this metric please consult 2.7.3.4. There was no significant difference in volume or sphericity between co-cultivated and control cells. For statistical analysis, a student's two-tailed ratio paired t-test was performed.

Next, changes in cell morphology upon co-cultivation with U87 with direct intercellular contact were analyzed. Cell volume and sphericity were analyzed. Sphericity was computed as defined by mathematician Wadell in 1935. The analyzed particle's volume is computed, then the surface area of a perfect sphere of obtained volume is calculated. This value is then divided by the particle's actual surface area. For a closer description of this, please consult 2.7.3.4. There was no significant difference in iMGL volume ($p = 0,7342$). Co-cultivation also didn't significantly affect iMGL sphericity ($p = 0,6458$).

3.5 TLR2 Stimulation

3.5.1 TLR2 Stimulation Upregulates Proinflammatory Genes in BJFF.6-derived iMGL

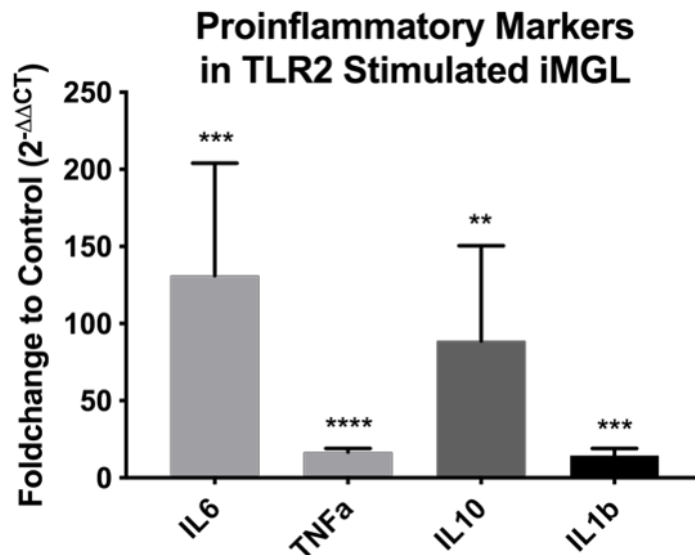


Figure 35 Upregulation of proinflammatory markers in BJFF.6 -derived iMGL upon TLR2 stimulation. IL-6, TNF α , IL-10 and IL-1 β were significantly upregulated. For statistical analysis, a student's two-tailed ratio paired t-test was performed.

After Pam2CSK4 stimulation, IL-6 ($p = 0.0007$, $t = 14.9$), TNF α ($p < 0.0001$, $t = 40.03$), IL-10 ($p = 0.0017$, $t = 10.69$) and IL-1 β ($p = 0.0006$, $t = 15.46$) were significantly upregulated in BJFF.6-derived iMGL.

3.5.2 TLR2 Stimulation Does Not Significantly Change GAM-Characteristic Gene Expression

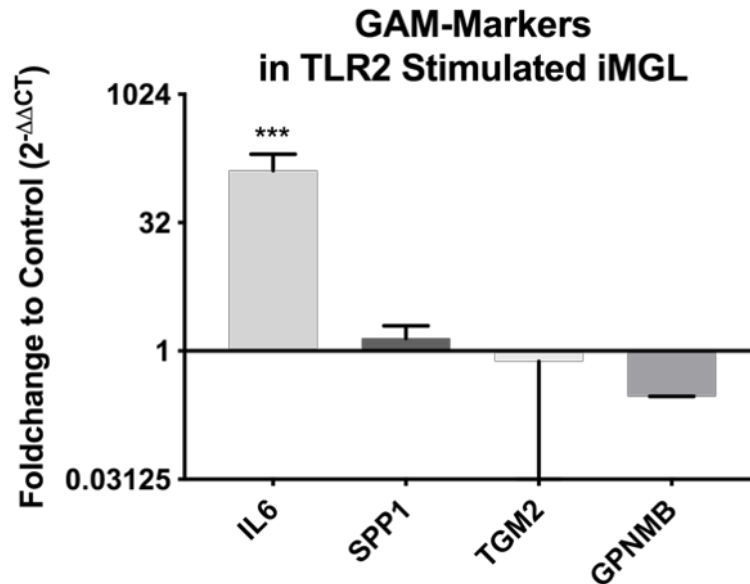


Figure 36 Fold changes of GAM-characteristic genes of BJFF.6-derived iMGL upon TLR2 stimulation with Pam2CSK4. IL-6 was significantly upregulated, otherwise there were no significant changes. For statistical analysis, a student's two-tailed ratio paired t-test was performed.

TLR2 stimulation with Pam2CSK4 did not significantly affect the gene expression of GAM-specific markers SPP1, TGM2 and GPNMB in BJFF.6- and XMOO1-derived iMGL. IL-6 was significantly upregulated ($p = 0.0007$, $t = 14.9$).

3.5.3 TLR2 Stimulation Does Not Significantly Upregulate MMP9 and MMP14 Expression in BJFF.6-derived iMGL

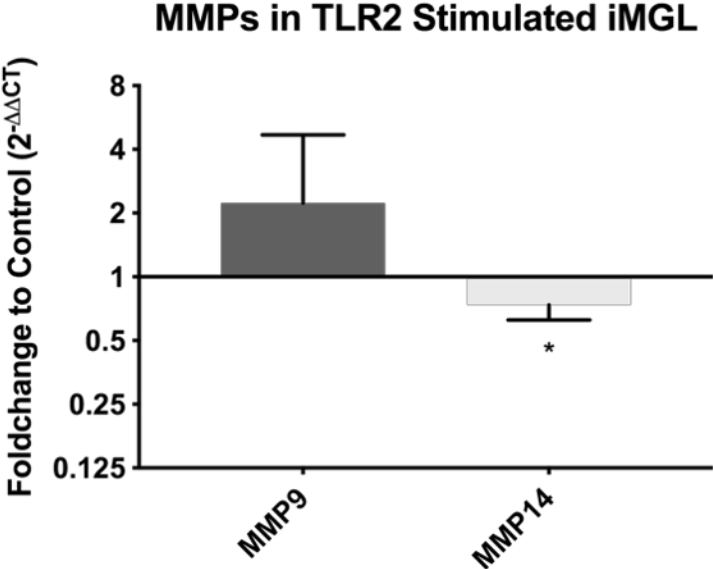


Figure 37 Fold changes in MMP9 and MMP14 expression of XMOO1- and BJFF.6 derived iMGL upon TLR2 stimulation with Pam2CSK4. MMP14 was significantly downregulated in BJFF.6-derived iMGL. For statistical analysis, a student's two-tailed ratio paired t-test was performed.

After TLR2 stimulation with Pam2CSK4, MMP14 was significantly downregulated in BJFF.6-derived iMGL ($p = 0.0296$, $t = 3.915$).

4. Discussion

In this thesis, the results of our basic characterization of induced pluripotent stem cell (iPSC)-derived microglia-like cells (iMGL) and their potential applications in models of glioma are presented. We differentiated iMGL from iPSC using a protocol published by Abud et al. (Abud, 2017) and simplified by McQuade et al. (McQuade, 2018). First, we will discuss our characterization of iMGL derived from XMOO1 iPSC cell line. Then, we will analyze our findings from transwell co-cultivation experiments, direct co-cultivation and TLR2 stimulation.

4.1 XMOO1-derived iMGL Exhibit Fundamental Microglia-Specific Properties

The basic characterization of iMGL derived from BJFF.6 iPSC line has previously been carried out in our lab and is to be published. In this thesis, we showed that XMOO1-derived iMGL exhibit a broad variety of microglial properties, namely upregulation of microglial signature genes, positive staining for microglial signature markers, upregulation of proinflammatory genes in response to LPS stimulation, migration into a scratch wound and phagocytosis of carboxylate microspheres.

The gene targets for our qPCR and immunohistochemical analysis are based on a recently published comprehensive gene expression meta-analysis that distinguishes microglia from peripheral monocytes and macrophages (Haage, 2019). Characteristic markers for microglia were found to be P2RY12, TMEM119, SLC2A5 and FCRL5, whereas monocyte / macrophage markers were EMILIN2, GDA, HP and SELL. Microglia-characteristic genes P2RY12, SLC2A5 and TMEM119 are upregulated in XMOO1-derived iMGL compared to U87 glioma cells, monocyte-like THP-1 cells differentiated to macrophage-like cells and hematopoietic progenitor cells (HPCs). The notion that HPCs mature towards a microglial phenotype is supported by upregulation of microglia-characteristic genes in iMGL compared to HPCs. Also, iMGL express more microglial signature genes than macrophage-like differentiated THP-1 cells, suggesting that they are more similar to microglia than peripheral macrophages. Moreover, peripheral macrophage-characteristic genes GDA, HP, SELL and EMILIN2 were not significantly upregulated in iMGL, compared to U87 cells, macrophage-like differentiated THP-1 and HPCs. This further supports that iMGL have a transcriptomic signature more similar to microglia than peripheral macrophages. This is an important

differentiation to make, especially in glioma research, since peripheral monocytes invade brains diseased with glioma (Herisson, 2018). For a clear grasp of glioma pathology, we must distinguish microglial and peripheral monocyte impact (Gutmann, 2019).

Also, XMOO1-derived iMGL stain positive for microglia-characteristic markers Iba1, P2RY12, TMEM119 and SLC2A5. Hence, canonical microglial markers can also be detected on a protein level on XMOO1-derived iMGL. iMGL differentiated by Abud et al. also stained positive for P2RY12 (Abud, 2017).

Furthermore, XMOO1-derived iMGL respond to LPS stimulation with an upregulation of proinflammatory genes IL-10, IL-1 β , IL-6 and TNF α . TGF- β 1 is downregulated by LPS, which is to be expected (Affram, 2017). In comparison, Abud et al. showed that their iMGL secreted more TNF α , IL6 and IL10 after stimulation with LPS (Abud, 2017). This goes in line with our qPCR results.

Also, we showed that XMOO1-derived iMGL are able to migrate into a scratch wound until the cells are nearly homogeneously distributed (see 3.1.5 Migration). After about 28 hours, maximal confluency is reached with 60 % of the scratch wound being covered by migrating cells. Next, stimulants of migration, such as 506, Pam2CSK4, LPS as well as glioma conditioned medium (GCM), should be tested. Abud et al. analyzed chemotaxis of iMGL triggered by ADP, not migration. Analyzing chemotaxis towards glioma cells may be especially interesting for brain cancer research, however, our established scratch assay is not suited for this. In order to study chemotaxis, we would have to make use of other experimental setups such as Boyden chamber or agarose spot assay.

Also, XMOO1-derived iMGL are able to phagocytose carboxylate beads, as shown by FACS-based phagocytosis. Phagocytosis is significantly downregulated by cytoskeletal inhibitor cytochalasin D from 44,93 % of phagocytosing cells with 1,39 phagocytosed beads per cell to 7,17 % phagocytosing cells with 0,13 beads per cell (see 3.1.7 FACS-Based Phagocytosis Assay – Analysis with LSRFortessa™ Analyzer and Quantification). 100 μ mol/l UDP did not significantly change phagocytosis. This is surprising, since it has been shown that UDP upregulates phagocytosis by stimulating P2RY6 for rat (Koizumi, 2007) and murine microglia (Wendt, 2017). In our laboratory, Wendt et al. used a UDP concentration of 100 μ mol/l

to stimulate phagocytosis (Wendt, 2017). Nevertheless, one could imagine that human iMGL need a higher UDP concentration to upregulate phagocytosis than murine microglia, since it has been shown that human microglia are less responsive to stimulants such as LPS (Landry, 2012) (Smith, 2014). Also, human microglia expressed less P2RY6 than their murine counterparts in transcriptomic studies. Gosselin et al. reported a 3.5-fold lower expression of P2RY6 in human microglia isolated post-mortem compared to murine microglia (Gosselin, 2017). Galatro et al. also report a lower expression of P2RY6 in their human dataset than in the murine datasets from Grabert et al. (Grabert, 2016), Matcovich-Natan et al. (Maticovitch-Natan, 2016) and themselves (Galatro, 2017). Furthermore, neither the function of P2RY6 on human microglia nor its mechanisms or stimulants have been fully elucidated to date. Hence, it could be that even if a sufficient amount of UDP binds P2RY6, phagocytosis is not upregulated. Also, the TGF- β 1 present in the microglia medium during our experiment could possibly have counteracted UDP stimulation, since TGF- β has been shown to induce a quiescent microglial phenotype (Abutbul, 2012). Positive controls are important for experiments to define effect size. Hence, it would be sensible to find a working positive control. This could be UDP at a higher concentration or TLR ligand LPS, since TLRs activate phagocytosis through MyD88-dependent pathways (Fu, 2014). Also, it could be interesting to test phagocytosis of other compounds. Abud et al. showed that iMGL phagocytose human synaptosomes, *E. coli* particles, A β protein and tau oligomers (Abud, 2017). McQuade et al. showed that iMGL phagocytose *S. aureus*, Zymosan and beta-amyloid fibrils (McQuade, 2018). For glioma research, examining phagocytosis of fluorescently marked glioma cells by flow cytometry may be especially interesting.

Since their aim was to validate their newly published differentiation protocol, Abud et al. characterized their iMGL more extensively than in this thesis (Abud, 2017). They carried out time-consuming and costly procedures such as transcriptome analysis to compare iMGL to iPSC, HPCs, monocytes, blood dendritic cells and human adult and fetal microglia. They also compared the transcriptome of control iMGL with iMGL co-cultivated with rat hippocampal neurons. Furthermore, they conducted experiments in which they co-cultivated iMGL with brain organoids (BORG) for morphologic examination under control conditions and in response to the piercing of BORG with a needle. Also, they conducted *in vivo* experiments, wherein fully differentiated iMGL were transplanted into immunodeficient MITRG quadruple knock-in (M-CSF, IL-3, GM-

CSF, TPO) mice. Two months post transplantation, cells were stained for P2RY12 and TMEM119. Microglia were highly ramified, similarly as to endogenous microglia under physiologic conditions. Here, we did not do a more thorough characterization because our aim was to show that we are able to robustly reproduce Abud et al.'s differentiation protocol.

4.2 iMGL Co-Cultivated with Human Glioma Cell Lines in a Transwell Setup Do Not Consistently Upregulate GAM-Characteristic Genes

Furthermore, we investigated changes of gene expression for iMGL co-cultivated with human glioma cell lines U87, LN229 and U251MG for 72 and 144 hours. We focused on four genes that had previously been shown to be upregulated in GAM, namely SPP1, TGM2, GPNMB and IL-6 (Szulzewsky, 2016) (Szulzewsky, 2017) (Walentynowicz, 2018) (a Dzaye, 2016). While there was a significant upregulation of SPP1 and TGM2 in iMGL under certain co-culture conditions, other conditions also led to a downregulation of these genes. Meanwhile, GPNMB was consistently downregulated and IL-6 did not significantly change. SPP1 was significantly upregulated in BJFF.6-derived iMGL after 72 hours of co-cultivation with U87 and in XMOO1-derived iMGL after 144 hours of co-cultivation with U251MG. However, SPP1 was also significantly downregulated in BJFF.6-derived iMGL after 72 hours of co-cultivation with LN229. TGM2 was significantly upregulated for BJFF.6-derived iMGL co-cultivated with U87 for 72 and 144 hours and in XMOO1-derived iMGL co-cultivated with LN229 for 72 hours, but also significantly downregulated in XMOO1-derived iMGL co-cultivated for 72 and 144 hours with U251MG. GPNMB was significantly downregulated for BJFF.6-derived iMGL co-cultivated with U251MG and LN229 for 72 hours and XMOO1-derived iMGL after 72 hours of co-culture with U87 and 144 hours of co-cultivation with U87, U251MG and LN229. There were no significant changes in IL-6 expression.

This rather inconsistent upregulation of GAM-typic genes in this *in vitro* setup using transwell inserts could have a myriad of reasons. It could be that iMGL cultivated *in vitro* and in monoculture are unsuited to study GAM-characteristic microglial changes, due to transcriptomic changes and divergent enhancer landscapes of microglia *in vitro* (Gosselin, 2017), (Bohlen, 2017), (Butovsky, 2014). Tumor microenvironments are highly complex ecosystems, defined by interactions of a myriad of cell types (Hambardzumyan, 2016) (Gutmann, 2019). Also, there is a growing uncertainty as to

whether conventional glioma cell lines are reliable tools for research. For instance, it has been shown that the U87 glioma cell line differs from its original cells in terms of its DNA profile, leaving the true origin of U87 cells unknown (Allen, 2016). A possible workaround for this uncertainty could be to use carefully characterized, patient-derived glioma cell lines. Furthermore, the long microglial differentiation protocol used here could have induced a high variability between iMGL batches.

Moreover, a lack of cell-cell contact in our experimental setup could have attenuated microglial conditioning by glioma cells. Direct cell-cell contact has been shown to be important for induction of a GAM-like phenotype (Hu, 2014). For further elaboration on this, see below. Furthermore, protein supplements added to microglial differentiation medium may have skewed results. Both TGF- β 1 (Wesolowska, 2008) (Wick, 2001) and M-CSF (Pyonteck, 2013) have been shown to be relevant for GAM-glioma cell interaction. Moreover, our protocol included seeding the iMGL in 500 μ l on Day 1, then, while adding transwell inserts with glioma cells or for control, another 100 μ l DMEM with supplements were added to wells. Then, on Days 1, 3 and 5 another 150 μ l microglial basal medium and supplements were added. This led to final medium volumes of 750 μ l after 72 hours and 1050 μ l after 144 hours. Such high medium volumes could have strongly diluted substances secreted from cells, significantly attenuating paracrine effects. For this reason, shorter timepoints may have been more suitable for this study.

Walentynowicz et al. showed an upregulation of GPNMB and TGM2 in rodent microglia stimulated with GCM, however, they only conditioned microglia for three and six hours (Walentynowicz, 2018). It is uncertain whether GAM-related genes remain upregulated for as long as 72 or 144 hours. Kim et al. studied upregulation of proinflammatory genes, including IL-6 in human monocytes in response to *Candida albicans* (Kim, 2005). Proinflammatory gene expression reached a peak after about six hours but came back down to baseline after 18 hours, despite a constant exposure to *Candida albicans*. Moreover, genes relevant for host defense against *C. albicans* also chiefly attained a peak after six hours, after which they remained only slightly upregulated. Correspondingly, for this long-term co-culture it would make sense to analyze changes on a proteomic level, such as by Enzyme-Linked Immunosorbent Assay (ELISA) or immunohistochemistry. These methods measure accumulation of secreted substances over a long time period.

4.3 iMGL Co-Cultivated with Human Glioma Cells in a Transwell Setup Exhibit a Morphology Not Typical for GAM

Our morphologic examination of iMGL co-cultivated with glioma cells showed that under co-culture conditions, iMGL become more ramified, whereas they took on amoeboid shapes in monoculture (see 3.3 Morphology of iMGL Co-Cultivated with Glioma Cells). Quantification of iMGL morphology based on Iba1 and DAPI staining using image analysis software Imaris 9.2 software (Bitplane, Zurich, Switzerland) showed that iMGL sphericity is significantly reduced after 144 hours of co-cultivation with U87 glioma cells. No significant changes in volume or nucleus to cytoplasm volume ratio could be shown. This goes in line with our abovementioned conclusions drawn from morphologic examination.

These changes in morphology are unexpected since microglia in context of pathologies have been shown to become more amoeboid, not ramified. This was first shown by Pio del Rio-Hortega (Rio-Hortega, 1919). An *in vitro* study on morphologic changes of murine microglia co-cultivated with glioma cells in a transwell setup was published by Walentynowicz et al. (Walentynowicz, 2018). The authors showed amoeboid changes of microglia co-cultivated with glioma cells. The reasons for our unexpected results may be similar to the possible reasons for unexpected gene expression listed above. Notably, a medium volume that was too large could have attenuated paracrine effects, or the lack of intercellular material may have prevented GAM-typic changes of iMGL. Possibly, despite the addition of medium supplemented with fresh cytokines every other day as during differentiation, monoculture may have activated iMGL, while the addition of a second cell type may have deactivated them, as previously shown by Abud et al., in which they compared transcriptomes of iMGL in monoculture with iMGL co-cultivated with rat hippocampal neurons (Abud, 2017). Possibly, co-cultivation with any type of cell could have changed the iMGL morphology to a less activated phenotype. Therefore, morphological studies conducted on murine organotypic brain slices (OBS), in brain organoids (BORG) or *in vivo* may be better-suited.

4.4 iMGL Upregulate GPNMB in Co-Culture with Direct Intercellular Contact

Since GAM-characteristic markers were not consistently upregulated in our transwell setup, we next examined the protein expression of SPP1 and GPNMB with immunohistochemistry in a direct co-culture setup. iMGL were seeded directly on top

of U87 mCherry cells for 48 hours. It is conceivable that direct co-culture may lead to more dramatic changes in iMGL, since closer proximity between cell types may enhance osmotic effects and direct intercellular contact may further strengthen induction of a GAM-like phenotype. For instance, extracellular matrix (ECM) component versican, a chondroitin sulfate proteoglycan, has been shown to induce MMP14 production in microglial cells in response to TLR2 binding (Hu, 2014). As an ECM component, versican cannot act via diffusion. No differences in SPP1 and GPNMB expression were visible at first sight. However, mean intensity of GPNMB inside iMGL was significantly higher in iMGL co-cultivated with U87 mCherry. Hence, closer proximity of glioma cells and iMGL could indeed induce stronger GAM-like transformations of iMGL. Also, an examination of GAM-markers on a proteomic level may be more informative than gene expression patterns. These findings should encourage the study of GAM-markers by immunohistochemistry in more comprehensive models of glioma such as OBS or BORG.

Moreover, direct co-culture setup did not significantly change iMGL volume or sphericity. As discussed above, in a transwell setup co-culture induced a less activated iMGL phenotype than monoculture. In contrast, a direct co-culture setup did not induce a less activated iMGL phenotype in iMGL co-cultivated with U87 compared to monocultivated control. The fact that direct co-cultivation did not deactivate iMGL as strongly as co-cultivation in a transwell setup could be explained by a less deactivating effect induced by pathogenic U87 cancer cells with intercellular contact. Also, monoculture in experimental setup including direct cell-cell contact lasted only 48 hours, whereas monoculture in transwell setup lasted 72 or 144 hours. Hence, longer monocultivation may have activated iMGL to a stronger degree in the transwell setup and led to the abovementioned amoeboid phenotype.

4.5 TLR2 Stimulation Upregulates Pro-Inflammatory but Not GAM-Characteristic Genes in iMGL

Furthermore, we investigated changes in gene expression of proinflammatory markers, GAM-characteristic markers and matrix-metalloproteases (MMPs) in iMGL stimulated with TLR2. TLR2 mediates expression of MMP14 by microglia and brain macrophages (Vinnakota, 2013). Vinnakota et al. showed that TLR2 stimulation of murine microglia with palmitoyl-3-cysteine-serine-lysine-4 (Pam3CSK4, TLR1/2), PG-LPS (TLR2), heat-killed *Listeria monocytogenes* (HKLM, TLR2) and macrophage-activating lipopeptide

2 (MALP2, TLR2/6) led to significant upregulation of MMP14 in murine microglia. In this study, we utilized TLR2/6 stimulant Pam2CSK4 as a stimulant. In response to stimulation with Pam2CSK4, proinflammatory genes IL-10, IL-6, TNF α and IL-1 β were significantly upregulated. However, GAM-characteristic genes SPP1, TGM2 and GPNMB were not significantly changed (see 3.5 TLR2 Stimulation). MMP9 was not changed by TLR2 stimulation, whereas MMP14 was significantly downregulated.

This contradicts the abovementioned results of Vinnakota et al. It is unlikely that this is due to the fact that an *in vitro* model was used here, since Vinnakota et al. also conducted their qPCR experiments *in vitro*. Also, it is unlikely that these differing results are due to a lower expression of TLR2 in human microglia compared to murine microglia, since according to the dataset by Gosselin et al., there is a 1.2-fold higher expression of TLR2 in human microglia compared to murine microglia (Gosselin, 2017).

Moreover, Vinnakota et al. used macrophage-activating lipopeptide 2 (MALP2) as TLR2/6 stimulant, whereas we used Pam2CSK4. Even though Vinnakota et al. showed a significant increase of MMP14 in response to MALP2, the increase was only 1.7-fold. Hence, it may be that MMP14 upregulation can only moderately be triggered by TLR2/6 stimulation and that a slightly different experimental setup may attenuate this effect.

It is also possible that the Pam2CSK4 concentration used here was wrong. We used a Pam2CSK4 concentration of 100 ng/ml for six hours. In our group, Buonfiglioli et al. also used a Pam2CSK4 concentration of 100 ng/ml for an ELISA of TNF α (Buonfiglioli, 2019). However, other concentrations of Pam2CSK4 have previously been used, such as 300 ng/ml for 24 hours by Ifuku et al. to examine TLR2 and TLR7 expression in qPCR experiments (Ifuku, 2016).

Nevertheless, it is conceivable that downregulated MMP14 expression in our experiments reflects dissimilarity between fetal and neonatal microglia. Vinnakota et al. used microglia extracted from neonatal mice for their experiments (Vinnakota, 2013). We used iPSC-derived iMGL. Abud et al., showed that iMGL differentiated by our protocol cluster closer to human adult and fetal microglia than HPCs, iPSC, blood dendritic cells, CD14 $^+$ /CD16 $^-$ monocytes and CD14 $^+$ /CD16 $^+$ inflammatory monocytes (Abud, 2017). In their whole-transcriptome differential gene expression analysis they showed that there are fewer differences in gene expression between human adult

microglia and iMGL than between human fetal microglia and iMGL. Hence, iMGL seem to be more similar to adult than fetal microglia, even though one could not assign them a specific age. Possibly, these different stages of iMGL maturity may have led to different responses to Pam2CSK4.

5. Outlook and Conclusion

It is becoming increasingly clear that there are important differences between murine and human microglia on a transcriptomic (Galatro, 2017) (Szulzewsky, 2016) and functional (Wolf, 2017) (Smith, 2014) (Landry, 2012) level. Studies with microglia isolated post-mortem have been used in the past to study human microglia (Gosselin, 2017) (Galatro, 2017). However, they have been rare and hard to implement. Also, it is not clear to what extent the donor's death and elapsed time before isolation may alter microglia. Brain tissue samples removed intraoperatively from patients suffering from conditions such as epilepsy, trauma or glioma have also been used to study microglia (Szulzewsky, 2016). Yet, also in this case it is not clear whether a microglial state is altered by the removal procedure or the patient's underlying condition, even when tissue samples were taken from the pathology's border. New knowledge on microglial embryology gained especially over the last decade (Ginhoux, 2010) (Schulz, 2012) (Kierdorf, 2013) has enabled the development of a series of protocols to differentiate iPSC towards a microglial phenotype (Muffat, 2018) (Haenseler, 2017) (Abud, 2017) (McQuade, 2018). Nevertheless, at present (March 2020), to the best of our knowledge, there are no publications on glioma that utilize iMGL. Importantly, glioma models utilizing iPSC-derived cells could be used to clearly discriminate microglial and peripheral monocytic impact on glioma pathology. It has been shown that under pathologic conditions, brain tissue is infiltrated by monocytes from the skull bone marrow (Herisson, 2018). Hence, two distinct cell populations, brain resident microglia and invading peripheral monocytes, may be impacting glioma pathology. This may have hampered glioma research in the past, since markers that clearly distinguish microglia and peripheral monocytes were only just recently published (Haage, 2019).

In this study, we showed that iMGL produced with the protocol from McQuade et al. (McQuade, 2018) exhibit microglia-characteristic properties and that they have a stronger expression of microglia-characteristic markers than peripheral macrophages. We then explored how iMGL may be used to model GAM in *in vitro* studies. It is very challenging to model interactions between microglia and glioma cells in *in vitro* settings, possibly due to the high complexity of glioma microenvironments. Therefore, we suggest investing additional effort into more comprehensive models of brain tissue such as OBS or BORG to model glioma.

BORG are *in vitro* grown brain-like mini organs (Lancaster, 2013). It has been shown that slight modifications of an original BORG protocol induce intrinsic development of microglia-like cells within BORG (Ormel, 2018). Also, iMGL co-cultivated with BORG have a microglia-typical morphology and injury response (Abud, 2017). BORG could be used as a high throughput system to model microglial interaction with other CNS and glioma cell types. Gene editing techniques can easily be applied to BORG. Also, BORG and iMGL could be differentiated from the same iPSC, resulting in the same genetic background. Hence, perhaps in the future, custom-made models consisting of BORG and microglia from patient-derived iPSC could be used to test therapy responses. These models could perhaps even include glioma cells from the patients themselves. Nevertheless, one should bear in mind that the transcriptomic profile of BORG is more similar to fetal than adult brain tissue and that BORG lack the structural organization of adult brains.

OBS are mouse brain slices that can be cultivated in special media for up to several weeks (Gähwiler, 1981). It has been shown that iMGL engrafted into the brains of immunodeficient mice, develop microglia-typic ramification and stain positive for canonical microglial markers (Abud, 2017). M-CSF knock-in of mice is sufficient for this (Hasselmann, 2019). Xenotransplanted microglia also exhibit a transcriptomic signature similar to human *in vivo* microglia, develop numerous subpopulations, survey their environment and respond to laser ablation, trauma and intraperitoneal LPS (Hasselmann, 2019) (Svoboda, 2019). Perhaps iMGL could be conditioned on OBS in a similar way. Experiments could also be carried out with brain slices from specific knock-out mice. OBS present a nearly intact brain environment with structural organization of a mature brain.

Overall, we have shown that microglia differentiated from the XMOO1 iPSC cell line as described by McQuade et al. (McQuade, 2018) exhibit fundamental microglia-specific properties. Upon co-cultivation with glioma cell lines utilizing a transwell setup, there is no consistent upregulation of GAM characteristic genes, and iMGL do not exhibit an exemplary GAM-like morphology. TLR2 stimulation of iMGL elicits upregulation of proinflammatory genes, but not of GAM-characteristic genes. Nevertheless, a co-cultivation with U87 glioma cells including direct cell-cell contact elicits an upregulation of GPNMB. These findings imply that iMGL may be a promising tool for glioma research, since iMGL appear transcriptionally and functionally close to microglia. IMGL

are especially interesting for glioma research, since human GAM and physiologic microglia have been poorly available for research to date. Models close to an *in vivo* setting such as OBS or BORG may be especially promising for brain tumor research. Subsequently, these novel tools may build the basis for a myriad of novel glioma therapies.

6. References

- a Dzaye, O.D., Hu, F., Derkow, K., Haage, V., Euskirchen, P., Harms, C., Lehnardt, S., Synowitz, M., Wolf, S.A. and Kettenmann, H. (2016) Glioma stem cells but not bulk glioma cells upregulate IL-6 secretion in microglia/brain macrophages via toll-like receptor 4 signaling. *Journal of Neuropathology & Experimental Neurology*, 75(5), pp. 429-440.
- Abud, E., Ramirez, R., Martinez, E., Healy, L., Nguyen, C., Newman, S., Yeromin, A., Scarfone, V., Marsh, S., Fimbres, C., Caraway, C., Fote, G., Madany, A., Agrawal, A., Kayed, R., Gylys, K., Cahalan, M., Cummings, B., Antel, J., Mortazavi, A., Carson, M., Poon, W., Blurton-Jones, M. (2017) iPSC-derived human microglia-like cells to study neurological diseases. *Neuron*, 94(2), pp. 278-293.
- Abutbul, S., Shapiro, J., Szaingurten-Solodkin, I., Levy, N., Carmy, Y., Baron, R., Jung, S. and Monsonego, A. (2012) TGF- β signaling through SMAD2/3 induces the quiescent microglial phenotype within the CNS environment. *Glia*, 60(7), pp. 1160-117.
- Affram, K. O., Mitchell, K. and Symes, A. J. 2017. Microglial Activation Results in Inhibition of TGF- β -Regulated Gene Expression. *Journal of Molecular Neuroscience*, 63(3-4), pp. 308-319.
- Allen, M., Bjerke, M., Edlund, H., Nelander, S. and Westermark, B. (2016) Origin of the U87MG glioma cell line: Good news and bad news. *Science translational medicine*, 8(354), 354re3-354re3.
- Badie, B. and Schartner, J.M. (2000) Flow cytometric characterization of tumor-associated macrophages in experimental gliomas. *Neurosurgery*, 46(4), pp. 957-962.
- Bohlen, C.J., Bennett, F.C., Tucker, A.F., Collins, H.Y., Mulinyawe, S.B. and Barres, B.A. (2017) Diverse requirements for microglial survival, specification, and function revealed by defined-medium cultures. *Neuron*, 94(4), pp. 759-773.
- Buonfiglioli, A., Efe, I.E., Guneykaya, D., Ivanov, A., Huang, Y., Orłowski, E., Krüger, C., Deisz, R.A., Markovic, D., Flüh, C., Newman, A.G., Schneider, U.C., Beule, D., Wolf, S.A., Dzaye, O., Gutmann, D.H., Semtner, M., Kettenmann, H. and Lehnardt, S. (2019) let-7 microRNAs regulate microglial function and suppress glioma growth through Toll-like receptor 7. *Cell Reports*, 29(11), pp. 3460-3471.
- Butovsky, O., Jedrychowski, M.P., Moore, C.S., Cialic, R., Lanser, A.J., Gabriely, G., Koeglsperger, T., Dake, B., Wu, P.M., Doykan, C.E., Fanek, Z., Liu, L., Chen, Z.,

- Rothstein, J.D., Ransohoff, R.M., Gygi, S.P., Antel, J.P. and Weiner, H.L. (2014) Identification of a unique TGF- β -dependent molecular and functional signature in microglia. *Nature neuroscience*, 17(1), pp. 131-143.
- Charles, N.A., Holland, E.C., Gilbertson, R., Glass, R. and Kettenmann, H. (2011) The brain tumor microenvironment. *Glia*, 59(8), pp. 1169-1180.
- Chen, Y. and Pruett-Miller, S.M. (2018) Improving single-cell cloning workflow for gene editing in human pluripotent stem cells. *Stem Cell Res*, 31, pp. 186-192.
- Douvaras, P., Sun, B., Wang, M., Kruglikov, I., Lallios, G., Zimmer, M., Terrenoire, C., Zhang, B., Gandy, S., Schadt, E., Freytes, D.O., Noggle, S. and Fossati, V. (2017) Directed differentiation of human pluripotent stem cells to microglia. *Stem cell reports*, 8(6), pp. 1516-1524.
- Ellert-Miklaszewska, A., Dabrowski, M., Lipko, M., Sliwa, M., Maleszewska, M. and Kaminska, B. (2013) Molecular definition of the pro-tumorigenic phenotype of glioma-activated microglia. *Glia*, 61(7), pp. 1178-1190.
- Engler, J.R., Robinson, A.E., Smirnov, I., Hodgson, J.G., Berger, M.S., Gupta, N., James, C.D., Molinaro, A. and Phillips, J.J. (2012) Increased microglia/macrophage gene expression in a subset of adult and pediatric astrocytomas. *PloS one*, 7(8), pp. e43339.
- Evans, M.J. and Kaufman, M.H. (1981) Establishment in culture of pluripotential cells from mouse embryos. *Nature*, 292(5819), pp. 154-156.
- Feng, X., Szulzewsky, F., Yerevanian, A., Chen, Z., Heinzmann, D., Rasmussen, R. D., Alvarez-Garcia, V., Kim, Y., Wang, B., Tamagno, I., Zhou, H., Li, X., Kettenmann, H., Ransohoff, R. M. and Hambardzumyan, D. (2015) Loss of CX3CR1 increases accumulation of inflammatory monocytes and promotes gliomagenesis. *Oncotarget*, 6(17), p. 15077.
- Fu, J., Yang, Q., Sai, K., Chen, F., Pang, J.C.S., Ng, H., Kwan, A. and Chen, Z. (2013) TGM2 inhibition attenuates ID1 expression in CD44-high glioma-initiating cells. *Neuro-oncology*, 15(10), pp. 1353-1365.
- Fu, R., Shen, Q., Xu, P., Luo, J.J. and Tang, Y. (2014) Phagocytosis of microglia in the central nervous system diseases. *Molecular neurobiology*, 49(3), pp. 1422-1434.

Gähwiler, B. H. (1981) Organotypic monolayer cultures of nervous tissue. *Journal of neuroscience methods*, 4(4), pp. 329-342.

Galatro, T., Holtman, I., Lerario, A., Vainchtein, I., Brouwer, N., Sola, P., Veras, M., Pereira, T., Leite, R., Moeller, T., Wes, P., Sogayar, M., Laman, J., den Dunnen, W., Pasqualucci, C., Oba-Shinjo, S., Boddeke, E., Marie, S. and Eggen, B. (2017) Transcriptomic analysis of purified human cortical microglia reveals age-associated changes. *Nature neuroscience*, 20(8), p. 1162.

Giering, A., Pszczolkowska, D., Bocian, K., Dabrowski, M., Rajan, W.D., Kloss, M., Mieczkowski, J. and Kaminska, B. (2017) Immune microenvironment of experimental rat C6 gliomas resembles human glioblastomas. *Scientific reports*, 7(1), p. 17556.

Ginhoux, F., Greter, M., Leboeuf, M., Nandi, S., See, P., Gokhan, S., Mehler, M.F., Conway, S.J., Ng, L.G., Stanley, E.R., Samokhvalov, I.M. and Merad, M. (2010) Fate mapping analysis reveals that adult microglia derive from primitive macrophages. *Science*, 330(6005), pp. 841-845.

Gosselin, D., Skola, D., Coufal, N.G., Holtman, I.R., Schlachetzki, J.C.M., Sajti, E., Jaeger, B.M., O'Connor, C., Fitzpatrick, C., Pasillas, M.P., Pena, M., Adair, A., Gonda, D.D., Levy, M.L., Ransohoff, R.M., Gage, F.H. and Glass, C.K. (2017) An environment-dependent transcriptional network specifies human microglia identity. *Science*, 356(6344), p. eaal3222.

Grabert, K., Michoel, T., Karavolos, M.H., Clohisey, S., Baillie, J.K., Stevens, M.P., Freeman, T.C., Summers, K.M. and McColl, B.W. (2016) Microglial brain region-dependent diversity and selective regional sensitivities to aging. *Nature neuroscience*, 19(3), p. 504.

Gutmann, D.H. and Kettenmann, H. (2019) Microglia/brain macrophages as central drivers of brain tumor pathobiology. *Neuron*, 104(3), pp. 442-449.

Haage, V., Semtner, M., Vidal, R.O., Hernandez, D.P., Pong, W.W., Chen, Z., Hambardzumyan, D., Magrini, V., Ly, A., Walker, J., Mardis, E., Mertins, P., Sauer, S., Kettenmann, H. and Gutmann, D.H. (2019) Comprehensive gene expression meta-analysis identifies signature genes that distinguish microglia from peripheral monocytes/macrophages in health and glioma. *Acta neuropathologica communications*, 7(1), p. 20.

Haenseler, W., Sansom, S.N., Buchrieser, J., Newey, S.E., Moore, C.S., Nicholls, F.J., Chintawar, S., Schnell, C., Antel, J.P., Allen, N.D., Cader, M.Z., Wade-Martins, R., James, W.S. and Cowley, S.A. (2017) A highly efficient human pluripotent stem cell microglia model displays a neuronal-co-culture-specific expression profile and inflammatory response. *Stem cell reports*, 8(6), pp. 1727-1742.

Hambardzumyan, D., Gutmann, D.H. and Kettenmann, H. (2016) The role of microglia and macrophages in glioma maintenance and progression. *Nature neuroscience*. 19(1), p. 20.

Hasselmann, J. and Blurton-Jones, M. (2020) Human iPSC-derived microglia: A growing toolset to study the brain's innate immune cells. *Glia*, 68(4), pp. 721-739.

Hasselmann, J., Coburn, M., England, W., Velez, D., Shabestari, S., Tu, C., McQuade, A., Kolahdouzan, M., Echeverria, K., Claes, C., Nakayama, T., Azevedo, R., Coufal, N., Han, C., Cummings, B., Davtyan, H., Glass, C., Healy, L., Gandhi, S., Spitale, R. and Blurton-Jones, M. (2019) Development of a chimeric model to study and manipulate human microglia in vivo. *Neuron*, 103(6), pp. 1016-1033.

Herisson, F., Frodermann, V., Courties, G., Rohde, D., Sun, Y., Vandoorne, K., Wojtkiewicz, G.R., Masson, G.S., Vinegoni, C., Kim, J., Kim, D., Weissleder, R., Swirski, F.K., Moskowitz, M.A. and Nahrendorf, M. (2018) Direct vascular channels connect skull bone marrow and the brain surface enabling myeloid cell migration. *Nature neuroscience*, 21(9), pp. 1209-1217.

Hu, F., Dzaye, O.D., Hahn, A., Yu, Y., Scavetta, R.J., Dittmar, G., Kaczmarek, A.K., Dunning, K.R., Ricciardelli, C., Rinnenthal, J.L., Heppner, F.L., Lehnardt, S., Synowitz, M., Wolf, S.A. and Kettenmann, H. (2014) Glioma-derived versican promotes tumor expansion via glioma-associated microglial/macrophages Toll-like receptor 2 signaling. *Neuro-oncology*, 17(2), pp. 200-2.

Ifuku, M., Buonfiglioli, A., Jordan, P., Lehnardt, S. and Kettenmann, H. (2016) TLR2 controls random motility, while TLR7 regulates chemotaxis of microglial cells via distinct pathways. *Brain, behavior, and immunity*, 58, pp. 338-347.

Janabi, N. (2002) Selective inhibition of cyclooxygenase-2 expression by 15-deoxy- Δ 12, 1412, 14-prostaglandin J2 in activated human astrocytes, but not in human brain macrophages. *The Journal of Immunology*, 168(9), pp. 4747-4755.

Kierdorf, K., Erny, D., Goldmann, T., Sander, V., Schulz, C., Perdiguero, E.G., Wieghofer, P., Heinrich, A., Riemke, P., Hölscher, C., Müller, D., Luckow, B., Brocker, T., Debowski, K., Fritz, G., Opdenakker, G., Diefenbach, A., Biber, K., Heikenwalder, M., Geissmann, F., Rosenbauer, F., Prinz, M. (2013) Microglia emerge from erythromyeloid precursors via Pu. 1- and Irf8-dependent pathways. *Nature neuroscience*, 16(3), p. 273.

Kim, H.S., Choi, E.H., Khan, J., Roilides, E., Francesconi, A., Kasai, M., Sein, T., Schaufele, R.L., Sakurai, K., Son, C.G., Greer, B.T., Chanock, S., Lyman, C.A. and Walsh, T.J. (2005) Expression of genes encoding innate host defense molecules in normal human monocytes in response to *Candida albicans*. *Infection and immunity*, 73(6), p. 37.

Koizumi, S., Shigemoto-Mogami, Y., Nasu-Tada, K., Shinozaki, Y., Ohsawa, K., Tsuda, M., Joshi, B.V., Jacobson, K.A., Kohsaka, S. and Inoue, K. (2007) UDP acting at P2Y₆ receptors is a mediator of microglial phagocytosis. *Nature*, 446(7139), pp. 1091-1095.

Kuan, C.T., Wakiya, K., Keir, S.T., Li, J., Herndon, J.E., Pastan, I. and Bigner, D.D. (2011) Affinity-matured anti-glycoprotein NMB recombinant immunotoxins targeting malignant gliomas and melanomas. *International journal of cancer*, 129(1), pp. 111-121.

Lancaster, M.A., Renner, M., Martin, C., Wenzel, D., Bicknell, L.S., Hurles, M.E., Homfray, T., Penninger, J.M., Jackson, A.P. and Knoblich, J.A. (2013) Cerebral organoids model human brain development and microcephaly. *Nature*, 501(7467), p. 373.

Landry, R.P., Jacobs, V.L., Romero-Sandoval, E.A. and DeLeo, J.A. (2012) Propentofylline, a CNS glial modulator does not decrease pain in post-herpetic neuralgia patients: in vitro evidence for differential responses in human and rodent microglia and macrophages. *Experimental neurology*, 234(2), pp. 340-350.

Lenhossek, M. (1895) *Bau des Nervensystems*.

Linnartz-Gerlach, B., Bodea, L., Klaus, C., Ginolhac, A., Halder, R., Sinkkonen, L., Walter, J., Colonna, M. and Neumann, H. (2019) TREM2 triggers microglial density and age-related neuronal loss. *Glia*, 67(3), pp. 539-550.

Louis, D.N., Perry, A., Reifenberger, G., Von Deimling, A., Figarella-Branger, D., Cavenee, W.K., Ohgaki, H., Wiestler, O.D., Kleihues, P. and Ellison, D.W. (2016) The

2016 World Health Organization classification of tumors of the central nervous system: a summary. *Acta neuropathologica*, 131(6), pp. 803-820.

Matcovitch-Natan, O., Winter, D., Giladi, A., Aguilar, S., Spinrad, A., Sarrazin, S., Ben-Yehuda, H., David, E., Gonzalez, F., Perrin, P., Keren-Shaul, H., Gury, M., Lara-Astaiso, D., Thaiss, C., Cohen, M., Halpern, K., Baruch, K., Deczkowska, A., Lorenzo-Vivas, E., Itzkovitz, S., Elinav, E., Sieweke, M., Schwartz, M., Amit, I. (2016) Microglia development follows a stepwise program to regulate brain homeostasis. *Science*, 353(6301), p. aad8670.

McQuade, A., Coburn, M., Tu, C.H., Hasselmann, J., Davtyan, H. and Blurton-Jones, M. (2018) Development and validation of a simplified method to generate human microglia from pluripotent stem cells. *Molecular neurodegeneration*, 13(1), pp. 1-13.

Muffat, J., Li, Y., Omer, A., Durbin, A., Bosch, I., Bakiasi, G., Richards, E., Meyer, A., Gehrke, L. and Jaenisch, R. (2018) Human induced pluripotent stem cell-derived glial cells and neural progenitors display divergent responses to Zika and dengue infections. *Proceedings of the National Academy of Sciences*, 115(27), pp. 7117-7122.

Ormel, P.R., de Sa, R.V., van Bodegraven, E.J., Karst, H., Harschnitz, O., Sneeboer, M., Johansen, L.E., van Dijk, R.E., Scheefhals, N., van Berlekom, A., Martinez, E., Kling, S., MacGillavry, H., Kahn, R., Hol, E., de Witte, L. and Pasterkamp, R. (2018) Microglia innately develop within cerebral organoids. *Nature communications*, 9(1), pp. 1-14.

Pandya, H., Shen, M.J., Ichikawa, D.M., Sedlock, A.B., Choi, Y., Johnson, K.R., Kim, G., Brown, M.A., Elkahloun, A.G., Maric, D., Sweeney, C.L., Gossa, S., Malech, H.L., McGavern, D.B. and Park, J.K. (2017) Differentiation of human and murine induced pluripotent stem cells to microglia-like cells. *Nature neuroscience*, 20(5), p. 753.

Paolicelli, R.C., Bolasco, G., Pagani, F., Maggi, L., Scianni, M., Panzanelli, P., Giustetto, M., Ferreira, T.A., Guiducci, E., Dumas, L., Ragozzino, D. and Gross, C.T. (2011) Synaptic pruning by microglia is necessary for normal brain development. *Science*, 333(6048), pp. 1456-1458.

Pyonteck, S.M., Akkari, L., Schuhmacher, A., Bowman, R., Sevenich, L., Quail, D., Olson, O., Quick, M.L., Huse, J., Teijeiro, V., Setty, M., Leslie, C., Oei, Y., Pedraza, A., Zhang, J., Brennan, C., Sutton, J., Holland, E., Daniel, D. and Joyce, J.A. (2013) CSF-

1R inhibition alters macrophage polarization and blocks glioma progression. *Nature medicine*, 19(10), p. 1264.

Rio-Hortega, P. (1919) " Tercer elemento" de Los Centros Nerviosos. II. Intervencion de la microglia en los procesos patologicos (Cellulas en bastocito y cuerpos granulo-adiposos). *Bol Soc Esp Biol*, 9, pp. 91-103.

—. (1919) El "tercer elemento" de los centros nerviosos. I. La microglia en estado normal. *Boll. Societed Esp. Biol*, 9, pp. 67-82.

—. (1919) El "tercer elemento" de los centros nerviosos. III. Naturaleza probable de la microglía. *Bol. Soc. Esp. Biol*, 9, pp. 108-115.

—. (1919) El " Tercer" elemento" de los centros nerviosos: poder fagocitario y movilidad de la microglia. *Boll. Societed Esp. Biol*, 9, pp. 108-115.

Robert Koch Institut (2017) Gesellschaft der epidemiologischen Krebsregister in Deutschland eV Krebs in Deutschland für 2013/2014. Berlin: Robert Koch Institut.

Schulz, C., Perdiguero, E.G., Chorro, L., Szabo-Rogers, H., Cagnard, N., Kierdorf, K., Prinz, M., Wu, B., Jacobsen, S.E.W., Pollard, J.W, Frampton, J., Liu, K.J. and Geissmann, F. (2012) A lineage of myeloid cells independent of Myb and hematopoietic stem cells. *Science*, 336(6077), pp. 86-90.

Schwartzbaum, J.A., Fisher, J.L., Aldape, K.D. and Wrensch. (2006) M. Epidemiology and molecular pathology of glioma. *Nature clinical practice Neurology*, 2(9), pp. 494-503.

Scudellari, M. (2016) How iPS cells changed the world. *Nature News*, 534(7607), p. 310.

Smith, A.M. and Dragunow, M. (2014) The human side of microglia. *Trends in neurosciences*, 37(3), pp. 125-135.

Smith, A.M., Graham, E.S., Feng, S.X., Oldfield, R.L., Bergin, P.M., Mee, E.W., Faull, R.L.M., Curtis, M.A. and Dragunow, M. (2013) Adult human glia, pericytes and meningeal fibroblasts respond similarly to IFN γ but not to TGF β 1 or M-CSF. *PloS one*, 8(12), p. e80463.

Stupp, R., Hegi, M.E., Mason, W.P., Van Den Bent, M.J., Taphoorn, M.J.B., Janzer, R.C., Ludwin, S.K., Allgeier, A., Fisher, B., Belanger, K., Hau, P., Brandes, A.A., Gijtenbeek, J., Marosi, C., Vecht, C.J., Mokhtari, K., Wesseling, P., Villa, S.,

Eisenhauer, E., Gorlia, T., Weller, M., Lacombe, D., Cairncross, J.G. and Mirimanoff, R. (2009) Effects of radiotherapy with concomitant and adjuvant temozolomide versus radiotherapy alone on survival in glioblastoma in a randomised phase III study: 5-year analysis of the EORTC-NCIC trial. *The lancet oncology*, 10(5), pp. 459-46.

Svoboda, D.S., Barrasa, M.I., Shu, J., Rietjens, R., Zhang, S., Mitalipova, M., Berube, P., Fu, D., Shultz, L.D., Bell, G.W. and Jaenisch, R. (2019) Human iPSC-derived microglia assume a primary microglia-like state after transplantation into the neonatal mouse brain. *Proceedings of the National Academy of Sciences*, 116(50), pp. 25293-25303.

Szondy, Z., Korponay-Szabó, I., Király, R., Sarang, Z. and Tsay, G. J. (2017) Transglutaminase 2 in human diseases. *BioMedicine*, 7(3).

Szulzewsky, F., Arora, S., de Witte, L., Ulas, T., Markovic, D., Schultze, J.L., Holland, E.C., Synowitz, M., Wolf, S.A. and Kettenmann, H. (2016) Human glioblastoma-associated microglia/monocytes express a distinct RNA profile compared to human control and murine samples. *Glia*, 64(8), p. 1416.

Szulzewsky, F., Schwendinger, N., Güneykaya, D., Cimino, P.J., Hambardzumyan, D., Synowitz, M., Holland, E.C. and Kettenmann, H. (2017) Loss of host-derived osteopontin creates a glioblastoma-promoting microenvironment. *Neuro-oncology*, 20(3), pp. 355-366.

Takahashi, K. and Yamanaka, S. (2006) Induction of pluripotent stem cells from mouse embryonic and adult fibroblast cultures by defined factors. *cell*, 126(4), pp. 663-676.

Takahashi, K., Tanabe, K., Ohnuki, M., Narita, M., Ichisaka, T., Tomoda, K. and Yamanaka, S. (2007) Induction of pluripotent stem cells from adult human fibroblasts by defined factors. *cell*, 131(5), pp. 861-872.

Takata, K., Kozaki, T., Lee, C., Thion, M., Otsuka, M., Lim, S., Utami, K., Fidan, K., Park, D., Malleret, B., Chakarov, S., See, P., Low, D., Low, G., Garcia-Miralles, M., Zeng, R., Zhang, J., Goh, C., Gul, A., Hubert, S., Lee, B., Chen, J., Low, I., Shadan, N., Lum, J., Wei, T., Mok, E., Kawanishi, S., Kitamura, Y., Larbi, A., Poidinger, M., Renia, L., Ng, L., Wolf, Y., Jung, S., Önder, T., Newell, E., Huber, T., Ashihara, E., Garel, S., Pouladi, M. and Ginhoux, F. (2017) Induced-pluripotent-stem-cell-derived primitive macrophages provide a platform for modeling tissue-resident macrophage differentiation and function. *Immunity*, 47(1), pp. 183-198.

Thomson, J.A., Itskovitz-Eldor, J., Shapiro, S.S., Waknitz, M.A., Swiergiel, J.J., Marshall, V.S. and Jones, J.M. (1998) Embryonic stem cell lines derived from human blastocysts. *science*, 282(5391), pp. 1145-1147.

Vinnakota, K., Hu, F., Ku, M., Georgieva, P.B., Szulzewsky, F., Pohlmann, A., Waiczies, S., Waiczies, H., Niendorf, T., Lehnardt, S., Hanisch, U., Synowitz, M., Markovic, D., Wolf, S.A., Glass, R. and Kettenmann, H. (2013) Toll-like receptor 2 mediates microglia/brain macrophage MT1-MMP expression and glioma expansion. *Neuro-oncology*, 15(11), pp. 1457-1468.

Virchow, R. (1862) *Gesammelte abhandlungen zur wissenschaftlichen medicin*. s.l. : Grote.

Walentynowicz, K.A., Ochocka, N., Pasierbinska, M., Wojnicki, K., Stepniak, K., Mieczkowski, J., Ciechomska, I.A. and Kaminska, B. (2018) In search for reliable markers of glioma-induced polarization of microglia. *Frontiers in immunology*, 9, p. 1329.

Wang, C.Y., Hsieh, Y.T., Fang, K.M., Yang, C.S. and Tzeng, S.F. (2016) Reduction of CD200 expression in glioma cells enhances microglia activation and tumor growth. *Journal of neuroscience research*, 94(12), pp. 1460-1471.

Wang, X., Sterr, M., Burtscher, I., Chen, S., Hieronimus, A., Machicao, F., Staiger, H., and Häring, H., Lederer, G., Meitinger, T., Cernilogar, F.M., Schotta, G., Irmeler, M., Beckers, J., de Angelis, M.H., Ray, M., Wright, C.V.E., Bakhti, M. and Lickert, H. (2018) Genome-wide analysis of PDX1 target genes in human pancreatic progenitors. *Molecular metabolism*, 9, pp. 57-68.

Wendt, S., Maricos, M., Vana, N., Meyer, N., Guneykaya, D., Semtner, M. and Kettenmann, H. (2017) Changes in phagocytosis and potassium channel activity in microglia of 5xFAD mice indicate alterations in purinergic signaling in a mouse model of Alzheimer's disease. *Neurobiology of aging*, 58, pp. 41-53.

Wesolowska, A., Kwiatkowska, A., Slomnicki, L., Dembinski, M., Master, A., Sliwa, M., Franciszkiewicz, K., Chouaib, S. and Kaminska, B. (2008) Microglia-derived TGF- β as an important regulator of glioblastoma invasion—an inhibition of TGF- β -dependent effects by shRNA against human TGF- β type II receptor. *Oncogene*, 27(7), p. 918.

Wick, W., Platten, M. and Weller, M. (2001) Glioma cell invasion: regulation of metalloproteinase activity by TGF- β . *Journal of neuro-oncology*, 53(2), pp. 177-185.

Wolf, S.A., Boddeke, H. and Kettenmann, H. (2017) Microglia in physiology and disease. *Annual review of physiology*, 79, pp. 619-643.

y Cajal, S. R. (1913) *Contribucion al conocimiento de la neuroglia del cerebro humano*.

Yin, J., Oh, Y.T., Kim, J., Kim, S.S., Choi, E., Kim, T.H., Hong, J.H., Chang, N., Cho, H.J., Sa, J.K., Kim, J.C., Kwon, H.J., Park, S., Lin, W., Nakano, I., Gwak, H., Yoo, H., Lee, S., Lee, J., Kim, J.H., Kim, S., Nam, D., Park, M. and Park, J.B. (2017) Transglutaminase 2 inhibition reverses mesenchymal transdifferentiation of glioma stem cells by regulating C/EBP β signaling. *Cancer research*, 77(18), pp. 4973-4984.

Yu, J., Vodyanik, M.A., Smuga-Otto, K., Antosiewicz-Bourget, J., Frane, J.L., Tian, S., Nie, J., Jonsdottir, G.A., Ruotti, V., Stewart, R., Slukvin, I.I. and Thomson, J.A. (2007) Induced pluripotent stem cell lines derived from human somatic cells. *Science*, 318(5858), pp. 1917-1920.

7. Statutory Declaration

Eidesstattliche Versicherung

„Ich, Marina Sophia Schnauß, versichere an Eides statt durch meine eigenhändige Unterschrift, dass ich die vorgelegte Dissertation mit dem Thema: „Aus iPSC Differenzierte Mikroglia: Charakterisierung und Veränderungen nach Co-Kultivierung mit Gliomzellen / iPSC-Derived Microglia: Characterization and Changes Upon Co-Cultivation with Glioma Cells“ selbstständig und ohne nicht offengelegte Hilfe Dritter verfasst und keine anderen als die angegebenen Quellen und Hilfsmittel genutzt habe.

Alle Stellen, die wörtlich oder dem Sinne nach auf Publikationen oder Vorträgen anderer Autoren beruhen, sind als solche in korrekter Zitierung (siehe „Uniform Requirements for Manuscripts (URM)“ des ICMJE - www.icmje.org) kenntlich gemacht. Die Abschnitte zu Methodik (insbesondere praktische Arbeiten, Laborbestimmungen, statistische Aufarbeitung) und Resultaten (insbesondere Abbildungen, Graphiken und Tabellen) entsprechen den URM (s.o) und werden von mir verantwortet.

Ich versichere ferner, dass ich die in Zusammenarbeit mit anderen Personen generierten Daten, Datenauswertungen und Schlussfolgerungen korrekt gekennzeichnet und meinen eigenen Beitrag sowie die Beiträge anderer Personen korrekt kenntlich gemacht habe (siehe Anteilserklärung). Texte oder Textteile, die gemeinsam mit anderen erstellt oder verwendet wurden, habe ich korrekt kenntlich gemacht.

Meine Anteile an etwaigen Publikationen zu dieser Dissertation entsprechen denen, die in der untenstehenden gemeinsamen Erklärung mit dem/der Betreuer/in, angegeben sind. Sämtliche Publikationen, die aus dieser Dissertation hervorgegangen sind und bei denen ich Autor bin, entsprechen den URM (s.o) und werden von mir verantwortet.

Weiterhin versichere ich, dass ich diese Dissertation weder in gleicher noch in ähnlicher Form bereits an einer anderen Fakultät eingereicht habe.

Die Bedeutung dieser eidesstattlichen Versicherung und die strafrechtlichen Folgen einer unwahren eidesstattlichen Versicherung (§156,161 des Strafgesetzbuches) sind mir bekannt und bewusst.“

11.10.2020

Datum

Unterschrift

Statutory Declaration

“I, Marina Sophia Schnauß, by personally signing this document in lieu of an oath, hereby affirm that I prepared the submitted dissertation on the topic „Aus iPSC Differenzierte Mikroglia: Charakterisierung und Veränderungen nach Co-Kultivierung mit Gliomzellen” / „iPSC-Derived Microglia: Characterization and Changes Upon Co-Cultivation with Glioma Cells“ independently and without the support of third parties, and that I used no other sources and aids than those stated.

All parts which are based on the publications or presentations of other authors, either in letter or in spirit, are specified as such in accordance with the citing guidelines. The sections on methodology (in particular regarding practical work, laboratory regulations, statistical processing) and results (in particular regarding figures, charts and tables) are exclusively my responsibility.

Furthermore, I declare that I have correctly marked all of the data, the analyses, and the conclusions generated from data obtained in collaboration with other persons, and that I have correctly marked my own contribution and the contributions of other persons (cf. declaration of contribution). I have correctly marked all texts or parts of texts that were generated in collaboration with other persons.

My contributions to any publications to this dissertation correspond to those stated in the below joint declaration made together with the supervisor. All publications created within the scope of the dissertation comply with the guidelines of the ICMJE (International Committee of Medical Journal Editors; www.icmje.org) on authorship. In addition, I declare that I shall comply with the regulations of Charité – Universitätsmedizin Berlin on ensuring good scientific practice.

I declare that I have not yet submitted this dissertation in identical or similar form to another Faculty.

The significance of this statutory declaration and the consequences of a false statutory declaration under criminal law (Sections 156, 161 of the German Criminal Code) are known to me.”

11.10.2020

Date

Signature

8. German Curriculum Vitae

Mein Lebenslauf wird aus datenschutzrechtlichen Gründen in der elektronischen Version meiner Arbeit nicht veröffentlicht.

9. Publication List

van Sluijs, R., Rondei, Q.J., Wilhelm, E., Jäger, L., Schnauss, M., Gall, M., Garn, H., Hewertson, V., Achermann, P., Landolt, H., Jenni, O., Riener, R. & Hill, C.M. (2018) Rocking bed therapy for sleep related rhythmic movement disorder: movement preference and acceptability in six children. *Special Issue: Abstracts of the 24th Congress of the European Sleep Research Society*, 27, pp. 431-432.

Flüh, C., Nanvuma, C., Huang, Y., Motta, E., Kuhrt, L., Yuan, Y., Xia, P., Lubas, M., Schnauss, M., Hu, F., Synowitz, M., Kettenmann, H., (2021) P16.05 Implementation of a novel ex-vivo brain slice model to study human glioblastoma and glioma-associated microglia, *Neuro-Oncology*, Volume 23, Issue Supplement_2, Pages ii56–ii57, <https://doi.org/10.1093/neuonc/noab180.197>

Huang, Y., Motta, E., Nanvuma, C., Kuhrt, L. D., Yuan, Y., Xia, P., Lubas, M., Zhu, S., Schnauss, M., Qazi, N., Hu, F., Zhang, H., Lei, T., Synowitz, M., Flueh, C. & Kettenmann, H. (2022). Microglia/macrophage-derived human CCL18 promotes glioma progression via CCR8-ACP5 axis analyzed in humanized slice model. *Cell Reports*, 39(2), 110670.

Kuhrt, L. D., Motta, E., Elmadany, N., Weidling, H., Fritsche-Guenther, R., Efe, I. E., ... & Kettenmann, H. (2023). Neurofibromin 1 mutations impair the function of human induced pluripotent stem cell-derived microglia. *Disease models & mechanisms*, 16(12)

Schnauss M., Corona L., Gong E. (2023) Roboter-Assistierte Appendikovesikostomie bei einem Kinderurologischen Patienten mit Augmentationszystoplastie. *DGU Kongress 2023*, Leipzig, Deutschland.

10. Statistical Certification



CharitéCentrum für Anästhesiologie, OP-Management und Intensivmedizin

Charité - Universitätsmedizin Berlin | D - 13344 Berlin

**Universitätsklinik für Anästhesiologie
mit Schwerpunkt operative Intensivmedizin
CCM / CVK**

Klinikdirektorin
Univ.- Prof. Dr. med. Claudia Spies

Campus Virchow-Klinikum

Augustenburger Platz 1
13353 Berlin

Tel: +49 30 450 551-001/002/022

Fax: +49 30 450 551909

anaesthesie-virchow-klinikum@charite.de



Campus Charité Mitte

Charitéplatz 1

10117 Berlin

Tel. +49 30 450 531012/52

Fax: +49 30 450 531911

anaesth@charite.de

<http://www.charite.de/ch/anaest/>

Zur Vorlage bei der
Promotionskommission der
Charité – Universitätsmedizin Berlin

Berlin, den 19. August 2020

Bescheinigung nach § 8 Abs. 2a PO 2017

Sehr geehrter Frau Schnauß,

hiermit bestätige ich Ihnen zum Zwecke der Vorlage beim Promotionsbüro der Charité die erfolgte Beratung zu Ihrem Promotionsprojekt. Die Durchführung und Beschreibung der statistischen Methoden der mir vorgelegten Schrift ist in Art und Umfang für die Erarbeitung adäquat. Nach Einsicht in ihre Arbeit und der mir vorgelegten Beschreibung von Methoden und Berechnungen sehe ich eine sehr gute und detaillierte statistische Bearbeitung, die sich auf eine deskriptive Darstellung der betrachteten Experimente beschränkt.

Im heutige Beratungsgespräch wurden die Primärdaten der Arbeit nicht mit begutachtet. Ergänzend erfolgte eine Beratung zu deskriptiven Statistik sowie der ANOVA, Anwendung von Standardabweichungen als Lagemaße, zu Abbildungen sowie dem Charakter von observationalen versus experimentellen Studien.

Ich wünsche Ihnen für die Zukunft alles Gute.

Priv.-Doz. Dr. med. Sascha Tafelski
akkreditierter Statistiker der Promotionskommission
Universitätsklinik für Anästhesiologie m. S. operative Intensivmedizin
Campus Virchow-Klinikum und Campus Charité Mitte
Charité-Universitätsmedizin Berlin
Charitéplatz 1
10117 Berlin
<http://anaesthesieintensivmedizin.charite.de/>

11. Acknowledgements

I would like to thank Prof. Dr. Kettenmann at MDC Berlin for letting me work in his group and his supervision. Notably, the historical insights he gave us on our field and campus were a great source of inspiration. Also, I would like to thank Dr. Charlotte Flueh for the early supervision of my thesis. Moreover, I am grateful for the advice and support of my other colleagues in the Kettenmann laboratory, including Leonardt Kurth, Maren Wendt, Regina Piske, Nadine Scharek, Yimin Huang, Fatih Yalcin, Nirmeen Elmadany, Pengfei Xia, Sarah Green, Roxanne Papavasiliou, Alexander Schattenberg, Celeste Franconi and Antonia Schreiner. I especially acknowledge Leonardt Kurth for allocating me his leftover BJFF.6-derived iMGL for a few of my experiments, most notably TLR2 stimulation and analysis of morphology upon co-cultivation. I would like to thank MDC's Stem Cell Core Facility. Last but not least, I would like to thank my parents, my sister and my boyfriend for their great support throughout my time at MDC. I would truly not stand where I am today without their support.